A novel theoretical and experimental approach permits a systems view on stochastic intracellular Ca^{2+} signalling

D I S S E R T A T I O N

zur Erlangung des akademischen Grades
doctor rerum naturalium
(Dr. Rer. Nat.)
im Fach Biophysik

eingereicht an der
Mathematisch-Naturwissenschaftlichen Fakultät I
Humboldt-Universität zu Berlin

von
Dipl.-Biophys. Kevin Thurley
geboren am 1. November 1980 in Berlin

Präsident der Humboldt-Universität zu Berlin:
Prof. Dr. Jan-Hendrik Olbertz

Dekan der Mathematisch-Naturwissenschaftlichen Fakultät I:
Prof. Dr. Andreas Herrmann

Gutachter:
1. PD Dr. Martin Falcke
2. Prof. Dr. Dr. h.c. Edda Klipp
3. Prof. Colin Taylor, Ph.D.

eingereicht am: 22. Februar 2011
Tag der mündlichen Prüfung: 6. Juli 2011

Abstract

Keywords: systems biology, noisy signalling, mathematical modelling, HEK cells.

Ca^{2+} is a universal second messenger in eukaryotic cells transmitting information through sequences of concentration spikes. A prominent mechanism to generate these spikes involves Ca^{2+} release from the endoplasmic reticulum (ER) Ca^{2+} store by Inositol(1,4,5)-trisphosphate(IP_3)-sensitive channels. Puffs are elemental events of IP_3-induced Ca^{2+} release through single clusters of channels. Intracellular Ca^{2+} dynamics are a stochastic system, but a complete stochastic theory has not been developed yet. This thesis presents a new modelling framework for spatially resolved stochastic systems in terms of measurable quantities, derives statistical properties emerging on the cell level from local dynamics, and verifies key results experimentally.

The new modelling framework follows emergent behaviour of Ca^{2+} channels over several levels of molecular organisation. It can potentially be applied to a wide range of biological systems consisting of coupled clusters of subsystems. The theory reproduces the typical spectrum of Ca^{2+} signals like puffs, spiking and over-stimulation in analytically treatable test cases as well as in more realistic simulations. The presented calculations show that signal form, average interspike intervals (ISIs) and their distributions depend sensitively on the details of cluster properties and their spatial arrangement. In difference to that, the relation between the average and the standard deviation of ISIs does not depend on cluster properties and cluster arrangement, and it is robust with respect to cell variability. The relation can be adapted to environmental changes or cell-type specific needs by details of global feedback processes in the Ca^{2+} signalling pathway, e.g. via Protein Kinase C or ER depletion. These results from the modelling, to a large extent, are verified by live cell imaging experiments in HEK cells.

In addition to statistics of cellular behaviour, this thesis also investigates statistical properties of the cluster dynamics by analysing high-resolution data from total internal reflection (TIRF) microscopy in two mammalian cell lines. That analysis shows that interpuff intervals (IPIs) are significantly shorter than cellular ISIs, that puff-activity is stochastic with a recovery time

much shorter than the cellular refractory period, and that IPIs show no sign of periodicity. These findings strongly suggest that Ca^{2+} spikes do not arise from oscillatory cluster dynamics, but that cellular repetitive spiking and its typical time scales arise from collective dynamics of the whole cluster array. Thus, they provide evidence for the proposed stochastic Ca^{2+} model based on *in vivo* data on the microscopic scale.

This thesis seeks to gain a systems view on emergent behaviour of spatially resolved stochastic dynamics by investigating intracellular Ca^{2+} signals as a model system. For that purpose, a multidisciplinary approach is employed, which ranges from solution of integro-differential equations to TIRF microscopy.

Zusammenfassung

Schlagworte: Systembiologie, verrauschte Signaltransduktion, mathematische Modellierung, HEK Zellen.

Ca^{2+}-Ionen werden in vielen eukaryotischen Zellen als sekundärer Botenstoff verwendet und übertragen Information durch wiederholte, kurzzeitige Erhöhungen der cytosolischen Ca^{2+}-Konzentration ('Ca^{2+} Spikes'). Ein bekannter Mechanismus, der solche Ca^{2+}-Signale erzeugt, beinhaltet die Freisetzung von Ca^{2+}-Ionen aus dem Endoplasmatischen Retikulum (ER) durch Inositol(1,4,5)-trisphosphate(IP_3)-sensitive Kanäle. 'Puffs' sind elementare Flüsse von Ca^{2+}-Ionen durch einzelne Cluster von Ca^{2+}-Kanälen. Intrazelluläre Ca^{2+}-Dynamik ist ein stochastisches System, allerdings konnte bisher keine vollständige stochastische Theorie entwickelt werden. Die vorliegende Dissertation stellt eine neue Herangehensweise für die Modellierung von räumlich aufgelösten, stochastischen Systemen vor, welche in messbaren Größen formuliert wird. Es werden emergente Systemeigenschaften hergeleitet, die aus der lokalen Cluster-Dynamik hervorgehen, und wichtige Ergebnisse werden experimentell überprüft.

Der neue Modellierungsansatz folgt dem emergenten Verhalten von Ca^{2+}-Kanälen über mehrere Ebenen molekularer Organisation. Er kann potentiell auf eine Vielzahl von biologischen Systemen angewandt werden, die durch Kopplung von clusterbildenden Subsystemen entstehen. Die hier vorgestellte Theorie reproduziert das typische Spektrum zellulärer Ca^{2+}-Signale aus Puffs, Spikes und Überstimulation in analytisch lösbaren Testsystemen und in realistischeren Simulationen. Mit Hilfe von Modellrechnungen wird gezeigt, dass die Signalform, das durchschnittliche Interspikeintervall (ISI) und die ISI-Verteilung sensitiv von den Eigenschaften und der räumlichen Anordnung der Kanalcluster abhängen. Im Gegensatz dazu hängt die Beziehung zwischen Mittelwert und Standardabweichung der ISIe nicht von den Clustereigenschaften und der Clusteranordnung ab, sondern ist robust in Bezug auf zelluläre Variabilität. Die Beziehung kann an Veränderungen der Umwelt oder an spezifische Bedürfnisse des Zelltyps angepasst werden, indem Details der globalen Feedback-Prozesse im Ca^{2+}-Signalweg verändert werden. Das kann z.B. durch Regulation der Protein-Kinase C oder der ER-Entleerung

realisiert werden. Die genannten Ergebnisse, die aus der neuartigen Modellierung resultieren, konnten zum großen Teil durch fluoreszenzmikroskopische Messungen an lebenden Zellen bestätigt werden.

Zusätzlich zur Statistik zellulärer Ca^{2+}-Dynamik untersucht die vorliegende Arbeit auch statistische Eigenschaften der Cluster-Dynamik, indem Daten aus hochauflösender Totalreflektionsfluoreszenz(TIRF) - Mikroskopie in zwei aus Säugetieren stammenden Zelllinien ausgewertet werden. Diese Analyse zeigt, dass Interpuff-Intervalle (IPIe) deutlich kürzer sind als zelluläre ISIe, dass die Puff-Aktivität stochastisch ist – mit bei weitem kleineren Refraktärzeiten als bei zellulären ISIen – und dass IPIe keine Anzeichen von Periodizität aufweisen. Diese Beobachtungen liefern starke Hinweise darauf, dass Ca^{2+}-Spikes nicht aus der oszillatorischen Dynamik einzelner Cluster entstehen, sondern dass repetetives Spiking mit typischen Zeitskalen vielmehr das Ergebnis kollektiven Verhaltens der Gesamtheit der Cluster ist. Insofern bestätigt diese Analyse das in dieser Arbeit vorgeschlagene stochastische Modell intrazellulärer Ca^{2+}-Dynamik mit Hilfe von Daten, die *in vivo* auf mikroskopischer Ebene gewonnen wurden.

Die vorliegende Arbeit wendet eine systembiologische Sichtweise auf emergentes Verhalten von räumlich aufgelöster stochastischer Dynamik an. Speziell werden intrazelluläre Ca^{2+}-Signale als Modellsystem untersucht. Zu diesem Zweck wird ein interdisziplinärer Ansatz verfolgt, der von der Lösung von Integro-Differentialgleichungen bis hin zu hochauflösender TIRF-Mikroskopie reicht.

Contents

List of Figures

List of Tables

Abbreviations

Abbreviation or Symbol	Meaning
c	Local stationary Ca^{2+} concentration
CCH	Carbachol
CPA	Cyclopyazonic acid
CICR	Ca^{2+}-induced Ca^{2+} release
DSSA	Delayed stochastic simulation algorithm
EGTA	Ethylene glycol tetraacetic acid
ER	Endoplasmic Reticulum
FPT	First-passage time
IP_3	Inositol(1,4,5)-trisphosphate
IP_3R	Inositol(1,4,5)-trisphosphate receptor
GPCR	G-Protein coupled receptor
HBS	Hepes Buffered Saline
IPI	Interpuff interval
ISI	Interspike interval
T_{av}	Average ISI or IPI
σ	Standard deviation of ISI or IPI sequences
PKC	Protein Kinase C
PLC	Phopholipase C
PTH	Human parathyroid hormone fragments
SERCA	Serco-Endoplasmic Reticulum Ca^{2+} ATPase
SOCE	Store-operated Ca^{2+} entry
TIRF	Total internal reflection fluorescence
U7	U73122
VIE	Volterra integral equation

Organisms can be characterised as 'Naturzweck', ... (in which) each part is conceived as if exists only through all the others, thus as if existing for the sake of the others and on account for the whole, that means as an organ.

(Immanuel Kant in his "Critique of Judgement" 1790, quoted from ref. [158])

In physics it is obvious that even in the simplest case such as an electron running around a proton one can do classical physics until one's dying day and never get a hydrogen atom out of it. In order to achieve this, one has to use the complementary approach. If one looks at even the simplest kind of cell, one knows it consists of the usual elements of organic chemistry and otherwise obeys the laws of physics. One can analyze any number of compounds in it but one will never get a living bacterium out of it, unless one introduces totally new and complementary points of view.

(Max Delbrück reasoning about a lecture given by Nils Bohr in 1932 [73])

All biology can be explained in terms of physics and chemistry.

(Francis Crick 1966, quoted from ref. [158])

Everything that living things do can be understood in terms of the jiggling and wiggling of atoms.

(Feynman *et al.* 1989, quoted from ref. [158])

The triumph of the reductionism of the Greeks is a pyrrhic victory: We have succeeded in reduceing all of ordinary physical behavior to a simple, correct 'theory of everything' [the basic equations of quantum dynamics, note from the author] only to discover that it has revealed exactly nothing about many things of great importance... The central task of theoretical physics in our time is no longer to write down the ultimate equations, but rather to catalogue and understand emergent behavior in its many guises, including potentially life itself.

(Laughlin and Pines 2000 [123])

What the studies do show so far very clearly is that life is indeed an emergent property.

(Heinz Penzlin 2009 [158])

1 Introduction

The dispute about the nature and the adequate description of biological processes has a long tradition. While in earlier times, it was common sense that living organisms are completely distinct from non-living matter [158], the discoveries of the last century, especially the development of molecular biology, demonstrated that the laws of physics and chemistry are also valid in biology. That view led to the dominance of reductionist approaches seeking to understand living organism on the molecular level or to find the "hydrogen atom of biology" [73] (see also page XV). In the last decades, the pendulum turned back, as it became evident that a systems view is necessary to understand biological processes [93, 112, 115, 239]. A living organism or an adequately defined submodule should be studied by considering all of its parts and their interactions, and not only by isolated investigation of the smallest subunits. This thesis contributes to such a systems view by developing a mathematical description of emergent behaviour of biomolecules (here, Ca^{2+} channels), by deriving emergent system properties from the model, and by verifying key results experimentally.

Emergent behaviour refers to system properties arising on the next higher level of description by collective dynamics of interacting subsystems (Fig. 1.1). It has been argued that emergent behaviour is the key to all processes relevant on the macroscopic scale, because attempts to derive properties of many-particle systems from a general 'theory of everything' have always failed [122, 123]. In the tradition of systems biology, applications of that 'principle of emergent behaviour' often emphasise on network topology: They conclude that critical properties for system function emerge from the whole network, rather than being controlled by a particular process. This idea is an important aspect of metabolic control theory [92, 93], which has been a cornerstone of modern systems biology [239]. It is also relevant for the more recent investigation of generic properties of genetic circuits or signal

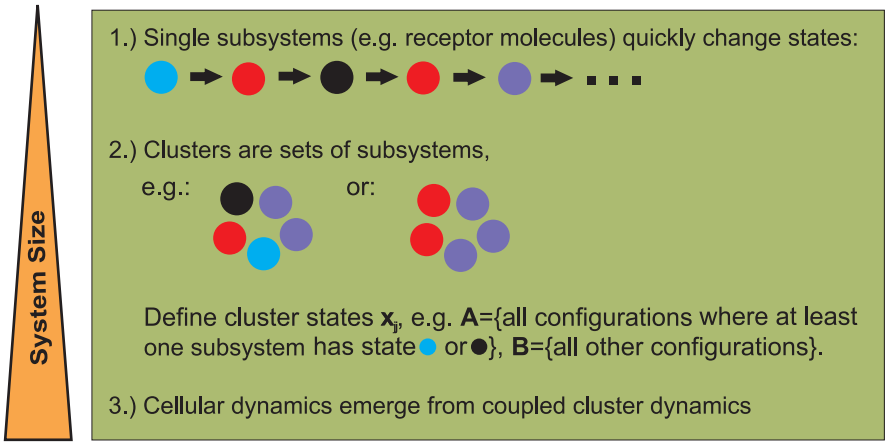

Figure 1.1: General framework of hierarchic stochastic modelling. Clusters of microscopic subsystems are considered as macroscopic entities, for which we define lumped states. Global dynamics arise by coupling of clusters. Thus, we follow emergent behaviour over three different levels, from single subsystems over single clusters to coupled clusters. That approach cirumvents the usual problem of state-space explosion due to the existence of micro- and submicrostates in a natural way.

transduction networks [2–5, 10, 30, 145] (cf. Section 2.2).

Max Delbrück was not only a pioneer of molecular biology, who – from the beginning – argued that understanding the molecules is not sufficient to understand biology [73]. He also was probably the first to investigate probability distributions arising from the fluctuations of biomolecules, in theory and experiment, rather than only considering averages [53, 54]. The significance of such fluctuations made him doubt that biology is really governed by the 'order from order principle' postulated by Erwin Schrödinger in his influential monograph "What is life" [55, 181]. In recent years, the investigation of stochastic fluctuations of biomolecules and their consequences has been a major issue of systems biology (see Section 2.2), and even the idea of an 'order from disorder principle' in biology was formulated [154].

Key terms in this context are robustness and adaptivity – biological systems should be sufficiently robust to molecular noise and fluctuations in the environment to function properly, but they should also be adaptive to changing needs in a changing world [62, 113, 185, 201, 235] (see Section 2.2). This thesis expands these ideas by demonstrating that robustness may arise from molecular noise. For that purpose, concepts from collective dynamics and from the study of biological

robustness are applied to an important eukaryotic signalling pathway, which is intracellular Ca^{2+} signalling.

Ca^{2+} is a versatile second messenger, which is released from intracellular stores into the cytosol in response to extracellular stimuli [28, 67, 212] (see Section 2.1). Signal transduction by Ca^{2+}-dependent pathways is crucial for a large number of processes determining development and physiology of all eukaryotic organisms, and therefore Ca^{2+} has been termed a "life and death signal" [26]. Ca^{2+} signals typically have the form of repeated short-lived increases in the cellular Ca^{2+} concentration (Ca^{2+} oscillations or spikes), and they have become a textbook example of a nonlinear biochemical oscillator [80, 93, 105, 150, 182]. However, more recent data show that interspike intervals are stochastic [58, 195]. Analyses of spike statistics and new types of mathematical models suggest that Ca^{2+} dynamics arise by an intrinsically stochastic mechanism rather than by limit-cycle oscillations [66, 67, 193, 194, 222, 231] (see also Section 2.1).

To account for the stochasticity, a corse-grained modelling strategy is required, because Ca^{2+} dynamics arise from cooperative action of rather few, i.e. 5 to 20 [196], Ca^{2+} channel clusters. Thus, mean-field or white-noise assumptions [105, 233] are not appropriate, and a complete analytical description with Master Equations [233] is not possible because of the astronomic number of states [67]. In addition to the problems arising from the spatial organisation of Ca^{2+} channels, the individual channels also have a carefully regulated intrinsic organisation and continuously switch between several open and closed conformations [211]. Rate-laws for those state-changes can only be estimated from *in vitro* experiments, and determination of kinetic parameters is not straight-forward, a problem often encountered in systems biology [114, 115, 128, 176, 177, 241].

The first part of this thesis will derive a hierarchic stochastic model of intracellular Ca^{2+} dynamics formulated in measurable quantities. That concept is a novel approach to deal with complex systems, since it splits the mathematical description into the appropriate levels of molecular organisation (Fig. 1.1). Further, it is formulated in terms of interevent distributions, which are often accessible *in vivo* [54, 135, 184, 196, 247], and it leads to results in the form of analytical expressions (Chapter 3). The modelling strategy will be presented as applied to Ca^{2+} signalling in this thesis, but it is a general framework that can be applied to

systems consisting of interacting clusters of subsystems. In practice, that can be assumed for a variety of spatially resolved biological systems from cyclic adenosine monophosphate (cAMP) and extracellular signal-regulated kinase (ERK) signalling [106–108] over chemotaxis [39, 83] to clustering of Iummunoglobolin E and of the T cell receptor [24, 76, 95, 96]. Clustering was even argued to be a general principle in cell signalling [38].

Mathematical analysis of the model will predict that experimentally measured Ca^{2+} signals stem from a stochastic process with valuable properties: The average interspike interval is determined by the extracellular stimulus and local cluster dynamics. However, the signal-to-noise ratio is independent of that stimulus – it can only be adapted to specific requirements by feedbacks from global Ca^{2+} spikes to the upstream signalling pathway (Chapter 4). The biological function of Ca^{2+} signals is to transmit reliable information [28, 67], and the information is often contained in the interspike interval [57, 127, 252]. Therefore, robustness of the signal-to-noise ratio means robustness of function of the Ca^{2+} signalling pathway. This thesis will derive a quantitative description of such *funtional robustness*, which is a generic property of cell-signalling pathways [113].

The second part of the thesis will comprise recordings of Ca^{2+} channel cluster dynamics and of cellular Ca^{2+} dynamics obtained by live cell imaging. Statistical analyis of the data will provide evidence for the stochastic mechanism of intracellular Ca^{2+} dynamics proposed in this thesis and for important model predictions. Analysis of Ca^{2+} spike-sequences recorded at different experimental conditions (Chapter 5) will show that stochastic Ca^{2+} signals can be *functionally robust*, sensitivite to stimulation and adaptive to environmental changes, at the same time. The methodologies to measure cellular Ca^{2+} dynamics are well established, but published spike-sequences are usually too short for a quantitative analysis, and a systematic analysis of Ca^{2+} spikes under different conditions in the same cell type has not been published before. The single-cell data from HEK cells presented in this thesis were collected by the author himself together with Dr Stephen C Tovey in the lab of Prof Colin W Taylor, Department of Pharmacology, University of Cambridge, UK, at the occasion of a short-term fellowship of the *European Molecular Biology Organisation*.

High-resolution recordings of Ca^{2+} channel cluster (called puff) dynamics are

investigated in Chapter 6 to establish statistical properties of the local Ca^{2+} dynamics on the single-cluster level. In particular, distributions and statistical moments of interevent intervals are characterised. The presented analysis rejects Ca^{2+} models based on oscillatory reaction-diffusion dynamics (see Section 2.1), and thus provides further support for a stochastic mechanism as proposed here (Chapter 3) and in earlier studies by the Falcke group [67, 193]. Recordings of Ca^{2+} puffs in SH-SY5Y neuroblastoma cells have recently been published by Ian Smith *et al* [197]. Similar data were obtained from the lab of Prof Ian Parker, University of California, Irvine, USA, by means of a collaboration, and could be analysed here. Additionally, puff-measurements in HEK cells were performed by the author and Dr Stephen C Tovey at a second stay in the UK funded by the *Functdyn* program of the *European Science Foundation*.

In summary, this thesis will refer to the concept of emergent behaviour in two ways: First, emergent behaviour will be the core idea behind the strategy of hierarchic stochastic modelling presented in the first part of the thesis (see Fig. 1.1). Second, that modelling strategy will allow for a quantitative analysis of emergent system properties of the Ca^{2+} signalling pathway. The experiments shown in the second part of the thesis will provide data for two levels of emergent behaviour, which are cluster dynamics and whole-cell dynamics, and thus permit experimental verification of both model assumptions and model predictions. Thus, the novel approach presented here provides a generalisation of emergent properties in deterministic networks to spatially resolved stochastic systems, and it reveals new mechanistic insights into the Ca^{2+} signalling machinery.

This thesis is organised as follows: Chapter 2 provides the biological background on intracellular Ca^{2+} signalling, especially in relation to mathematical models, and on robustness and evolvability of cell signalling, as far as these topics are required for the further discussion. At the end of Chapter 2, the research aims of the thesis will be given in detail. The following two chapters will contain the mathematical model and different solution techniques (Chapter 3) and the results and predictions obtained from the model (Chapter 4). The theory is presented in such a way that the first section of Chapter 3 contains the essential definitions and assumptions required to follow Chapter 4, while a detailed derivation of the theory follows in

Sections 3.2-3.5. Finally, Chapters 5 and 6 contain analyses of experimental data, providing evidence for the predicted robustness properties of cellular dynamics and for validity of the stochastic Ca^{2+} model.

2 Ca^{2+} Signalling and Biological Robustness

Ca^{2+} is one of the most important second messengers in eukaryotic cells. It plays a major role in many signalling pathways throughout physiology and development of the human body [26, 28, 130, 212]. Thus, a better understanding of the core mechanism of intracellular Ca^{2+} dynamics is highly relevant for cell biology and many related medical applications. The present chapter reviews some important achievements concerning intracellular Ca^{2+} dynamics and their analysis by mathematical modelling. It then aims to develop a broader perspective on cell signalling in the context of internal and environmental fluctuations and of evolution. That perspective paves the road for the analyses by hierarchic stochastic modelling and experiments presented in the following chapters.

2.1 Intracellular Ca^{2+} Signals in the Context of Mathematical Modelling

Ca^{2+} signals are typically evoked by an agonist of a G-protein coupled receptor (GPCR) in the plasma membrane, which subsequently initiates the release of inositol-1,4,5-trisphosphate (IP_3) [21]. The discovery that IP_3 triggers the activation of Ca^{2+} channels in the membrane of the endoplasmic reticulum (ER) [202] put forward the basic mechanism of intracellular Ca^{2+} dynamics depicted in Fig. 2.1, and it marks the starting point for the detailed investigation of that system (see refs. [25, 217] for historical reviews). Ca^{2+} as a second-messenger has since been investigated with a multitude of experimental and theoretical techniques [25, 67, 217]. Involved physiological elements are well studied and allow for a detailed

mathematical description [27, 28]. This section will focus on the main results required as background for the following chapters.

Ca^{2+} is a versatile second messenger occuring in diverse intracellular signalling cascades

The most astonishing property of Ca^{2+} signalling is that such a simple particle is involved in such a huge number of different signalling cascades [28, 212]. It is still unclear how that kind of unspecific signalling can induce highly specific cellular responses like enhanced expression of a certain gene. The most common answer is that a certain cell type uses a certain mode of the Ca^{2+} signalling toolkit [28] only for a restricted set of functions [22]. That property relates to the theory of facilitated variation discussed in Section 2.2.

The increase in cytosolic Ca^{2+} resulting from IP_3 release can directly induce the activation of transcription factors [28, 57], or it can induce store-operated (also called capacitative) Ca^{2+} entry (SOCE) through the plasma-membrane [27, 168]. The molecular mechanism of SOCE has long been under investigation, before it was finally resolved recently [72, 213]. SOCE can evoke large sustained increases in cytosolic Ca^{2+}, and therefore it is particularly relevant in cell-fate decisions, e.g., in T cell development [24, 72]. The long-lasting repetitive Ca^{2+} signals observed in stable cell lines like HEK cells (see Chapter 5) also involve SOCE, but there it is mainly required for signal persistence, not for downstream signals like Protein Kinase C [31].

Ca^{2+} signals often occur in the form of repetitive increases in the Ca^{2+} concentration [67, 246], which are refered to as Ca^{2+} spikes in this thesis. In many cell types, the information transmitted by Ca^{2+} spikes is encoded in the interspike interval [22, 57, 127, 252]. That is one of the reasons that Ca^{2+} signalling has long been regarded as one of the standard examples of a regular biological oscillator. Another reason is probably the availability of good fluorescence indicators for Ca^{2+}, which permit observation of Ca^{2+} spikes for long time frames and in many different conditions. Furthermore, the observation of Ca^{2+}-induced Ca^{2+} release (see below) seemed to provide a straight-forward explanation for regular oscillations. However, more recent studies and results in this thesis question that

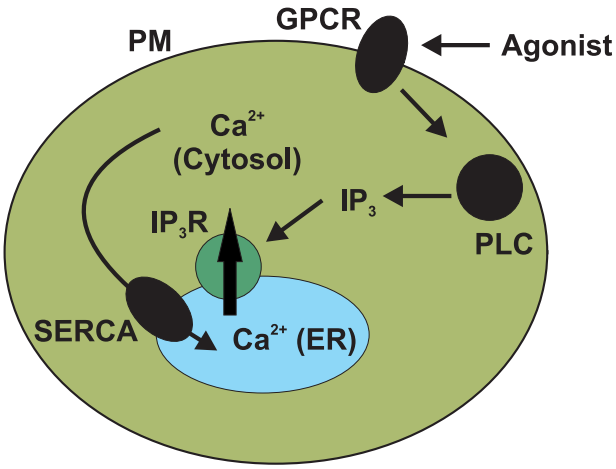

Figure 2.1: Schematic representation of the basic mechanism of intracellular Ca^{2+} signalling. An agonist binds to a G-Protein coupled receptor (GPCR) [130], leading to activation of Phospholipase C (PLC). That enzyme cleaves a phospholipid in the Plasma Membrane (PM), causing release of inositol-1,4,5-trisphosphate (IP_3), which subsequently can bind to IP_3 receptors (IP_3Rs) and enhance the opening probability of this type of intracellular Ca^{2+} channels: It releases Ca^{2+} molecules stored in intracellular compartments like the lumen of the Endoplasmic Reticulum (ER) into the cytosol. When the stores are empty or the IP_3R becomes inactive (cf. Fig. 2.2), Ca^{2+} is pumped out of the cytosol by continuously active pumps, e.g. the sarco-endoplasmic reticulum Ca^{2+} ATPase (SERCA). This scheme describes only a simplified version of the basic mechanism [21, 25]. For more details and the stochastic mechanism proposed in this thesis see Figs. 2.2-2.5, for a more complete picture of the processes contributing to Ca^{2+} signalling see refs. [27, 28].

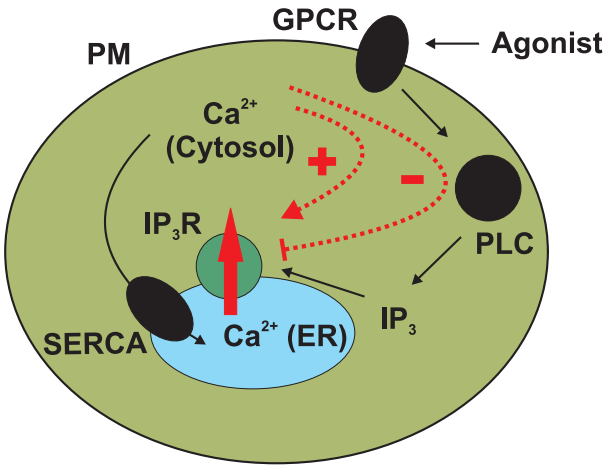

Figure 2.2: Ca^{2+}-induced Ca^{2+} release (CICR) and Ca^{2+}-mediated inhibition. Additionally to the reactions depicted in Fig. 2.1, Ca^{2+} molecules released into the cytosol further increase the opening probability of the IP_3R. By that process, which is often called CICR, Ca^{2+} release is further enhanced until the cytosolic Ca^{2+} concentration reaches very high levels, which cause inhibition of the IP_3R (Ca^{2+}-mediated inhibition) [29, 67].

hypothesis and provide evidence for a stochastic mechanism generating Ca^{2+} spikes (see end of this section and Chapter *Discussion*).

Minimal Ca^{2+} models are based on Ca^{2+}-induced Ca^{2+} release

Mathematically, the basic requirement for a biochemical stable oscillator, a so-called Hopf-oscillator, with two components (here: cytosolic and non-cytosolic Ca^{2+}), is at least one trimolecular reaction [93, 150]. In Ca^{2+} modelling, such a reaction is usually introduced by cooperation of the 4 subunits of the IP_3R (see below), which in simple models is described by a Hill-coefficient of 4.

A further requirement for a Hopf-oscillator is the existence of positive and negative feedbacks. It is well known that Ca^{2+} has a biphasic effect on its own release [23, 29, 67, 141, 211]: Upon stimulation, Ca^{2+} triggers its own release from intracellular stores into the cytosol, until a concentration threshold is reached, which causes inhibition of Ca^{2+} release. Ca^{2+} is pumped back into the stores by

the sarco-endoplasmic reticulum Ca^{2+} ATPase (SERCA). These feedbacks are often refered to as Ca^{2+}-induced Ca^{2+} release (CICR) and Ca^{2+}-mediated inhibition (see Fig. 2.2). Note that CICR and Ca^{2+}-mediated inhibition act locally on the level of individual IP_3R molecules and must be discerned from the global feedbacks described below.

There are earlier Ca^{2+} models based on IP_3 oscillations [146], but the first Ca^{2+} model for nonexcitable cells based on CICR is the classic work by Goldbeter *et al* [81], which reads:

$$\begin{aligned} \frac{dZ}{dt} &= \nu_0 + \nu_1\beta - \nu_2 + \nu_3 + k_f Y - k_z Z \\ \frac{dY}{dt} &= \nu_2 - \nu_3 - k_f Y. \end{aligned} \tag{2.1}$$

Z denotes the cytosolic Ca^{2+} concentration, Y the Ca^{2+} concentration in the endoplasmic reticulum (ER), $\nu_1\beta$ is IP_3-dependent Ca^{2+} release, ν_2 is the Ca^{2+} efflux mediated by SERCA pumps (modelled by a Hill-function with exponent 2), and ν_3 refers to CICR. The other terms describe leak fluxes. In ref. [81], CICR is modelled by the product of two Hill-functions, one for Ca^{2+} influx (exponent 2) and one for subunit cooperativity (exponent 4).

It can be shown by a detailed analysis of the Jacobian [93] or by the negative criterion of Poincare-Bendixson [80] that Eqs. **2.1** evoke oscillations if the positive feedback from CICR is strong enough, while the negative feedback at high Ca^{2+} concentration alone is not sufficient. This is in accordance with the general statement that in a two-component system at least a negative and a positive feedback are required for oscillations [151].

At this point, there are many possibilities to achieve a more accurate description of the opening of the IP_3R or of the other fluxes in the above equations. For reviews of simple heuristic Ca^{2+} models, see refs. [67, 182].

The structure of the IP_3R is the basis of first mechanistic models

Apart from the minimal Ca^{2+} models described so far, there have been considerable efforts to develop a more realistic description of intracellular Ca^{2+} dynamics. The first step into that direction is a mechanistic description of structure and function of the most prominent Ca^{2+} channel, which is the IP_3R. It consists of four subunits, which are identical or similar, and each have approximately 2700 residues (see refs. [214, 217] for review). In mammals and birds, there exist three different isoforms, which differ in binding affinities but are very similar in structure and function. They are encoded by genes which are similar in cells of all higher animals [214].

All subunits of the IP_3R have one binding site for IP_3 and several binding sites for Ca^{2+}. The standard model is that some of the Ca^{2+} binding sites inhibit the channel if occupied, while others lead to activation, which accounts for the typical bell-shaped Ca^{2+} response curve [29, 142, 215, 217]. Intermediate-resolution structures down to 24 Å [49, 99, 214, 244] of the IP_3R confirmed the proposition [142, 211] of several distinct conformations of the IP_3R, depending on the occupancy of different binding sites. However, our picture of the mechanism of IP_3R regulation is still incomplete, since attempts to resolve the structure of the IP_3 binding-pore in absence of IP_3 failed, and also the resolution of available structures is too low [214, 217].

The described findings have led to a class of mathematical models, which describe IP_3R-dynamics in terms of states of three binding sites (Fig. 2.3): The IP_3 binding site, and an activating and an inhibitory binding site for Ca^{2+} [67]. The most prominent example, which will also be used in this thesis (Section 3.2), is the model from De Young and Keizer [51]. It assumes that the IP_3R is in an open conformation if three out of the four subunits have IP_3 and activating Ca^{2+}, but not inhibitory Ca^{2+}, bound to the appropriate binding sites. The state-changes are governed by differential equations, depending on the cytosolic IP_3 and Ca^{2+} concentrations.

Other models differ from the De Young-Keizer model in the definition of the active state, in the type of the Ca^{2+} and IP_3 dependences of state changes, and in

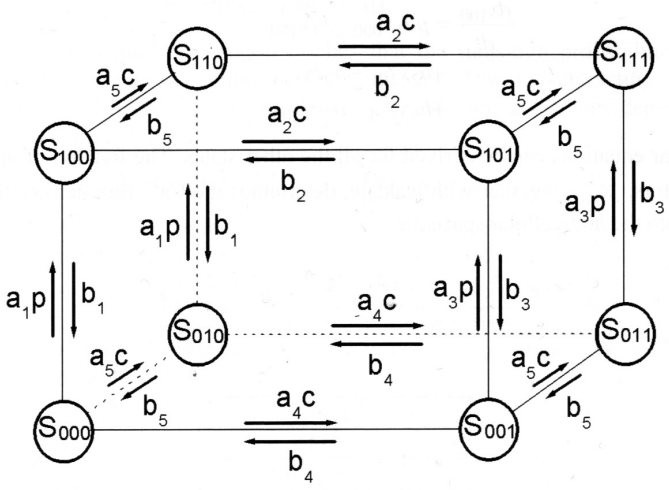

Figure 2.3: Schematic representation of the De Young-Keizer model for IP_3R subunits. The four subunits of the IP_3R are assumed to be characterised by the occupancy of three different binding sites, and therefore by its state variable S_{ijk}. The first index i describes binding of IP_3, $(j = 1)$ corresponds to binding of activating Ca^{2+}, and $(k = 1)$ to binding of inhibitory Ca^{2+}. In the De Young-Keizer model [51], the channel is said to be open if three subunits are in state S_{110}. The rates depend on the IP_3 (p) and Ca^{2+} (c) concentrations. The set of parameters used in this thesis is given in Appendix A.1.

the sequential order of state-changes (see refs. [67, 199, 208] for reviews). All models reproduce the bell-shaped Ca^{2+} response curve and the sigmoidal IP_3 response curve observed in patch-clamp measurements [29], to which the model parameters are usually fitted.

Global feedbacks are an important element of intracellular Ca^{2+} dynamics

Many Ca^{2+} models are based on the assumption that Ca^{2+} oscillations arise by Ca^{2+}-induced Ca^{2+} release, while IP_3 serves only as a parameter that regulates the stimulation strength. However, it is an experimental fact that IP_3 can oscillate together with Ca^{2+} [216]. Taking IP_3 as a constant parameter has the conceptual advantage that it can be seen as the control parameter that dictates the oscillation frequency, which carries the information contained in the Ca^{2+} signal [57, 127, 252]. The drawback is that the large interspike intervals observed in many cell types

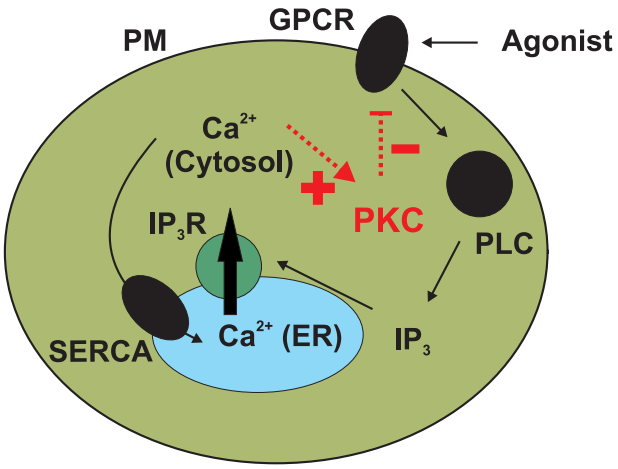

Figure 2.4: Protein Kinase C (PKC) as a possible effector of global negative feedback in the Ca^{2+} signalling machinery. In addition to the reactions depicted in Fig. 2.1, global Ca^{2+} release events cause activation of PKC. That enzyme is involved in a number of signalling cascades downstream of second-messenging by Ca^{2+} [130], and its activities include inhibition of certain GPCRs [152, 216]. Negative feedback may also arise via PLC, IP_3-3-kinase, store depletion or other mechanisms [27, 216].

can, without IP_3 dynamics, only be explained with additional pathway elements like buffer dynamics or mitochondria [27, 105] – or with stochastic models (see Chapter 4 and refs. [67, 194]).

There has been a controversy about the question if IP_3-dynamics, and especially global feedbacks acting from Ca^{2+} on the IP_3 metabolism, are necessary to explain experimentally observed Ca^{2+} spikes [61, 162, 163]. But, since newer results question the whole concept of limit-cycle induced Ca^{2+} spikes and suggest an intrinsically stochastic mechanism (see below), for this thesis that question is not as relevant as simply the fact that such feedbacks exist.

The IP_3 metabolism has been found to be sensitive for Ca^{2+} at several points [27, 105, 152, 216]: First, all isoforms of Phospholipase C, which catalyses IP_3 release in response to extracellular stimuli, are activated by Ca^{2+} ions. Second, IP_3 degradation by IP_3-3-kinase is activated by Ca^{2+}. And third, Protein Kinase C, an effector molecule downstream of the Ca^{2+} signalling cascade, may inhibit action of G-protein coupled receptors (Fig. 2.4) or other elements of the Ca^{2+}-signalling machinery.

In addition to the IP_3 metabolism, also other pathway elements can mediate global feedbacks from a cellular Ca^{2+} release event to the activity of Ca^{2+} channels. A prominent example is the Ca^{2+} loading of intracellular stores: It has been shown that the IP_3R is regulated also by luminal Ca^{2+}, in addition to cytosolic Ca^{2+} [21, 25, 147]. Therefore, Michael Berridge proposed that the oscillation pattern of the Ca^{2+} signal can be controlled by the rate at which stores are refilled after a Ca^{2+} spike [25] – some of the experiments presented in Chapter 5 will support that concept (see also Chapter *Discussion*). Other feedbacks can possibly be mediated by cAMP signalling, mitochondrial Ca^{2+} uptake, etc. [27, 28].

Such interactions can provide for a number of global positive and negative feedbacks and will be an important element of the analysis presented in the following chapters.

More detailed Ca^{2+} models include spatial effects, mitochondria and gap-junctions

Intracellular Ca^{2+} dynamics are often described by ordinary differential equations, implicitly assuming that Ca^{2+} diffusion is rapid, so that the Ca^{2+} concentration is approximately homogeneous inside a particular compartment like the cytosol or the ER. However, it has been shown experimentally [137, 220, 248] and computed from detailed diffusion models [67, 221] that the cytosolic Ca^{2+} concentration is not homogeneous. Rather, huge gradients occur in the surrounding of a Ca^{2+} channel [18, 221].

Due to these facts, lots of effort has been spent to investigate spatial Ca^{2+} models, which mostly have the form of diffusion equations for the Ca^{2+} concentration and apply mean-field assumptions for the interaction of IP_3Rs. That leads to approximately correct results if channels are equally distributed in the cytosol [105]. Such models often induce interesting spatial phenomena like spiral waves. The first mean-field model was published by Atri *et al* [8], see refs. [67, 105] for excellent reviews. Despite the success of these early diffusion models, they all have the drawback that they neglect the spatial organisation of Ca^{2+} channels into clusters (see below).

The observation that mitochondria encode and decode Ca^{2+} signals [85, 98]

also had a considerable impact on the development of mathematical Ca^{2+} models. Biologically, this is important because mitochondria can induce apoptosis by means of intracellular Ca^{2+} signalling [45, 89]. IP_3-mediated Ca^{2+} signalling has also been found to interact with the energy metabolism and with reactive oxygen species in mitochondria [237]. In this field, the focus was first on the development of an accurate description of the electrochemical gradients between mitochondria and the cytosol [136, 139, 183]. Later, spatial phenomena emerging from the presence of mitochondria were investigated [67, 68].

A further generalisation is the spreading of Ca^{2+} waves among neighboured cells by gap-junctions, which has been observed in many different cell types throughout the human body [67]. It is generally assumed that not Ca^{2+}, but rather IP_3 is the diffusing messenger between cells. Wave propagation can occur by CICR in the receiving cell [198], eventually being restricted by IP_3-induced feedbacks [97].

Channel clustering requires stochastic modelling

As mentioned above, spatial models with mean-field and continuum approximation have in common the drawback that they neglect the geometrical arrangement of Ca^{2+} channels. It was convincingly shown with different experimental techniques and in different cell types [137, 155, 197, 210, 227, 248] that IP_3Rs form internally stongly coupled clusters. These clusters are capable of responding to low agonist concentrations directly, in the form of localised Ca^{2+} signals (called puffs) in their surrounding, and they cooperate with other clusters to induce global waves in response to stronger stimuli (Fig. 2.5).

Therefore, realistic Ca^{2+} models must take into account that there are at least two different spatial scales relevant for Ca^{2+} signalling: Small distances inside clusters, where Ca^{2+} channels are strongly coupled, and large distances between cluster, which are weakly coupled: The Ca^{2+} concentration directly at an open channel is higher than the Ca^{2+} concentration typical cluster distances away from it by several orders of magnitude [137, 221].

The problem for mathematical modelling is then, that on the one hand, due to the relatively small numbers of clusters per cell and of channels per cluster (both in the order of 10 [67]), stochastic fluctuations are not longer negligible (see

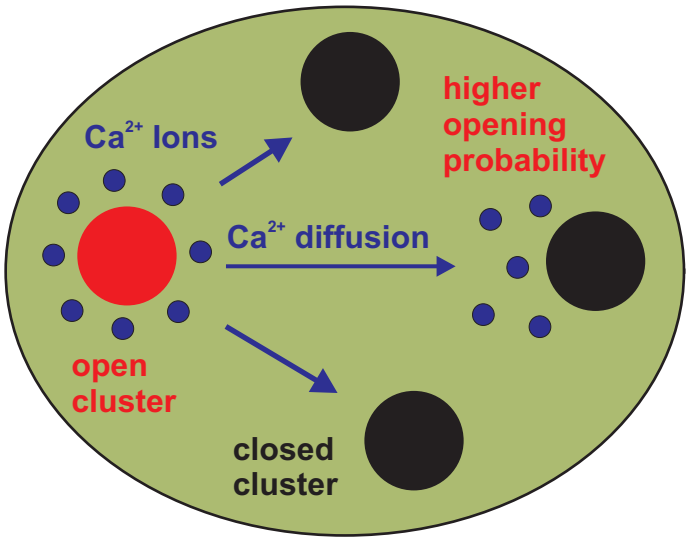

Figure 2.5: Schematic representation of the hierarchic stochastic mechanism of Ca^{2+} dynamics as proposed in this thesis. IP_3Rs aggregate to clusters with cluster distances much larger than the typical diffusion distance of Ca^{2+} [221]. Therefore, diffusive coupling by CICR is strong within a cluster and weak between clusters. Clusters open and close stochastically, where the opening probability depends on the local Ca^{2+} concentration, which is determined by the number of nearby open clusters. That spatial organisation implies that intrinsic fluctuations cannot average out due to the small numbers of clusters per cell and of IP_3Rs per cluster (see text). Moreover, stochastic dynamics arising from that mechanism can induce Ca^{2+} spikes in a realistic parameter regime, and with spike statistics similar to experimental data, in contrast to spatially homogeneous limit-cycle oscillations [67, 193, 222]. Note that the cluster arrangement in general is not symmetric, potentially leading to a large number of possible cluster configurations (see Section 3.5).

also Section 2.2). On the other hand, direct stochastic simulations coupled to spatiotemporal Ca^{2+} dynamics on multiple scales are intractable even for modern high-speed parallel computing. A probabilistic approach in terms of Master Equations also fails due to the extremely high number of states. That is especially true if we remember that we cannot ignore the various substates of the IP_3R subunits ($3^8 \approx 6500$ in the De Young-Keizer model) and the various feedbacks in IP_3 signalling, not even considering buffer dynamics, gap-junctions and the interaction with mitochondria or the extracellular medium [27, 28].

For that reason, the first stochastic models restricted themselves to the simulation of channel dynamics within one cluster [207]. As an alternative to stochastic simulations, Shuai *et al* proposed a description by Fokker-Planck Equations and also succeeded in reproducing experimental results [189] (see refs. [129, 172, 233] for an introduction to Fokker-Planck Equations). However, that approach implicitly assumes a high number of channels per cluster, for which there is no experimental evidence. More recent stochastic simulations of Ca^{2+} channel clusters achieved many interesting results concerning statistical properties of single-cluster events and predictions for the numbers of channels per cluster [59, 206, 231].

The first stochastic simulations of the induction of Ca^{2+} waves by cooperation of several clusters (Fig. 2.5) came up by Martin Falcke [65, 66, 69]. His model is based on the De Young-Keizer model for single-channel dynamics (see above) and relies on the superposition of stationary diffusion profiles around clusters, which in turn depend on the number of open channels in the cluster. The Falcke model could reproduce the whole spectrum of Ca^{2+} signals observed by Parker *et al* and Bootman *et al* [33, 137, 227, 248]. The astonishing success of this model "... calls into serious question the relevance of deterministic approaches to Ca^{2+} waves and oscillations that are caused by small numbers of stochastic IP_3Rs ", as pointed out by James Sneyd [105]. It led to the idea that, instead of a mechanism based on limit-cycle oscillations, Ca^{2+} spikes might be generated by a completely different mechanism, namely repetitive stochastic pulses arising from an excitable medium. Indeed, further analysis has shown that in a realistic parameter regime, the De Young-Keizer model does only generate spikes of the excitably medium type, and not in the regime of homogeneous limit-cycle oscillations [222].

Such seemingly regular global dynamics based on emergent behaviour of lo-

calised stochastic excitable elements are known from physics in the context of array-enhanced coherence resonance [7, 160]. It has recently been proposed that also circadian rhythms might be generated by such a noise-driven oscillator [240].

Recent results and outlook

The new concept of Ca^{2+} spiking in the regime of a stochastic excitable medium inspired a new series of experimental studies, which investigated wether Ca^{2+} spikes are really as regular as they have been thought to be. Several independent labs came to similar results, indicating that indeed interspike intervals of Ca^{2+} signals have comparatively large standard deviations, which in addition increase with the average [58, 195]. In this thesis, further evidence for this fact will be provided by analysing data from one cell type (HEK cells) in different experimental conditions (Chapter 5).

In recent work, Skupin and Falcke also demonstrated that such spiking statistics, where the standard deviation of interspike intervals increases with the average, cannot be explained by limit-cycle models, even if those are supplemented by additive noise [193]. Furthermore, Skupin and Falcke showed that stochastic Ca^{2+} signals are not worse than deterministic ones by means of information processing [192], and that spiking statistics can be correctly reproduced by a rather extensive multiple-scale modelling approach [191, 193, 194].

This thesis seeks to explore that topic further by a different type of stochastic mathematical model and by testing key results experimentally, and it seeks to investigate stochastic Ca^{2+} spiking in the broader context of biological robustness and evolvability (see Sections 2.2 and 2.3).

2.2 Robustness and Evolvability in Cell Signalling

"Nothing in biology makes sense except in the light of evolution", as pointed out by Theodosius Dobzhansky [56]. To persist in evolution, eukaryotes, and especially multicellular organisms, need precise signalling mechanisms to synchronise and adjust action of different cellular compartments or different cells. There is for

instance a variety of different signalling pathways transmitting signals from the plasma membrane to the nucleus, and Ca^{2+} signalling is an integral part of many of those pathways. Typically, each element of a signalling pathway is carefully regulated and serves a precise function [130]. But apart from that precise function, evolutionarily conserved biological systems usually meet two other requirements as well: Robustness to noisy fluctuations or to changes of environmental conditions [113, 201, 235], and evolvability, which is the quick adaptation to a different set of conditions over a few generations [62, 109, 185, 235]. These topics will be studied by the example of Ca^{2+} signalling in this thesis, particularly in Chapters 4 and 5, and therefore they are introduced in this section.

Cellular noise stems from intrinsic and extrinsic fluctuations

Robustness is not only important to persist changing conditions and stochasticity in the environment, but it is also a necessary condition for a biological system to deal with the unavoidable internal fluctuations [170]. The most obvious source of noise are the limited copy numbers of biomolecules present on the spatial scales relevant in prokaryotic cells and compartments of eukaryotic cells. That implies the occurence of so called Poisson noise, which stems from the fact that a physical quantity can only be accurate up to fluctuations of the order of $1/\sqrt{n}$. Here, n is the number of 'possible measurements', like the number of particles, e.g. Indeed, in an early investigation of the number of phages liberated from infected bacteria [53, 54], Max Delbrück found significant variability of that number and analysed the probability distribution. Another striking example is the DNA molecule, which exists in only two copies per cell – a fact that came up much later than the Delbrück study. Even though individual genes are often present on several loci, fluctuations arising in gene transcription usually cannot average out [62, 169].

Reasoning about Poisson noise in biological systems, Erwin Schrödinger [181] hypothesised that a lower boundary for the size of an organism is given by a sufficiently high number of important biomolecules that can be placed into it. That is, he argued, because only a sufficiently high number of any type of involved molecules can produce the degree of organisation required for higher body func-

tions. In this spirit, one could suppose that one of the most important issues in the step from prokaryotes to eukaryotes was simply the up to 1000-fold increase in cell volume [148]. Indeed, most evidence for noisy fluctuations in living organisms comes from bacteria, where several important proteins are expressed in very small copy numbers of the order of 10 [101, 131, 185, 247]. Nevertheless, stochastic fluctuations in eukaryotic organisms are not negligible, because there other sources of noise add up to the molecular fluctuations (see below).

Particularly well studied model systems for biological noise are bacterial chemotaxis [6, 11, 19, 20, 116, 117, 186] and prokaryotic gene expression [43, 44, 63, 135, 153, 171, 173]. In this context of gene expression, Elowitz *et al* [63, 205] discovered that stochasticity for a given system arises from two sources: Intrinsic noise stems from fluctuations in the machinery that directly triggers the considered system, and extrinsic noise summarises the noise contributions from other processes like upstream signalling cascades or diffusion-limited reactions [185]. An important source of extrinsic noise are also fluctuations in the environment, which challenge cell to cell communication and chemotaxis, e.g. Intrinsic and extrinsic noise can be discriminated by correlation analysis of two identically regulated but differently labeled subsystems (e.g. proteins), as demonstrated in ref. [63].

In this thesis, the focus lies on eukaryotic cell signalling. Although noisy fluctuations are less investigated there, it has been shown that protein levels are subject to huge variability over time and between individual cells, and that subsequent cellular decisions can be highly susceptible to that variability [32, 70, 74, 101, 131, 171, 190]. Importantly, data from yeast cells indicate that variability in eukaryotic gene expression is different from gene to gene and is subject to natural selection [74, 101, 171]. At first glance, that is surprising, because a typical signalling protein with a concentration of $\approx 10^4$ molecules per cell [180] would cause Poisson fluctuations of the order of 1 %. That is far away from the accuracy typically gained in statistical physics, but much better than what is usually achieved in biophysical experiments. Thus, one could assume that eukaryotic cells have evolved to a cell volume sufficienly large to restrict noise. However, this is not true, because in eukaryotic organisms other sources of noise add up to fluctuations in molecule numbers [101].

For instance, it is now well established in theory and experiment that gene ex-

pression occurs in a burst-like fashion, which means that the effect of stochastic chromatine remodelling persists up to the level of protein expression [32, 144, 171, 249]. In this context, it was even argued that gene expression in eukaryotes is impossible without stochastic chromatine remodelling, so that noise would be rather a *conditio sine qua non* than a side-effect of life at the single-cell level [154]. However, such concepts will have to be elucidated by further research. Notably, also spatial effects can considerably reduce precision on the length scales of eukaryotic cells [226], and network topologies have a considerable impact on the noise level [40, 43, 62, 101, 126, 219].

Living with noise – cells can both exploite molecular fluctuations and aquire robustness to them

How does a living organism deal with the various sources of intrinsic and extrinsic noise? There is an increasing number of studies demonstrating that internal fluctuations can be beneficial for the cell, by means of providing a biological random number generator (see refs. [12, 119] for review). That can be exploited, e.g., by bacteria, which have a higher competitive ability in rapidly changing environments if they stochastically switch their phenotype [1, 9, 174]. Another example are immune cells, where stochastic protein expression ensures phenotypic variability [70, 140]. Even sensitivity in signal transduction can be increased by noise exploitation [157]. Recently, it has been demonstrated that a genetic circuit present in living organisms causes even higher fluctuations than an alternative circuit, at the same mean value, and that this difference generates a survival advantage in bacteria [43, 203, 204].

Nevertheless, the more general task for biological systems certainly is to generate reliable output despite noisy input and internal fluctuations [12]. That problem is especially relevant in cellular decision-making: In fact, “cells must infer from noisy signals the probable current and anticipated future state of their environment” as a prerequisite to “weigh the costs and benefits of each potential response”, as emphasised by Perkins and Swain [159]. In general, that problem can be dealt with in several ways. The most obvious is to restrict internal fluctuations. It was shown that the precision of protein expression levels can be optimised by adapting

production and degradation rates [218], as well as by long signalling cascades [219], both at the cost of higher energy consumption. Mechanisms that control variability in protein levels are plausible, since that variability differs much between different proteins, being especially high in stress genes [12].

However, such mechanisms are not suitable to deal with extrinsic fluctuations, and they are very costly: In a recent investigation [126], it has been shown that the signal precision increases at best with the quartic root of the number of signalling events, for arbitrarily complex feedback regulation. Therefore, a better strategy is to design pathways which do not depend so much on precise signal propagation, because the structure of the regulatory circuit ensures tolerance to fluctuations. Such a property has first been discovered in the context of bacterial chemotaxis [6, 11] – it is usually termed *robustness* [88, 90, 113, 201, 235].

That concept of robust regulatory circuits has been applied successfully to a variety of biological systems, and it has become one of the defining concepts of systems biology [4, 5, 111–113, 115]. Recent studies of robustness properties in eukaryotes considered signal-transduction in yeast [118, 254], DNA replication [41], circadian clocks [46] and initiation of T cell proliferation [42].

The terminology of 'robustness to noise' or 'robustness to environmental changes' though has to be taken with caution: In each case, it needs to be defined exactly which property is robust to which kind of uncertainty [201, 235]. Beeing unaware of that problem can lead to subtle misunderstandings even in simple systems. For example, it is often said that negative feedbacks provide robustness, because they maintain the value of a certain variable for a broad range of system parameters [16, 101, 170]. At the same time, positive feedbacks also provide robustness, but of a different type: They ensure that state-changes happen with almost certainty in response to weak and noisy input signals, in particular in the context of cell-fate decisions [15, 42, 101]. Another type of robustness applies to biological oscillators, where instead of maintenance of a system state, it usually means that a certain system property like amplitude or period is robust to intrinsic or extrinsic fluctuations [46, 84, 201].

This thesis will employ the concept of *functional robustness* [113]. That property refers to robustness of the biological function of a certain system, rather than to low variability in system dynamics. In stochastic systems, *functional robustness* can

imply robustness of the relation of statistical moments rather than just robustness of the average system behavior, as will be demonstrated in Chapter 4.

Rapid evolvability requires *functionally robust*, conserved core units

The concept of evolvability has a long and turbulent history [109, 110, 235]. The idea that organisms can regulate their evolutionary adaptability to environmental changes ('evolvability') has been under discussion from the beginning of modern evolutionary theories in Darwin's "The Origin of Species". Since then, that idea was mostly rejected and replaced by selection as the active or 'creative' force: Evolvability was regarded as a passive property driven by selection by the environment.

However, that notion poses serious problems to the Darwinian theory of evolution: Genetic variability and selective pressure can explain evolution towards optimised structures like highly effective enzymes. But, it can hardly explain huge evolutionary steps like invention of the eye or the human brain, especially if intermediate structures cannot be expected to improve competitive ability [110]. Indeed, it has been suggested that evolution can be compared to the motion of a street-car, which travels (evolutionarily optimises) towards intermediate goals, which can only be left after introduction of significantly new mutant alleles [87]. So how do these huge steps arise?

Gerhart and Kirschner [75, 110] proposed that in general, biological organisms consist on several conserved 'core modules' that remain unchanged, and of a large set of connections and regulatory elements between those core units. Then, evolution of complex structures is made possible by 'facilitated variation': The connections between core units can be reorganised by only a few point mutations. Therefore, apparently huge steps in evolution can be generated by recombination of existing structures, without the need for evolutionarily stable intermediate structures. Furthermore, the core units guarantee basic functions like gene expression, cell division or body plans in higher animals, making it more likely that recombination of core-units results in viable organisms. Defining characteristics of core units are conservation in evolution, precise function and versatility – the

latter demonstrating adaptability to different conditions by modified links to other systems.

Facilitated variation necessarily implies different levels of evolvability at different biological systems: It can be expected, in the extreme case, that the core units are completely robust to evolutionary change. However, connections and modules which are sensitive to environmental change should be subject to rapid evolution at changing environmental conditions. Indeed, in recent years, lots of evidence has been collected indicating that systems which are challenged by rapid environmental changes or physiologic stress can adapt their genotypes over a few generations. Well-known examples are Calmodulin, Haemoglobin and the lac-Operon in *E.coli* [109, 110, 235]. Recently, it has also been suggested that prion-switching can enhance evolvability as a stress response [229, 230]. In contrast to that, other systems have remained unchanged for millions of years, like metabolism and the gene expression machinery [110].

Further support for rapid evolvability of subsystems comes from a combined theoretical and experimental study by Dekel and Alon [52]. It has shown that protein concentrations in bacteria can rapidly adapt to a predicted optimal value, in ≈ 500 generations. Another study from the Alon lab showed that evolutionary tuning is faster if trained on rapid changes of the objective [102, 156], especially when local extinctions of subpopulations are considered [103]. That means, it is possible to evolve towards evolvability, as predicted by Gerhart and Kirschner [109].

Moreover, Alon *et al.* find that such training on changing goals often leads to a modular structure of the system [102]. Modularisation is a prerequisite for facilitated variation, because it permits differentiation to core modules and links between them [110]. Since modularity is a property found in many biological systems [3, 4, 91], the connection between modularisation and evolvability can be seen as another piece of evidence for facilitated variation. However, note that modularity could also be not more than a byproduct of evolution [64, 235] – which mechanism actually generates modularity in living systems needs to be elucidated by further research.

Gerhart and Kirschner predicted the occurence of *functionally robust*, conserved core modules only phenomenologically, as a prerequisite for facilitated variation, but they do not state how it can be attained mechanistically, at the

level of the genome. There exist several hypotheses how the paradoxical requirements of robustness and evolvability can be realised within the same machinery, which is the gene code supplemented by mutation and recombination of gene fragments [50, 125, 235, 236]. The most prominent theory exploits the idea of neutral evolutionary spaces: Robust core modules are encoded in such a way that most point mutations do not change the phenotype, or change it only in such a way that the core function of the module is not affected [235, 236].

The concept of conserved core modules facilitating variation is highly relevant to Ca^{2+} signalling, because it offers an explanation for the long-raised question how one second messenger can transmit so many different signals [28, 212]. If the Ca^{2+} signalling toolkit is a core module, input and output connections should be adaptive, while the mechanism should be *functionally robust* – this topic will be one of the main issues investigated in this thesis.

2.3 Research Aims

Experimental and theoretical studies indicate that repetitive Ca^{2+} spikes are generated by a stochastic process based on the cooperative action of IP_3R clusters (Section 2.1). But, a realistic and analytically treatable mathematical model describing this process still lacks. Therefore, the first aim of this PhD thesis will be to proceed to a mathematical description of Ca^{2+} dynamics that is realistic but still sufficiently compact to be comprehensive. The model should be based on measurable quantities and should reproduce experimental results. Further, it should provide a deeper understanding of the mechanism and the role of individual players in generating the specific spike statistics obtained from single-cell measurements. Last not least, it is intended to avoid determination of a large number of kinetic parameters describing microscopic state-changes. This thesis will approach these goals with the new concept of hierarchic stochastic modelling, which follows the emergent behavior of Ca^{2+} channel clusters (Chapter 3).

In addition to the development of a novel, sound analytic Ca^{2+} model, this thesis aims to broaden the perspective to the biological role of structure and function of the spike-generating mechanism. Apart from pure functionality of the mechanism to transmit information, important properties to be discussed are also robustness and evolvability of the Ca^{2+} signalling toolkit. In Section 2.2, we have seen that it is not always necessary to attenuate internal fluctuations, even if the purpose of the system is not to provide a random number generator, but to transmit a reliable signal. Ca^{2+} signals, though apparently based on a cascade of stochastic processes with large standard deviation, can generate precise output, as demonstrated by the linear relation of average and standard deviation of experimentally measured interspike intervals (Section 2.1).

This thesis seeks to investigate the mechanism generating such precision. It will find that statistical properties of the macroscopic dynamics are robust to a wide range of perturbations, at the same time being highly adaptive to the needs of a specific cell type – a system property called *functional robustness* throughout this thesis (Chapter 4).

After building and analysing of the model, the author had the opportunity to test key results experimentally in the lab of Prof Colin Taylor (see Introduction).

With the data obtained from this collaboration, the robustness properties of spike statistics found in model simulations can be tested. To this end, we will consider data from single-cell imaging of Ca^{2+} spike-sequences in HEK cells for a variety of experimental conditions. The data support both robustness and adaptivity of spike statistics arising from a stochastic Ca^{2+} signalling mechanism (Chapter 5).

Since the model is formulated in terms of cluster dynamics, another aim will be to obtain an experimental characterisation of the microscopic dynamics. Opening events of single IP_3R clusters have been known as Ca^{2+} puffs for more than a decade [248], but only recently, high resolution data of puffs in mammalian cell lines have become available [197]. As part of research collaborations with Prof Ian Parker and Prof Colin Taylor (see Introduction), such data from SH-SY5Y cells and HEK cells can be investigated here. Different methods to analyse puff data will be presented, with the focus on a statistical characterisation of the stochastic process generating Ca^{2+} puffs. That analysis will provide further evidence from the microscopic scale for the stochastic mechanism generating global Ca^{2+} spikes proposed in this thesis (Chapter 6).

In summary, this thesis will contain a multidisciplinary approach for the purpose of a mechanistic characterisation of intracellular Ca^{2+} dynamics. It will range from the solution of integral equations over model simulations and spike-train analysis to fluorescence microscopy. Most importantly, the thesis will provide new insights to robustness and evolvability of a stochastic signal transduction machinery.

Part I

Theory

3 Hierarchic Stochastic Model

This chapter is organised in such a way that the basic modelling principles required to follow Chapter 4 are outlined in Section 3.1. Section 3.2 will give a more detailed description of the input data to the Ca^{2+} model investigated in this thesis, which are probabilities for cluster state transitions and Ca^{2+} diffusion profiles. The mathematical formulation of the model in terms of integral equations will be provided in Section 3.3. It contains a closed form analytical description of Ca^{2+} spike statistics, which can however only be evaluated by extensive numerical integration. Therefore, Sections 3.4 and 3.5 will seek for more efficient solution techniques. That will be done by two different approaches: Section 3.4 will present direct analytical solutions for stationary statistics of a simplified test model, which is realistic in small cells. Larger asymmetric cluster arrangements and dynamics of the system can only be obtained from stochastic simulations (Section 3.5). Importantly, Gillespie's algorithm for stochastic simulations [77] is not directly applicable here, because the model will be non-Markovian. Therefore, to simulate larger cluster arrangements, an efficient delayed stochastic simulation method is required.

3.1 Modelling Concept

The elemental events of cellular Ca^{2+} signals are Ca^{2+} puffs (see Section 2.1). Consequently, a model of cellular Ca^{2+} signalling should be formulated in terms of puff properties, since they are experimentally accessible – in contrast to the rates of state-switches of IP_3R subunits, which are the basis of most recent Ca^{2+} models (see Section 2.1). The challenge to develop a whole-cell Ca^{2+} model based on statistics of local events was met in the framework of hierarchic stochastic modelling, which exploits the principle of emergent behavior (see Fig. 1.1): On each

level of cellular organisation, dynamics of subsystems induce statistical properties of macroscopic variables defined on the next higher level. The novel approach circumvents fitting of kinetic parameters. It leads to analytical solutions for a simple but nontrivial test case and allows for very efficient stochastic simulations in more complex situations. The modelling concept is introduced here in the context of Ca^{2+} signalling, where the subsystems correspond to Ca^{2+} channels, but it should be applicable to other systems without difficulty (see Chapter *Introduction*).

Figure 3.1 gives an overview over the new modelling concept. This Section will give an outline how the hierarchic stochastic model describes cluster dynamics based on the properties of single channels and Ca^{2+} diffusion. Since spatial coupling will be an important read-out of the mathematical model in Chapter 4, it requires a precise definition, which is also provided in this Section. The spatial coupling depends on the geometrical arrangement of clusters. Details of data input and mathematical techniques used to investigate the model are presented in Sections 3.2-3.5. The main results from that investigation concerning spiking regimes, robustness of pathway function and the biological advantages of a stochastic mechanism will be the topic of Chapter 4.

Transition probabilities and Ca^{2+} diffusion drive cluster dynamics

Ca^{2+} channels form internally strongly coupled clusters. Each cluster has many states even if it comprises only a few channels. However, it is only relevant for the Ca^{2+} concentration dynamics whether a cluster releases Ca^{2+} or not. Therefore, we consider lumped cluster states. We lump all cluster states with at least one open channel into the cluster state open (O) and all the other states into the cluster state closed (C) (cf. Figs. 1.1 and 2.5). Single opening events of individual Ca^{2+} channel clusters are often referred to as Ca^{2+} puffs [27, 137, 248], in contrast to Ca^{2+} spikes, which reflect whole-cell events (see Section 2.1). Thus, the lumped state O corresponds to a puff.

Consider the probability density distributions for transitions between cluster states as input data specifying the dynamics of clusters of subsystems. If these probability densities were exponential distributions, than the model would be a

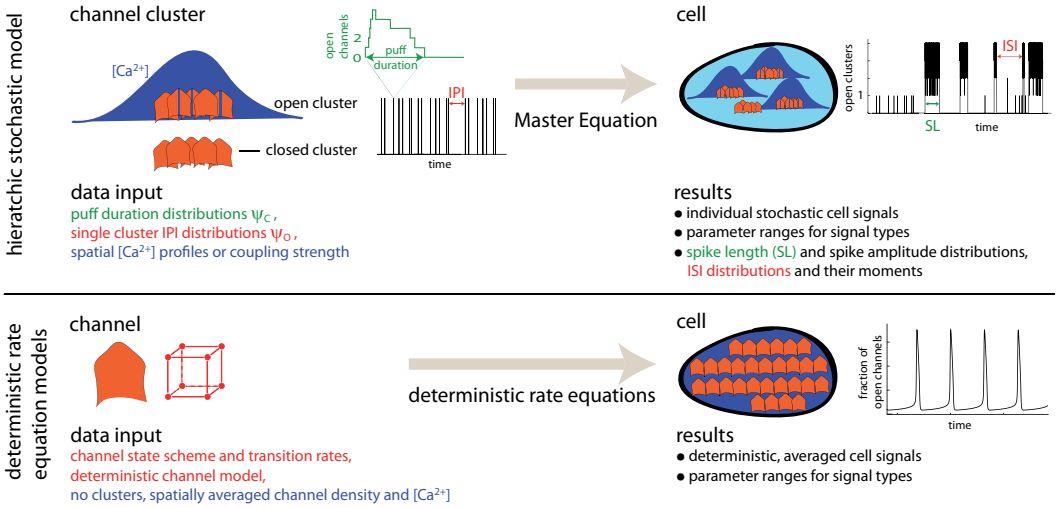

Figure 3.1: Summary of the modelling concept and comparison with traditional concepts. The stochastic hierarchic model takes advantage of the structural and functional hierarchy formed by channels, channel clusters and the cell. It subsumes the dynamics of the lower structural level into waiting time distributions on the next higher one. Channels cause the interpuff interval distribution ψ_o and closing time distributions ψ_c of clusters, and clusters generate the interspike interval distributions on cell level. The waiting time distributions on cluster level can be measured *in vivo*. That circumvents the problems arising from using parameter values from *in vitro* experiments for cell simulations, as deterministic rate equation models usually do. The involvement of many channels is required for the validity of rate equation models, such that average deterministic dynamics apply. Therefore, they are based on the assumption of continuous channel densities neglecting channel clustering. The additional assumption of fast Ca^{2+} diffusion entails neglecting spatial gradients and a mathematical description of cell behavior by ordinary differential equations. But this is in contradiction to the steep concentration gradients occurring during Ca^{2+} release. See text for details.

simple two-state Markovian Process, which can be easily described by rate equations [233]. That assumption would imply that at each time interval, system dynamics depend only on the current cluster state. However, while the cluster is in O, it switches between individual open states including changes of the number of open channels. Similarly, it explores all its individual closed states while in C. Such intermediate microscopic dynamics on the level of subsystems (Ca^{2+} channels) would be completely lost by a rate-equation description. Microscopic dynamics can however be incorporated by allowing for more general types of probability densities, without treating the dynamics of single subsystems explicity (Fig. 3.1).

Dynamics of the lumped states O and C can be described by the probability densities for the first transition to the other state, which is denoted by $\psi_o(c, t-\tau)$ for opening and $\psi_c(t-\tau)$ for closing. They depend on the time $t-\tau$ elapsed since the transition into the actual state at time τ. ψ_o also depends on the Ca^{2+} concentration c at the cluster site, i.e., also on Ca^{2+} diffusing from open clusters towards other clusters. That provides for the spatial coupling.

Details of the transition probabilities and the diffusive coupling are given in Section 3.2. Briefly, the closing probability can be derived from the constraint that the channels in a cluster close independently, which was suggested by a recent experimental study [196]. The opening probability is a quantity measurable *in vivo* (see Section 6.2, ref. [197] and Chapter *Discussion*). However, currently available data are not sufficient for quantitative modelling, and therefore in this thesis, ψ_o is computed from single-channel models by methods developed previously in the Falcke group [94, 223, 224]. ψ_o is computed from the DeYoung-Keizer model [51], which is one of the standard models in the field and largely based on *in vitro* data from patch-clamp recordings. The dynamics of the Ca^{2+} concentration can be described by a diffusion equation with spatial δ-sources at the locations of open clusters, since clusters are small compared to the cell volume. The calculations shown in this thesis apply stationary diffusion profiles computed with free boundary conditions, but more complicated diffusion problems can be introduced to the modelling framework without difficulty.

The cluster arrangement is an important element of spatial coupling

In Chapter 4, we will see that stochastic Ca^{2+} spikes can be characterised, to a large extent, by the strength of spatial coupling between clusters. The strength of spatial coupling can be defined by the probability for a transition from one to two open clusters driven by Ca^{2+}-induced Ca^{2+} release (see also Section 3.4). It is essentially the splitting probability C_{12} that upon opening of the first cluster, a second cluster opens before the first cluster recloses [233]. Later on, in order to exclude independent opening events, we will subtract the probability C_{12}^{∞} that two clusters far away from each other open simultaneously (Section 4.1).

If the model would contain only two clusters, C_{12} would be obtained by integration over the opening probability of the second cluster times the survival probability of the open state of the first cluster:

$$C_{12} = \int_0^{\infty} \psi_o(c,\theta) \left(1 - \int_0^{\theta} \psi_c(t')dt'\right) d\theta, \tag{3.1}$$

where $\theta = t - \tau$, and c represents the local stationary Ca^{2+} concentration at the second (closed) cluster (see above).

In genereal, it is necessary to compute the sum over all closed clusters m:

$$\begin{aligned} C_{12} = \int_0^{\infty} \sum_{m=2}^{N_{\mathrm{cl}}} \psi_o(c_m,\theta) \left(1 - \int_0^{\theta} \psi_c(t')dt'\right) \\ \times \prod_{\substack{n=2 \\ n\neq m}}^{N_{\mathrm{cl}}} \left(1 - \int_0^{\theta} \psi_o(c_n,t')dt'\right) d\theta, \end{aligned} \tag{3.2}$$

where the $c_m,\ m > 1$ are computed from the Ca^{2+} diffusion profiles given below (Eq. **3.7**) with only the first cluster open. The factors after the product sign assure that none of the other clusters opens before cluster m when calculating the opening probability of the mth cluster. Note that the sum and the product both run only over the closed clusters – the closing probability ψ_c is independent of the local Ca^{2+} concentration (see above). Eq. **3.2** holds for cluster interactions where

all cluster positions are equivalent, like in a tetrahedral cluster arrangement or in next-neighbour interactions in a cube. In irregular cluster arrangements, it is necessary to take the average over all possible cluster numberings.

In practice, C_{12} can be measured directly by the pair-wise correlation of puffs. However, while there are plenty of published examples of puff-sequences [100, 197, 248], the systematic measurements of puff correlations are still missing. Therefore, C_{12} is computed by Eq. **3.2** in this thesis, and cluster state transitions are governed by computed opening probability distributions (see Section 3.2). The definition of spatial coupling in terms of C_{12} is further discussed in Secion 3.4.

The spatial coupling, as given by Eq. **3.2**, arises by short-lived increases of the local Ca^{2+} concentrations at closed clusters, which stem from opening events of nearby clusters (puffs). An important element setting the spatial coupling is the geometrical arrangement of clusters. This thesis employs arrangements of clusters on the vertices of a tetrahedron or cube. The major reason for the choice of regular arrangements are their symmetries (cf. Section 3.4), which are convenient for solution of Eq. **3.2** and for the analytical calculations shown in Sections 3.3 and 3.4. Chapter 4 also presents simulations with irregular arrangements of 8 clusters.

The small numbers of clusters used in this thesis are justified in small cells like SH-SY5Y neuroblastoma cells, where on average four clusters participate in a Ca^{2+} signal [197]. They may also apply to pacemaker-sites in other cells, from which global signals nucleate and spread throughout the cell. As shown in Chapter 4, crucial results do not depend on the spatial arrangement of clusters, due to robustness properties. That is shown by simulations with more clusters, and irregular arrangements produce very similar results [194].

3.2 Data Input and Standard Parameter Values

Hierarchic stochastic modelling requires two types of input data, which provide all essential ingredients for a stochastic spiking mechanism: First, dynamics of individual clusters are described by probability distribution densities for cluster state transitions. Second, interaction of clusters is mediated by a coupling function, which in the case of Ca^{2+} dynamics is derived from a Ca^{2+} diffusion problem. The

values of some cellular parameters determining cluster properties and the Ca^{2+} diffusion profile are also needed in order to perform model simulations in a realistic regime of Ca^{2+} dynamics. Standard parameter values used in this thesis are given at the end of this Section.

Transition probability distributions

The closing probability density ψ_c can be derived from experimental results by Smith and Parker [196]: They indicate that the individual channels in a cluster close independently with closing rate γ, which does not depend on $[Ca^{2+}]$. Therefore, the cluster closing time distribution $\psi_c(t-\tau)$ can be computed as [233]:

$$\psi_c(t-\tau) = N_{\mathrm{ch}}\gamma e^{-\gamma(t-\tau)}\left(1-e^{-\gamma(t-\tau)}\right)^{N_{\mathrm{ch}}-1}, \tag{3.3}$$

where N_{ch} denotes the number of IP_3Rs per cluster.

As mentioned in Section 3.1, the opening probability density $\psi_o(c, t-\tau)$ is obtained by the method developed by Rüdiger Thul, Erin Higgins and Heiko Schmidle in the Falcke lab [94, 223, 224] on the basis of the De Young-Keizer model [51] (see Appendix A.1 for a brief description). Since the probability densities obtained that way are sums of more than 1000 exponentials, making computation of function values rather extensive, it is convenient to assume that the ψ_o can be described by the two-parametric γ-distribution

$$\psi_o(c,\theta) = \frac{\theta^{\alpha(c)-1}e^{-\theta/\beta(c)}}{\Gamma(\alpha(c))\beta(c)^{\alpha(c)}}, \tag{3.4}$$

where $\theta = t-\tau$, $\Gamma(x)$ is the Euler Γ function, α is the shape parameter and β is the scale parameter.

If α is an integer, the γ-distribution describes the probability density for the αth Poisson event with rate $1/\beta$ in a process consisting of α subsequent Poisson processes. Since within a cluster, many independent state transitions of individual clusters can occur before an open cluster configuration is achieved, this is a realistic model for our purposes. For $\alpha = 1$, the γ-distribution is equal to the exponential

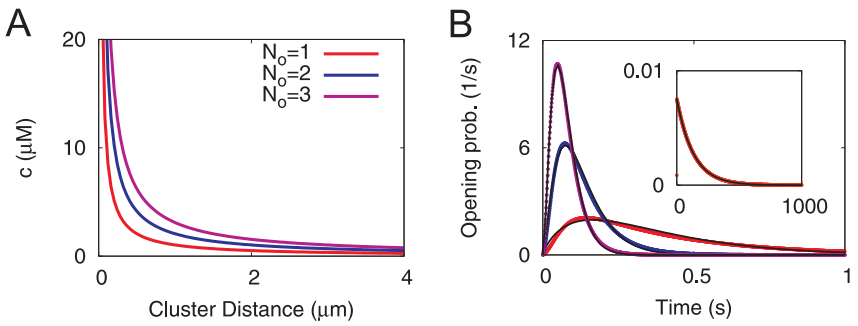

Figure 3.2: Calculation of opening transition times. (A) The Ca^{2+} concentration c at a closed cluster depends on the distances to the open clusters. Shown is the diffusion profile as obtained from Eq. **3.7** for the tetrahedron model (cf. Fig. 3.4), where all N_o open clusters have the same cluster distance. (B) Opening transition times for base-level $[Ca^{2+}]$ (inset, orange) and for the Ca^{2+} diffusion profiles depicted in A (same color-code as in A). The transition times were computed from the De Young-Keizer model (Fig. 2.3) with parameters given in Tab. A.1, and were fitted (black lines) to exponential (inset) and γ-distributions (see text). The cluster distance is 1.5 μm, for parameter values not mentioned in this caption see Tab. 3.1.

distribution describing a Markovian rate process:

$$\psi_o(c,\theta) = \lambda(c)e^{-\lambda(c)\theta}, \quad \lambda(c) = \frac{1}{\beta(c)}. \tag{3.5}$$

Figure 3.2 shows the ψ_o computed from the DeYoung-Keizer model for diffusion profiles computed according to Eq. **3.7** below. The computed ψ_o fit Eq. **3.4** well at high values of $[Ca^{2+}]$, which are expected during a spike, while at resting $[Ca^{2+}]$, Eq. **3.5** is sufficient to describe ψ_o. That is reasonable, because it can be expected that at resting $[Ca^{2+}]$ the recovery processes causing non-monotonous distributions are not active. Therefore we fit the probability distribution for opening of the first cluster by Eq. **3.5** and refer to the parameter λ as the puff-rate (see Tab. 3.1). In Section 6.2, it will be shown that the computed opening probabilities are similar to measured interpuff interval distributions presented in this work.

Ca^{2+} diffusion

As mentioned in Section 3.1, we describe Ca^{2+} dynamics by a diffusion equation with spatial δ-sources at the locations of open clusters. Ca^{2+} pumps transport

Ca^{2+} ions out of the cytosol into the ER or the extracellular space with rate p (Tab. 3.1). Their spatial density is assumed to be continuous. Therefore, the Ca^{2+} concentration is governed by a linear reaction-diffusion equation:

$$\frac{\partial}{\partial t}[Ca^{2+}](\vec{r},t) = D\Delta[Ca^{2+}] + \rho \sum_{\substack{n=1 \\ r\neq r_n}}^{N_o} \delta(\vec{r}-\vec{r}_n) - p[Ca^{2+}]. \tag{3.6}$$

D denotes the Ca^{2+} diffusion coefficient, ρ the average Ca^{2+} current through a cluster, and p the rate at which Ca^{2+} is pumped out of the cytosol by Ca^{2+} pumps. The vector $\vec{r}$ is the spatial coordinate, $\vec{r}_n$ is the position of cluster n. $\delta(\vec{r})$ and Δ are the Dirac δ-function and the Laplacian in three dimensions, respectively, and the sum runs over all N_o open clusters.

An open cluster causes a concentration rise in its vicinity, and concentrations between 20 µM and 200 µM at the cluster itself [221]. They decrease with gradients of 2-3 orders of magnitude per micrometer distance from the cluster [34, 221]. The large local concentration at the open cluster fluctuates with the number of open channels in the cluster. These fluctuations are large at the open cluster itself, but they are much smaller in a typical distance to a neighboring cluster, since they are smoothed by diffusion (Appendix A.2). Therefore, the concentration rise caused by open clusters at neighboring clusters can be well approximated by a constant rise lasting as long as the cluster is open. We describe it by the stationary spatial concentration profile corresponding to the average current ρ through an open cluster.

With free boundary conditions, i.e. $\lim_{r\to\infty}[Ca^{2+}] = 0$, and if we take the continuous presence of a resting Ca^{2+} concentration c_0 into account, the stationary solution to Eq. **3.6** at closed clusters c_m is [14]

$$c_m = \frac{\rho}{D} \sum_{\substack{n=1 \\ n\neq m}}^{N_o} \frac{e^{-\sqrt{\frac{p}{D}|r_m - r_n|}}}{4\pi|r_m - r_n|} + c_0. \tag{3.7}$$

Ca^{2+} diffusion profiles computed from Eq. **3.7** are shown in Fig. 3.2, together with the corresponding opening transition probabilities $\psi_o(c, t-\tau)$. Parameter values and an estimation of the Ca^{2+} release current ρ are given below.

More general boundary conditions leading to more complex Ca^{2+} diffusion profiles can be used instead of Eq. **3.7** without difficulty for what follows: The Ca^{2+} concentration enters the upcoming calculations only via the Ca^{2+}-dependence of the opening probability distributions ψ_o. But those need to be computed only one time for a given cluster arrangement, which determines the cluster distances and therewith the Ca^{2+} diffusion profiles for all possible combinations of open and closed clusters in the cell.

Standard parameter values

Table 3.1 shows the set of standard parameter values used in simulations if not stated otherwise. Since single channel dynamics are not considered in detail, but rather described by probability distributions, the only parameters needed are the IP_3 and Ca^{2+} base-level concentrations and parameters that determine the cluster geometry and the Ca^{2+} diffusion profile.

The used parameter values are widely accepted and applied in established Ca^{2+} models [67], only a few parameters require a bit of explanation: The puff-rate λ was derived from the base-level $[Ca^{2+}]$ by fitting of the computed opening probability at resting $[Ca^{2+}]$ $\psi_o(c_o, t-\tau)$ (see above) to Eq. **3.5**. The channel closing rate γ is used as a free parameter in model simulations (see Chapter 4), since it has not yet been determined experimentally to high precision, but it is probably a molecular property depending on the IP_3R isotype (cf. Section 2.1). The cluster distance is understood as the nearest neighbour distance between two clusters in the lattice. That means that in the cube model, it is the edge of the cube, and the small and large diagonal of the cube are derived from that value.

The only parameter posing problems with unit conversion is the release current of the IP_3R: It is required in units μmol/s for Eq. **3.6**, but it can only be measured by patch-clamp experiments in units pA (Tab. 3.1 shows a typical value). The units can be converted as follows: By Faraday's law, $\rho = I/(zF) \approx 10^{-12}$ μmol s^{-1}, if I is the release current of 0.2 pA given in Tab. 3.1, $z = 2$ is the valency of Ca^{2+} ions, and $F \approx 10^5$ As mol^{-1} is Faraday's constant. However, the 3D δ-function multiplied to ρ in Eq. **3.6** has dimension μm^{-3}, while the left-hand side has dimension $(\mu M\ s)^{-1}$, so that by the transformation from liter to μm^3 a factor

Table 3.1: Standard parameter values.

Parameter	Symbol	Value	Unit
Cluster distance	a	0.5–5	μm
Channels per cluster	N_{ch}	5	–
IP_3 concentration	$[IP_3]$	1.0	μM
Base-level $[Ca^{2+}]$	c_0	0.03	μM
Puff-rate	λ_0	0.00755	s^{-1}
Channel closing rate	γ	5–100	s^{-1}
Ca^{2+} Diffusion constant	D	220	$\mu m^2 s^{-1}$
Release current of the IP_3R	ρ	0.2	pA
SERCA pumping rate	p	80	s^{-1}

of 10^{15} enters ρ. Further, assume that on average three channels are open during a puff, to end up with $\rho = 3000$ μmol s^{-1}, which is the value used in simulations.

3.3 Mathematical Formulation of the Hierachic Stochastic Model

The hierarchic stochastic model of intracellular Ca^{2+} dynamics describes emergence of cellular Ca^{2+} dynamics from channel cluster dynamics. The cluster dynamics, as input data, are formulated in such a way that they take into account the underlying single-channel dynamics without considering them explicitly (see Figs. 1.1 and 3.1). The system variables of the hierarchic stochastic model are sojourn probabilities of cluster configurations. In their most general form, they are solutions of a set of Volterra Integral Equations, which will be derived in this section. The procedure is a generalisation of the formalism developed by Tobias Prager *et al.* [165–167] to more states and state-transitions. Statistical moments of spike statistics are derived by means of a first-passage time problem. At the end of the section, also numerical solutions of time-dependent spike statistics will be shown.

Cluster state transitions are governed by a non-Markovian Master Equation

In the hierarchic stochastic model, the state of the cell is described by the configuration of open and closed clusters among its N_{cl} clusters. To formulate these ideas mathematically, we introduce the state variable x_j for all clusters $j = 1,\ldots,N_{cl}$, which can assume the values O or C for open and closed clusters, respectively. A system configurations S_i is defined as the set of all cluster states: $S_i = \{x_1^i, \ldots, x_{N_{cl}}^i\},\ i = 0, \ldots, N_{conf}$, where N_{conf} is the number of configurations with at least one open cluster, and $x_j^i \in \{O, C\}$ is the state of cluster j in a system in configuration S_i.

Due to Ca^{2+}-induced Ca^{2+} release (see Section 2.1), transitions between system configurations will depend on the Ca^{2+} concentrations at closed clusters. We denote by $c_m(S_i)$ the Ca^{2+} concentration at a closed cluster m in configuration S_i. Then, the stationary solution to our diffusion problem (Eq. **3.7**) becomes

$$c_m(S_i) = \frac{\rho}{D} \sum_{\substack{n=1 \\ n\neq m}}^{N_o} \frac{e^{-\sqrt{\frac{p}{D}}|r_m - r_n|}}{4\pi|r_m - r_n|} + c(S_0). \tag{3.8}$$

The sum runs over all N_o open clusters. The indices m and n will be exclusively used for closed and open clusters, respectively, throughout this section. S_0 is the configuration with all channels closed, and $c(S_0) = c_0$ is the resting Ca^{2+} concentration (see Tab. 3.1).

The probability $P(S_i, t)$ to be in configuration S_i at time t obeys the Master Equation

$$\frac{\partial}{\partial t} P(S_i, t) = \sum_{\substack{l=0 \\ l\neq i}}^{N_{conf}} I_{li}\left(S_l, t\right) - I_{il}\left(S_i, t\right), \tag{3.9}$$

with the probability fluxes I_{il} for a transition from S_i to S_l. In the case of a Markovian rate process, each transition would only depend on the configuration at the last time-step, and we would be able to write

$$I_{il}(S_i, t) = r_{il}(t) P(S_i, t), \tag{3.10}$$

with transition rates r_{il} determined uniquely by the configuration S_i, and potentially on the system time t [233]. But, instead of transition rates, the input data to our model are the probability density distributions for opening and closing of clusters, $\psi_o(c, t-\tau)$ and $\psi_c(t-\tau)$ (cf. Section 3.2). They depend not only on the configuration at the actual time, but also on the time-interval that has passed since the last state-change, $t-\tau$. Therefore, the Master Equation **3.9** is non-Markovian, and the problem does not lead to a set of differential equations, but it requires derivation of integral equations.

To introduce the calculation of the probability fluxes I_{il} in terms of the $\psi_{o,c}$, we first consider the simplest possible setup with only one cluster and two configurations, S_0={C} and S_1={O}. Then, the I_{il} are solutions of a system of integral equations [47, 166]:

$$\begin{pmatrix} I_{01}(t) \\ I_{10}(t) \end{pmatrix} = \int_0^t \begin{pmatrix} 0 & \psi_o(c_0, t-\tau) \\ \psi_c(t-\tau) & 0 \end{pmatrix} \begin{pmatrix} I_{01}(\tau) \\ I_{10}(\tau) \end{pmatrix} d\tau + \begin{pmatrix} f_{01}(t) \\ f_{10}(t) \end{pmatrix}, \quad (3.11)$$

where $f_{il}(t)$ is the initial flux vector (or initial function) containing fluxes from the starting configuration S_i to configuration S_l (see below). An intuitive explanation for Eq. **3.11** can be given as follows: The opening (closing) probability flux at time t is the sum of the initial flux $f_{01}(t)$ ($f_{10}(t)$) and the flux that results from reopening (re-closing). The latter equals the integral over the probabilities to have closed (opened) at earlier times $t-\tau$ multiplied by the probabilities to re-open (re-close) at t.

In general, the system contains more than one cluster, but we only consider transitions between configurations which are identical except for the state of one cluster. Simultaneous state changes of several clusters can be neglected as higher-order events [233]. Therefore, in Eq. **3.9**, all probability fluxes describing transitions with more than one cluster changing its state are set to zero. Note that the generalised transition probability distribution for a transition from S_i to S_l depends on the Ca^{2+} concentrations c_m at all closed clusters m (see Eq. **3.8**). Therefore, we denote the probability distribution for such a transition by $\psi_{il}(\{c_m(S_i)\}_m, t-\tau)$, where braces $\{\cdot\}_m$ indicate dependence on all m.

With these considerations, the general form of Eq. **3.11** is

$$I_{il}(t) = \int_0^t \psi_{il}(\{c_m(S_i)\}_m, t-\tau) \sum_{\substack{k=0 \\ k\neq i}}^{\mathrm{N_{conf}}} I_{ki}(\tau)d\tau + f_{il}(t). \tag{3.12}$$

The generalised transition probability ψ_{il} describes the state change of a certain cluster j, while all other clusters remain in their states (see above). In the remaining part of this section, we denote the time elapsed since the last transition by $\theta = t - \tau$. Then, the generalised transition probability has the following form:

$$\begin{aligned}\psi_{il}(\{c_m(S_i)\}_m, \theta) = \psi_{o,c}(c_j(S_i), \theta) \\ \times \prod_{m\neq j} \left[1 - \int_0^\theta \psi_o(c_m(S_i), t')dt'\right] \\ \times \prod_{n\neq j} \left[1 - \int_0^\theta \psi_c(t')dt'\right].\end{aligned} \tag{3.13}$$

As before, m indexes the subset of closed clusters and n indexes the subset of open clusters. If ψ_{il} describes cluster closing, the dependence on $c_j(S_i)$ can be omitted, because only ψ_o depends on the local Ca^{2+} concentration.

The ψ_{il} are normalized such that

$$\sum_{\substack{i=0 \\ i\neq l}}^{\mathrm{N_{conf}}} \int_0^\infty \psi_{il}(t')dt' = 1, \tag{3.14}$$

for all configurations S_l, which can be shown by integration by parts. This means that the system does not possess an absorbing state, which is a necessary condition for repetitive spiking – and that is the dynamical regime expected from a model describing intracellular Ca^{2+} signals.

Volterra integral equations need to be supplemented by initial functions

The integral equation **3.12** belongs to the class of Volterra Integral Equations (VIEs) with convolution kernels [164]. In contrast to differential equations, VIEs

always possess a unique solution and do not require additional initial values for uniqueness. Nevertheless, the initial properties of VIEs are governed by the function added to their integral part, often called initial function. The trivial solution is always zero: In Eq. **3.12** e.g., $f_{il}(t) = 0 \Rightarrow I_{il}(t) = 0$, regardless of the kernel ψ_{il}.

To determine the correct initial functions for our problem, we start in configuration $S_0 = \{C, ..., C\}$, so that all initial fluxes are zero apart from those out of S_0. In the case of one cluster, the initial condition is $P(S_0, 0) = 1,\ P(S_1, 0) = 0$, and we have $\psi_{01}(c_j(S_i), \theta) = \psi_o(c_0(S_0), \theta)$, according to Eq. **3.13**. The initial function as it appears in Eq. **3.11** should describe system dynamics in the absence of reclosing events, i.e. for $I_{10} = 0$. That implies $\theta = t$ and $P(S_0, t) = 1 - \int_0^t \psi_o(t')dt'$. Because $I_{10} = 0$, we infer from Eq. **3.12** that

$$f_{01}(t) = -\frac{\partial}{\partial t} P(S_0, t) = \psi_o(t). \tag{3.15}$$

In general, this means

$$\begin{aligned} &P(S_i, 0) = 1, \quad P(S_k) = 0, \quad k \neq i \\ &\Rightarrow f_{il}(t) = \psi_{il}(\{c_m(S_i)\}_m, t), \quad f_{kl}(t) = 0, \quad k \neq i. \end{aligned} \tag{3.16}$$

The initial functions **3.16** complete the mathematical formulation of the model, which provides a unique description of the systems dynamics. A good direct test for the model equations is their reduction to simple cases. For that purpose, assume a Markov Process, where the waiting times $\psi_{o,c}$ are exponential distributions $\lambda \exp[-\lambda(t - \tau)]$, with λ depending on the transition type. Then Eqs. **3.12** and **3.16** can be transformed to Eq. **3.10** by the standard method described in ref. [164].

Statistical moments of interspike intervals arise as solutions of related integral equations

Since spike patterns can be characterised in terms of average (T_{av}) and standard deviation (σ) of interspike intervals (ISIs), we wish to compute these quantities from the model. Fortunately, the ISI distribution is the solution of a well-known

first-passage time (FPT) problem: Let $\psi_{\mathrm{FPT}}(S_i, S_l, t)$ denote the probability distribution that S_l is visited for the first time after starting in S_i. Then the ISI distribution is equal to $\psi_{\mathrm{FPT}}(S_0, S_{\mathrm{sp}}, t)$, so that σ and $\mathrm{T_{av}}$ can be computed as its standard deviation and average, respectively. S_{sp} is a system configuration identified with a cellular Ca^{2+} spike. If several such configurations exist – which is the typical case in cluster arrangements with more than 4 clusters (see Section 3.4) – than it is appropriate to compute the average over all the resulting values of σ and $\mathrm{T_{av}}$.

$\psi_{\mathrm{FPT}}(S_0, S_{\mathrm{sp}}, t)$ can be computed from Eqs. **3.12-3.13** by inversion of the following Volterra Integral Equation of the first kind [233]:

$$P(S_0, S_{\mathrm{sp}}, t) = \int_0^t P(S_{\mathrm{sp}}, S_{\mathrm{sp}}, t-\tau)\psi_{\mathrm{FPT}}(S_0, S_{\mathrm{sp}}, \tau)d\tau, \tag{3.17}$$

where $P(S_i, S_j, t)$ is the probability to be in S_j at time t after having started in S_i. However, numerically it is more effective to transform that equation into a VIE of the second kind – i.e., into the form of Eq. **3.12** – which can be done by differentiation [164]. Since $P(S_{\mathrm{sp}}, S_{\mathrm{sp}}, 0) = 1$, differentiation yields

$$\psi_{\mathrm{FPT}}(S_0, S_{\mathrm{sp}}, t) = \frac{\partial}{\partial t}P(S_0, S_{\mathrm{sp}}, t) - \int_0^t \frac{\partial}{\partial t}P(S_{\mathrm{sp}}, S_{\mathrm{sp}}, t-\tau)\psi_{\mathrm{FPT}}(S_0, S_{\mathrm{sp}}, \tau)d\tau. \tag{3.18}$$

Average $\mathrm{T_{av}}$ and standard deviation σ of interspike intervals, which are the key variables characterising Ca^{2+} spike-sequences in this thesis (see Chapters 4 and 5), are the statistical moments of ψ_{FPT} and thus can be obtained by appropriate integration of the solution to Eq. **3.18**. That equation depends merely on $(\partial/\partial t)P(S_0, S_{\mathrm{sp}}, t)$, which is already known from Eq. **3.9**. Therefore, Eqs. **3.9**, **3.12-3.16** and **3.18** form a complete system that uniquely determines spike statistics on the basis of puff characteristics.

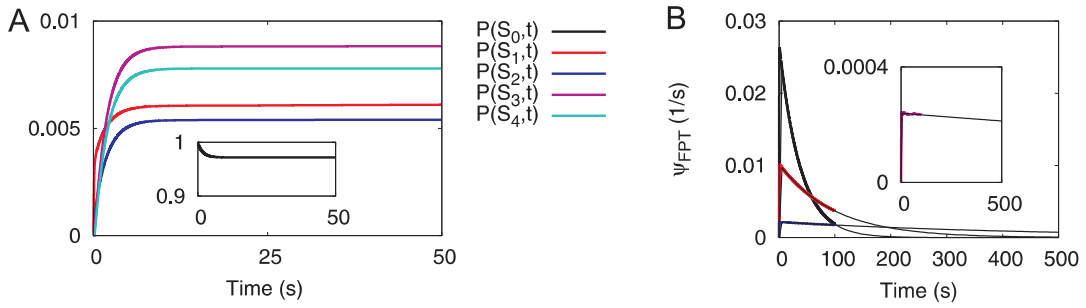

Figure 3.3: Solution of the time-dependent analytic model. (A) The probabilities $P(S_i, t)$ attain stationarity after a few seconds. The probability that all clusters are closed, $P(S_0, t)$ (inset) is highest. However, the probabilities for more open clusters also have probabilities different from zero, suggesting short spikes and longer time intervals in between. The cluster distance is 1.5 µm, the channel closing rate is γ=15 s^{-1}. (B) Calculation of the first-passage-time distribution ψ_{FPT} by integral equations. The colors indicate different values of the channel closing probability γ (black, 5 s^{-1}; red, 15 s^{-1}; blue, 25 s^{-1}; pink (inset), 40 s^{-1}). Average (T_{av}) and standard deviation (σ) of interspike intervals are obtained as central moments of ψ_{FPT} (see text). Since they have large nonzero tails, direct computation of the moments would require solution of the integral equations **3.12** for > 500 s, for which there are no efficient numerical procedures. Therefore, the FPTs are fitted to the normalised, initially zero double exponential $\lambda_1\lambda_2/(\lambda_2-\lambda_1)\times(\exp(-\lambda_1 t)-\exp(-\lambda_2 t))$ (thin black lines). The values shown in Tab. 3.2 (Section 3.4) are computed from these fits. Parameters not mentioned in this caption are given in Tab. 3.1.

Solution for complete time-dependent spiking statistics requires numerical integration

Equations **3.12-3.16** define a system of linear Volterra Integral Equations with convolution kernel, which has a unique solution [164]. Such equations can sometimes be solved directly by reduction to differential equations or by Laplace Transform methods, but this is not possible here due to the rather complicated form of the kernel $\psi(t)$. Therefore, it requires direct numerical integration. We have implemented the integral equations of the tetrahedron model (cf. Section 3.4) by the two-step method described by Wolkenfelt [245]. For this algorithm, Lubich proved absolute stability – i.e., the numerical solution attains stationarity if the real solution does – for a prototypic system of integral equations [133].

Figure 3.3A shows a typical solution of the time development of the $P(S_i, t)$, indicating that they rapidly attain stationarity. Solutions for $\psi_{\mathrm{FPT}}(t)$ are depicted

in figure 3.3B. The probability to spike fast clearly is high if the channel closing probability is low. From $\psi_{\mathrm{FPT}}(t)$, we can easily derive the standart deviation (σ) and average ($\mathrm{T_{av}}$) of interspike intervals as the first and second central moments (Tab. 3.2 in Section 3.4). Therefore, we have derived the complete behavior of cellular spike statistics on the basis of a Ca^{2+} diffusion profile and the probability distributions for cluster opening and closing, which can be measured experimentally.

3.4 Stationary Statistics and the Tetrahedron Model

Since numerical solution of the integral equations derived in Section 3.3 is tedious, we sought to derive direct analytical expressions for steady state values describing spike statistics. That is useful as a test for the stochastic algorithm described in Section 3.5, and it turns out that many of the results shown in Chapter 4 were obtained more efficiently on the basis of the analysis presented here.

The tetrahedron model is both simple and realistic in small cells

We will see below that stationary statistics are particularly easily obtained if transitions between configurations compose a linear chain indexed by the number of open clusters. The only non-trivial realisation of that property for our model system is the tetrahedron model depicted in Fig. 3.4: Here, all configurations with equal number of open clusters are topologically equivalent, since the Ca^{2+} diffusion profiles are equal. This is not true for the next easiest cluster arrangements, which are the hexaeder (or cube) and the octaeder.

For computation of the probability fluxes I_{il} of the tetrahedron model, it is convenient to define equivalence classes of system configurations, rather than considering all configurations individually. In the following, the S_i, I_{il} and ψ_{il} are to be understood in this sense of equivalence classes of configurations, and thus they have a slightly different meaning than in the previous section. We identify

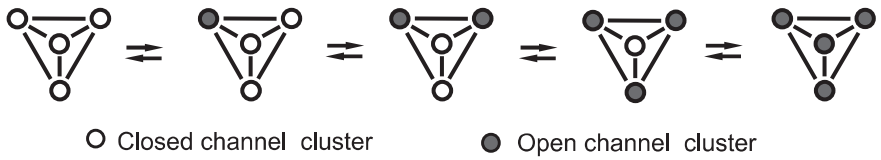

Figure 3.4: Schematic representation of the tetrahedron model. All configurations with the same number of open clusters are equivalent, so that transitions ψ_{il} can be represented by a linear chain.

S_i with the class of configurations with i open clusters. In the ψ_{il}, it must be taken into account that there can be different possibilities to switch from S_i to S_l. For instance, starting from S_0, opening of either of the 4 closed clusters induces a switch to S_1.

Since only one cluster can change state at a time (see Section 3.3), we can write $\psi_{il} = \psi_{i,i+1}$ for an opening transition and $\psi_{il} = \psi_{i,i-1}$ for a closing transition, now. This leads to the following expressions, which should be used here instead of Eq. **3.13**:

$$\psi_{i,i+1}(\theta) = N_i^c \psi_o(c_j(S_i),\theta) \left[1 - \int_0^\theta \psi_o(c_m(S_i),t')dt'\right]^{N_{i-1}^c} \left[1 - \int_0^\theta \psi_c(t')dt'\right]^{N_i^o}$$

$$\psi_{i,i-1}(\theta) = N_i^o \psi_c(\theta) \left[1 - \int_0^\theta \psi_o(c_m(S_i),t')dt'\right]^{N_i^c} \left[1 - \int_0^\theta \psi_c(t')dt'\right]^{N_{i-1}^o},$$

where depence of the ψ_{il} on the c_m is omitted. $N_i^o = i$ and $N_i^c = \mathrm{N_{cl}} - i$ are the numbers of open and closed clusters in configuration S_i, respectively. They account for the numbers of possible closing and opening events in the given configuration. The $N_i^{o,c}$ in the exponents assure that all other clusters remain in their states in the considered time interval, in which cluster j changes state.

Now, the time-dependent model equations can be given explicitly in matrix notation:

$$\mathbf{I}(t) = \int_0^t \boldsymbol{\psi}(t-\tau)\mathbf{I}(\tau)d\tau + \mathbf{f}(t), \tag{3.19}$$

with

$$\mathbf{I} = \begin{pmatrix} I_{01} \\ I_{10} \\ I_{12} \\ I_{21} \\ I_{23} \\ I_{32} \\ I_{34} \\ I_{43} \end{pmatrix}, \quad \boldsymbol{\psi} = \begin{pmatrix} 0 & \psi_{01} & 0 & 0 & 0 & 0 & 0 & 0 \\ \psi_{10} & 0 & 0 & \psi_{10} & 0 & 0 & 0 & 0 \\ \psi_{12} & 0 & 0 & \psi_{12} & 0 & 0 & 0 & 0 \\ 0 & 0 & \psi_{21} & 0 & 0 & \psi_{21} & 0 & 0 \\ 0 & 0 & \psi_{23} & 0 & 0 & \psi_{23} & 0 & 0 \\ 0 & 0 & 0 & 0 & \psi_{32} & 0 & 0 & \psi_{32} \\ 0 & 0 & 0 & 0 & \psi_{34} & 0 & 0 & \psi_{34} \\ 0 & 0 & 0 & 0 & 0 & 0 & \psi_{43} & 0 \end{pmatrix}.$$

As mentioned before, the ψ_{il} used here should not be confused with those in the general case given in Eq. **3.13**. Note that the formulation in terms of equivalence classes of configurations, as presented here for the tetrahedron model, can also be used for simplification of larger systems with symmetries. For instance, nearest-neighbour interactions in the cube model (see Section 3.5) can be handled as an equivalence class. However, the tetrahedron model is the largest system that can be completely described by classes of configurations representing the number of open clusters.

Stationary statistics of linear chain models can be obtained directly in the form of analytical expressions

The basic assumption in the forthcoming calculations is that the spike-generating stochastic process is stationary, i.e. $(\partial/\partial t)P(S_i, t) = 0$. Then, from Eq. **3.12**,

$$\bar{I}_{il} = I_{il}(\infty) = C_{il} \sum_{\substack{k=0 \\ k \neq i}}^{\mathrm{N_{conf}}} \bar{I}_{ki}, \tag{3.20}$$

where $C_{il} = \int_0^\infty \psi_{il}(t')dt'$ is the splitting probability to reach configuration S_l before returning to the ground state S_0 when starting in S_i. Note that we omit the argument c of the distribution functions in this section for convenience. The $\psi_{il}(\theta)$, $\theta = t - \tau$, were defined in Eq. **3.13**. It follows immediately (Eq. **3.14**) that $\sum_l C_{il} = 1$.

At this point, one might guess that the solutions of Eq. **3.20** will determine the

relative number of occurences of each configuration, leading to

$$\bar{P}(S_i) = \frac{T_i \sum\limits_{\substack{l=0 \\ l\neq i}}^{\mathrm{N_{conf}}} I_{il}}{\sum\limits_{l=0}^{\mathrm{N_{conf}}} \left(T_l \sum\limits_{\substack{k=0 \\ k\neq l}}^{\mathrm{N_{conf}}} I_{lk} \right)}, \tag{3.21}$$

where $T_i = \int_0^\infty t' \sum_l \psi_{il}(t') dt'$ is the mean residence time in configuration S_i, and $\bar{P}(S_i)$ is the stationary sojourn probability. Equation **3.21** is confirmed by Eq. **3.27** below and by simulations.

Now, we approach the problem in a different way. If we dealt with a Markov process, the probabilities for state-changes would be exponentially distributed with parameters r_{il} [233], and that parameter could be computed from T_i and C_{il}:

$$\psi_{o,c}(\theta) = r_{il} \exp(-r_{il}\theta) \tag{3.22}$$

$$\Rightarrow \psi_{il}(\theta) = r_{il} e^{-\theta \sum_l r_{il}}, \quad \left(T_i = \sum_{\substack{l=0 \\ l\neq i}}^{\mathrm{N_{conf}}} r_{il} \right)^{-1}, \quad C_{il} = r_{il} \left(\sum_{\substack{l=0 \\ l\neq i}}^{\mathrm{N_{conf}}} r_{il} \right)^{-1} \tag{3.23}$$

$$\Rightarrow \quad r_{il} = \frac{C_{il}}{T_i}. \tag{3.24}$$

Equation **3.23** is a direct consequence of the definitions of T_i and C_{il}, in the case of a Markov process. The expression for T_i is sometimes used as characteristic time of a chemical reaction [93].

To proceed with our non-Markovian process, consider an interesting result from Cox [47] for the alternating renewal process (Eq. **3.11**): The stationary probability to be in configuration S_i, $\bar{P}(S_i)$, does not change if the transition time distribution $\psi_\omega(\theta)$ is replaced by an exponential distribution with the same average transition time. As a generalization, we assume that the stationary statistics of the process with general transition probabilities ψ_o and ψ_c (Section 3.2) are equal to those of the Markov process with exponentially distributed transition probabilities. That means, we assume that Equation **3.24** is valid in more general circumstances.

Then, we can apply the theory of birth and death processes in the case of a linear chain $S_0 \rightleftharpoons S_1 \rightleftharpoons \cdots \rightleftharpoons S_{\mathrm{N_{conf}}}$ [233]. In particular for the tetrahedron

Table 3.2: Comparison of the different methods of computation described in Sections 3.3-3.5 for cluster distance a=1.5 µm and parameters given in Tab. 3.1.

	Integral Equations	**Direct Solution**	**DSSA**
$\bar{P}(S_0)$	0.9719	0.9720	0.9715
$\bar{P}(S_4)$	0.0078	0.0078	0.0079
$\bar{\mathrm{T}}_{\mathrm{av}}$	98.39 s	98.44 s	98.68 s
$\bar{\sigma}$	98.07 s	98.11 s	98.68 s

model with $\mathrm{N_{conf}} = \mathrm{N_{cl}} = 4$, C_{14} is the probability that a puff (S_1) generates a spike (S_4) before all clusters are closed again. It can be expressed in terms of single-step transition probabilities:

$$C_{14} = \frac{C_{12}C_{23}C_{34}}{1 + C_{12}(C_{23} - 1) + C_{23}(C_{34} - 1)}. \tag{3.25}$$

With $[Ca^{2+}]$ at closed clusters below the values causing Ca^{2+}-dependent inhibition, $C_{12} < C_{23} < C_{34} < 1$ applies due to Ca^{2+} induced Ca^{2+} release. Equation **3.25** shows that $C_{14} \approx C_{12}$ for large C_{12}. In Section 3.1, we identified C_{12} with cluster coupling and derived a general expression for it (Eq. **3.2**). The finding that $C_{14} \approx C_{12}$ supports this definition in the sense that the probability to open a second cluster C_{12} is also an indicator for spiking (cf. Section 4.1).

$\bar{\mathrm{T}}_{\mathrm{av}}$ and $\bar{\sigma}$ are in fact moments of the first passage time to go from S_0 to S_4 and can be obtained from recursion relations derived by Gillespie [78], as well as the stationary probabilities. The relations for $\bar{\mathrm{T}}_{\mathrm{av}}$ and $\bar{P}(S_0)$ are rewritten as analytic formulas in terms of model variables by simple algebra (the others are too long to give them explicitly):

$$\bar{\mathrm{T}}_{\mathrm{av}} = \frac{T_0 + T_1}{C_{14}} + \frac{T_1 C_{21}}{C_{23}C_{34}} + \frac{T_2}{C_{23}C_{34}} + \frac{T_3}{C_{34}} \tag{3.26}$$

$$\bar{P}(S_0) = \left[1 + \frac{T_1 C_{21} C_{32}}{T_0 C_{10} C_{21} C_{32}} + \frac{T_2 C_{12} C_{32}}{T_0 C_{10} C_{21} C_{32}} + \frac{T_3 C_{12} C_{23}}{T_0 C_{10} C_{21} C_{32}} + \frac{T_4 C_{12} C_{23} C_{34}}{T_0 C_{10} C_{21} C_{32}}\right]^{-1}. \tag{3.27}$$

Table 3.2 shows that values calculated by the described direct method are in excellent agreement with the exact solution presented in Section 3.3 and the stochas-

tic simulations presented in Section 3.5, which confirms validity of the assumption made by Eq. **3.24**.

3.5 Stochastic Simulations and the Cube Model

This chapter so far derived analytical expressions for statistical properties of Ca^{2+} spiking by means of the hierarchic stochastic model. However, the temporal evolution of the configurations $S_i(t)$, which illustrates the actual spiking pattern, needs to be resolved with a stochastic simulation algorithm. Since the hierarchic stochastic model is non-Markovian, the standard method from Gillespie [77] cannot be applied, and this section will describe a suitable delayed stochastic simulation algorithm (DSSA). Such an algorithm is also required for the determination of statistic properties of model systems larger than the tetrahedron model (e.g. the cube model). Larger models cannot be represented by linear chains, so that the expressions obtained in Section 3.4 are not applicable, and the full problem considered in Section 3.3 becomes too large for available numerical methods. Furthermore, Chapter 4 will show that realistic simulations require the addition of global feedback processes to the model presented so far. Implementation of such feedbacks into our DSSA is straight-forward, as demonstrated at the end of this section.

The cube model defines a larger cluster arrangement used to verify key results on a larger scale

The basic larger model considered in this thesis is the cube model (Fig. 3.5). In fact, it is the next easiest model after the tetrahedron model, since it is the second platonic solid and has only three different cluster distances. However, it already leads to 22 configurations and 80 fluxes - i.e., Eq. **3.12** would be a system of 80 integral equations. Moreover, we will not only consider the regular cube model, but also random deviations from it. That means, the positions of the clusters (nodes in the cube) are subject to random variation in all three dimensions. That is only possible with a fast stochastic simulation algorithm.

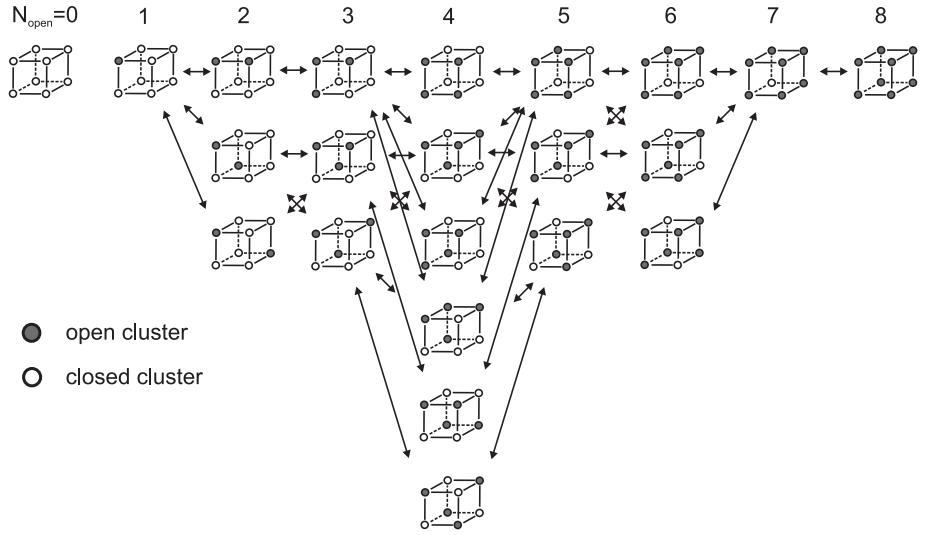

Figure 3.5: Schematic representation of the cube model. Three different cluster distances appear in each configuration, which requires superposition of the diffusion profiles in Eq. **3.7**. Altogether we count 22 configurations and 80 transitions, which makes solution of the integral equation **3.12** impossible.

We will find that the cube model and the irregular cube model lead to results which are qualitatively very similar to the tetrahedron model (see Figs. 3.7 and 4.7). That can be rationalised by the fact that for not too irregular cluster arrangements, system dynamics depend to a large extend on the probability C_{12} for opening of a neighbour of an open cluster (see Eq. **3.25**). C_{12} crucially depends on the number of nearby clusters and the distances to them, and not so much on the detailed cluster arrangement farther away from it. Once an array of clusters in one part of the cells has been activated, the Ca^{2+} concentration is usually high enough to induce a global spike – configurations with intermediate numbers of open clusters are short-lived in realistic simulations (see Fig. 3.7).

Thus, we do not consider more complex cluster arrangements than the irregular cube model here, since it is unlikely that system dynamics would qualitatively change by this.

A delayed stochastic simulation algorithm (DSSA) is required for dynamic simulations

As mentioned above, the hierarchic stochastic model is non-Markovian, so that waiting-times between successive events are not exponentially distributed, and the standard method from Gillespie [77] cannot be applied. Therefore, a DSSA was developed, which is similar to those investigated in [13, 37, 179]. However, unlike those studies, the algorithm employed here (Fig. 3.6) does not draw random numbers from the waiting time distributions in advance to determine the transition times. Instead of that, it integrates stepwise over the distributions until the obtained value exceeds a random number drawn from the unit interval. The time is reset when a transition occurs. That procedure does not depend on drawing random numbers from non-uniform intervals, which is a numerically extensive task [79, 172]. Moreover, it can directly incorporate survival probabilities as analytical functions, and therefore it is very efficient for the purposes of this thesis (see below).

Typical simulations are shown in Fig. 3.7. The tetrahedron model and the cube model both reproduce spike sequences similar to experimental data for the same set of parameters. Ca^{2+} spikes (most clusters open) emerge from basal puff-activity (1 cluster open) at irregular intervals. Long-term simulations ($\approx 10^6$ s) are used to compute spike statistics and are in excellent agreement with the analytical solutions (see Tab. 3.2).

The presented DSSA is particularly efficient with input data expressed by analytical functions

The DSSA is particularly efficient if the integral of $\psi(c_j, t-\tau, x_j)$ in the above notation of the pseudocode is an analytic funtion. Then, at every time-step, instead of applying a subroutine for numerical quadrature, we only need to compute the value of the survival function

$$\Psi(c_j, t-\tau, x_j) = 1 - \int_{\tau}^{t} \psi(c_j, t', x_j) dt', \tag{3.28}$$

Data: Initial cluster states x_j; Transition probabilities $\psi(c_j, t-\tau, x_j)$; Transition types $\nu(x_j)$; Total simulation time T; Time step h.
Result: Dynamics of the configurations $S_i(t)$ indicating Ca^{2+} spikes

```
begin
    generate {U_k}_{k=1..N_cl} as U(0,1) random variables
    τ = 0; {P_k}_{k=1..N_cl} = 0
    while t < T do
        for (j = 1; j <= N_cl; j++) do
            if U_j > P_j:
                P_j+ = ∫_{t-τ}^{t-τ+h} ψ(c_j, t', x_j) dt'
            else:
                x_j = x_j + ν(x_j)
                generate {U_k}_{k=1..N_cl} as U(0,1) random variables
                τ = t; {P_k}_{k=1..N_cl} = 0
                break
        t=t+h
end
```

Figure 3.6: Pseudocode of the delayed stochastic simulation algorithm (DSSA). $U(0,1)$ random variables means random numbers drawn from a uniform distribution in the interval $(0,1)$. In our case, the type of the transition $\nu(x_j)$ is uniquely determined for each state (open if closed and close if open). Therefore, $\psi(c_j, t-\tau, x_j)$ is $\psi_o(c_j, t-\tau)$ or $\psi_c(t-\tau)$, depending on the actual cluster state x_j. In general, we would need a second random number to decide over the transition type, analogously to the original stochastic simulation algorithm from Gillespie [77].

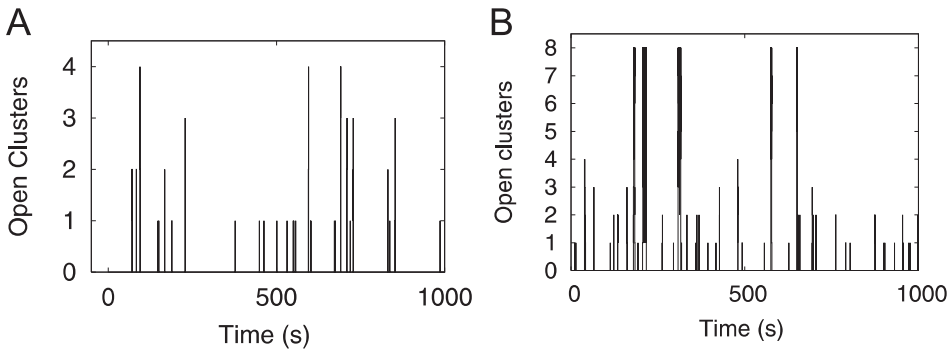

Figure 3.7: Stochastic simulations. The tetrahedron model (A) and the cube model (B) show similar spike patterns with the same set of parameters (Tab. 3.1, $\gamma = 25\ s^{-1}$). Calculations are performed with the delayed stochastic simulation algorithm (Fig. 3.6).

which gives us the probability that the present configuration survives until time t. We thus only need to check if

$$U_j > \Psi(c_j, t - \tau, x_j), \tag{3.29}$$

i.e. if the state survives even longer.

Integrals of the γ-distributions used for the opening transitions (Section 3.2) are incomplete Γ-functions, and integrals of exponentials as employed for the closing transitions (Eq. **3.3**) are exponentials again. Therefore, the described DSSA is very efficient in our case, and we can compute 10^6 s of simulated time of the tetrahedron model in minutes on a standard personal computer. Parameter-scans of the irregular cube model like shown in chapter 4 can be performed in 1-2 days. Note that for the tetrahedron model, it is still faster to compute the direct solution from Section 3.4.

Implementation of global feedback

In addition to the basic spike-generating mechanism described so far, Ca^{2+} spikes are modulated by global feedback processes from Ca^{2+} spikes to IP_3R dynamics. Such feedbacks arise e.g. by Ca^{2+}-dependent activation of kinases interacting with the IP_3R, or by store-depletion (see Section 2.1). We model global feedbacks by modification of the probability distribution for opening of the first cluster (i.e., for a puff), which up to now was described as a rate-process with puff-rate λ (see Section 3.2). With global feedback, the puff-rate dependends on the time elapsed since the last global spike:

$$\lambda = \lambda(t - t_{sp}). \tag{3.30}$$

Chapter 4 will provide details of that dependence (Eq. **4.1**), and it will show that global feedbacks shift both the slope and the intercept of the σ-T_{av} relation (Figs. 4.7 and 4.8). This section provides details of the implementation of that feedback.

The probability density for opening of the first cluster is $\psi_o(c_0, t - \tau)$, where $t - \tau$ denotes the time elapsed since the last state-change, and c_0 is the local resting Ca^{2+} concentration (see Section 3.1). $\psi_o(c_0, t - \tau)$ can be modeled by an

exponential distribution $\lambda \exp[-\lambda(t-\tau)]$, where the parameter λ is the puff-rate (Section 3.2). As stated in the context of Eq. **4.1**, the global feedback to this first opening probability can be applied by assuming a dependence of the puff-rate on the time elapsed since the last global spike, $t - t_{sp}$. Further, in the case of $\psi_o(c_0, \cdot)$, the last state transition which occured at time τ is always a transition from one to zero open clusters, so that we can identify τ with the time of the last puff, $\tau = t_p$, and $\psi_o(c_0, \cdot)$ depends on three different times: The actual time t, the time of the last puff t_p and the time of the last spike t_{sp}. These considerations lead to the following expression for the first opening time:

$$\psi_o(c_0, t, t_p, t_{sp}) = \lambda(t - t_{sp}) e^{-\int_{t_p}^{t} \lambda(t'-t_{sp})dt'}, \tag{3.31}$$

which can be evaluated analytically with the expression for $\lambda(t - t_{sp})$ given by Eqs. **4.1** or **4.2**.

From Eq. **3.31**, it is immediately clear that the formalism derived in Sections 3.3 and 3.4 is not applicable anymore, because therein, it was a prerequisite that state transitions depend only on time-differences between subsequent state-transitions. That is also evident from a physical point of view: Remembrance of the last occurence of a specific configuration is far stronger non-Markovian than just remembrance of the time of the last configuration change.

But for such reasons, we delveloped the DSSA presented in Tab. 3.6, which was tested against the analytic solutions for suitable test cases (Tab. 3.2). Indeed, that DSSA is particularly useful for applications such as Eq. **3.31**, because, rather than ψ_o, it requires the survival probability Ψ_o as input data (see Eqs. **3.28**-**3.29**). With global feedback the survival probability can be written as

$$\begin{aligned} \Psi_o(c_0, t, t_p, t_{sp}) &= 1 - \int_{t_p}^{t} \psi_o(c_0, t', t_p, t_{sp}) dt' \\ &= e^{-\frac{\lambda_0}{\xi}[\lambda_1(e^{-\xi(t_p - t_{sp})} - e^{-\xi(t-t_{sp})}) + \xi(t-t_p))}, \end{aligned} \tag{3.32}$$

where the second line applies Eq. **4.2**. Therefore, the only change to the pseudocode provided in Tab. 3.6 is that we remember the occurence of the last spike, in order to compute the expression given by Eq. **3.32**.

3.6 Summary

The concept of hierarchic stochastic modelling presented in this chapter naturally follows the emergent behavior of biomolecules (see Introduction). Our theory covers two transitions from lower to higher levels of emergence: First, waiting-time probability distributions describe the dynamics of cluster states, which emerge from rapid fluctuations of channel states. Remarkably, these probabilities are well described by simple two-parametric distribution functions (Section 3.2). And second, coupling of cluster dynamics generates cellular dynamics.

Three ways to compute cellular dynamics from the hierarchic stochastic model were presented: A non-Markovian Master Equation approach leading to a system of integral equations (Section 3.3); the assumptions made by Eq. **3.24** allowing for the application of birth-death processes (Section 3.4); and an efficient delayed stochastic simulation algorithm, which uses the survival probabilities of cluster states as input data (Section 3.5). Results for key stationary observables like sojourn probabilities and average and standard deviation of interspike intervals computed with the three methods are in excellent agreement (Tab. 3.2). Chapter 4 will show that the emerging cellular dynamics also can be described by simple distribution functions, which are the first-passage times describing Ca^{2+} spikes computed in Eq. **3.18**: Their stationary moments $\bar{\sigma}$ and $\bar{T}_{av}$, which were computed in Sections 3.4 and 3.5, obey a linear relation.

The modeling concept presented here is not only relevant in the context of Ca^{2+} signaling, but it can be applied to any system that consists of coupling of clusters of subsystems (see Introduction). Therefore, its analysis not only serves to prepare the more specific theoretical investigations in Chapter 4, but it is also relevant as a general new modelling framework with broad potantial applicability.

4 Model Predictions and Analytic Approximations

Ca^{2+} spikes have been extensively investigated, but the relation between puff characteristics and cellular signals has not been established yet. In particular, the conditions for spiking in terms of puff characteristics and spatial cluster arrangement remain unknown. Are typical spiking patterns, average interspike interval (ISI) and the cell type specific signalling determined by channel and cluster properties or are they the result of emergent behavior of the complete pathway? Here we use the model derived in the previous chapter (see Section 3.1 for a short version) to study these questions. Section 4.1 investigates how the spiking regime depends on cellular parameters. In Section 4.2, robustness properties of the Ca^{2+} signalling machinery are derived on the basis of the relation between average and standard deviation of interspike intervals. Finally, Section 4.3 proposes a simplified version of the model that can be introduced to larger signalling cascades in future research.

4.1 The Spike Pattern is Controlled by Cellular Parameters

There is no clear separation between a cellular spike and local events. In order to obtain nonetheless a criterium for the occurrence of a global spike, a release event is called a spike if more than three quarters of all clusters are open at the same time. Opening of fewer clusters defines a local event. Each spike starts with a puff, which corresponds to opening of a single cluster. It can cause a global spike, if the probability that more clusters open before itself closes is sufficiently large. The Ca^{2+} released by open clusters increases the propensity of other clusters to

open, as described in Figs. 2.5 and 3.1.

ISI distributions depend on the details of cluster dynamics, cluster arrangement and concentration dynamics

The probability to open early increases with the number of open clusters N_o (Fig. 4.1A). This characterises the properties of Ca^{2+} -induced Ca^{2+} release. The probability to open early increases also with the IP_3 concentration (Fig. 4.1B). The signal types puffs, spikes, bursting and over-stimulation shown in Fig. 4.1C were obtained by varying the IP_3 concentration (other parameters are given in Tab. 3.1). At low $[IP_3]$, only puffs occur. Spikes can be found with slightly higher $[IP_3]$. Increasing the IP_3 concentration further causes longer more frequent spikes and finally steady release at over-stimulation. This spectrum of signal types and their sequence with increasing $[IP_3]$ is in good agreement with experimental observations [67]. The model only considers puff properties characterised by distributions of opening and closing times of clusters and spatial coupling between clusters mediated by Ca^{2+} diffusion (Section 3.1). This means that the properties of these distribution functions are sufficient to generate a wide range of Ca^{2+} signals.

We are interested in particular in spike trains because of their function in signalling. Their average interspike interval T_{av} depends on the parameters of channel state dynamics and spatial coupling. Fig. 4.2 shows four dependencies: T_{av} decreases with increasing number of channels per cluster N_{ch} and $[IP_3]$, since the cluster open probability is proportional to N_{ch}, and it also increases with $[IP_3]$. Another important parameter for the cluster dynamics is the channel closing rate γ. The larger γ, the sooner a cluster closes, and the less likely a second cluster opens before closing of the first cluster. Therefore, T_{av} increases with γ. T_{av} depends also on the buffer concentration, the channel current and the density of Ca^{2+} pumps [66]. The IP_3- and buffer-dependencies are experimentally verified [67, 195]. The other parameters are difficult to measure, but the T_{av}-dependencies comply with current ideas on IP_3R regulation by Ca^{2+} and IP_3 [215]. T_{av} and the standard deviation of interspike intervals σ can also be modulated by changing the spatial arrangement of clusters [194].

With these dependencies of T_{av} on so many details and the usually observed cell

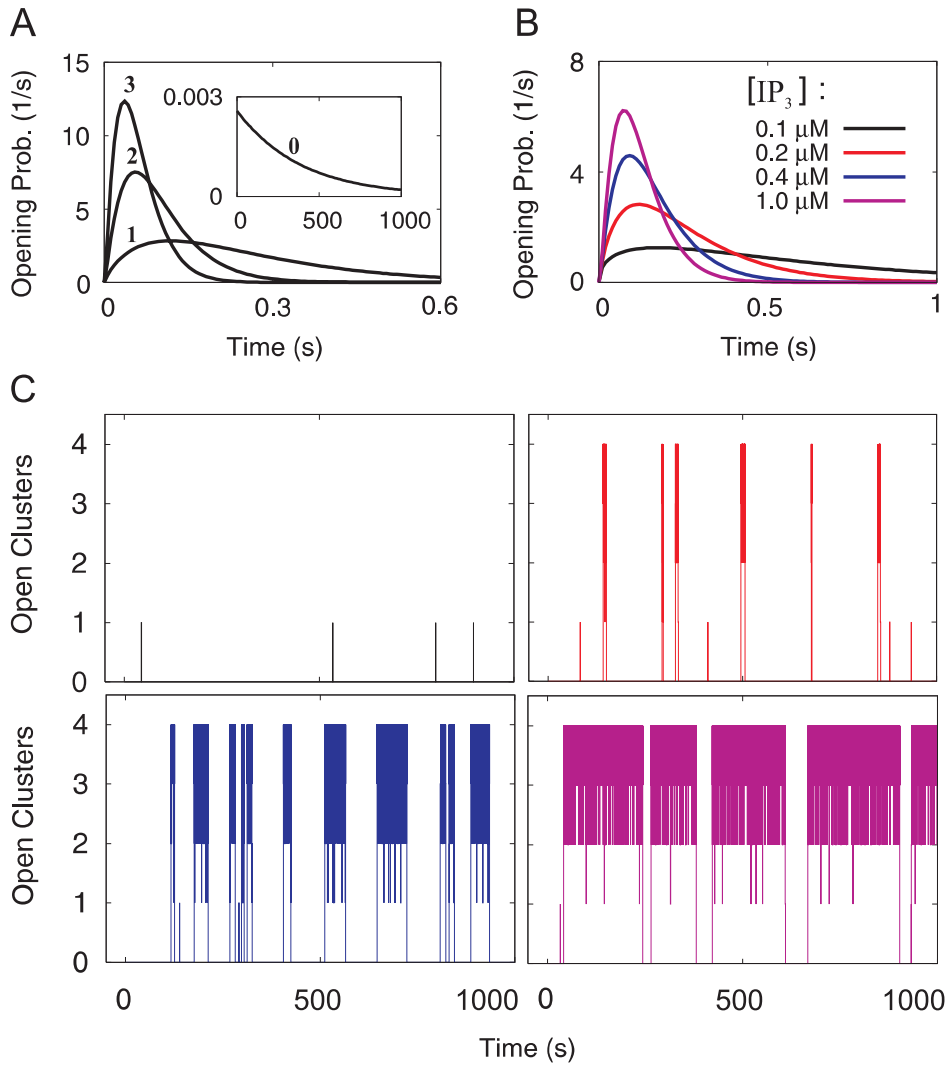

Figure 4.1: Various patterns of Ca^{2+} signals can be inferred from properties of single clusters. (A) Left: Waiting time distribution for the opening of a cluster in the rest state (0) and with $N_o = 1$, 2 or 3 clusters open. The probability to open early increases with N_o (number at lines). Since N_o determines $[Ca^{2+}]$, this corresponds to CICR. Right: Probability to open the second cluster at $[IP_3]$ as indicated. It is very unlikely that the second cluster opens before the first one closes with small $[IP_3]$. (B) Stochastic simulations reveal different types of Ca^{2+} signals at various $[IP_3]$, from top left to bottom right: Only puffs, spiking, bursting and over-stimulation. The colors indicate $[IP_3]$ as in B, p=3.85 s^{-1}. Parameter values not mentioned in this caption are given in Tab. 3.1.

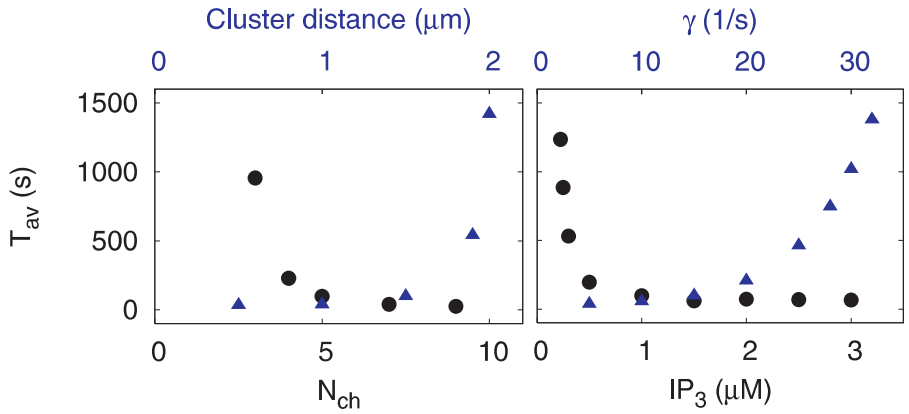

Figure 4.2: The average interspike interval T_{av} depends on cellular parameters. Here the left panel shows its dependence on the number of channels per cluster N_{ch} (black dots) and the cluster distance a (blue triangles), and on the IP_3 concentration (black dots) and the channel closing rate (blue triangles) in the right panel. Other parameters are given in Tab. 3.1.

variability even within one cell type, how can cells actually maintain the ability of spiking and frequency encoding at all? Many control processes converge on Ca^{2+} signalling [26, 27, 215]. Why does their combined action not destroy the ability to spike rather than controlling it? These parameter dependencies also pose questions for typical properties: With T_{av} and signal forms depending so sensitively on parameters which vary greatly among cells of a single cell type, which features of Ca^{2+} spiking could actually characterise a pathway or cell type? We will see below that a property of the system, which is called *functional robustness* here, suggests answers to these questions, and that the relation between T_{av} and σ is pathway specific.

The spike pattern is determined by cluster coupling

Intracellular Ca^{2+} signals are initiated by puffs, which eventually evoke opening of nearby clusters and induce a global spike, and in the case of over-stimulation may cause sustained increases in the global Ca^{2+} concentration. These transitions are well established by experiments (Section 2.1), and they can be reproduced by the model presented here (Fig. 4.1). How can we describe those transitions mathematically, and is there a universal criterion for the spike pattern as a function

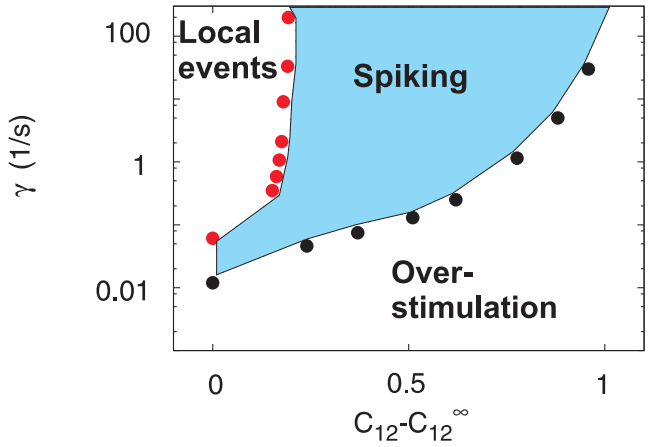

Figure 4.3: Cluster coupling controls the spike pattern. The coupling $C_{12} - C_{12}^{\infty}$ is defined as the probability to open a second cluster by diffusive coupling before the first one recloses (Section 3.1). The channel closing rate γ is a molecular property of the IP_3R and therefore constant. Spiking is defined by an average interspike interval lager than zero, a finite average spike length and a not too large number of local events between two spikes (see text for details). The blue area indicating the spiking regime was chosen by visual inspection of the long-T_{av} criterion (red circles) and the short-T_{av} criterion (black circles).

of important parameters like stimulation strength (IP_3 concentration) or cluster arrangement?

Ca^{2+} spikes result from a cascade of single cluster opening events, where by Ca^{2+} diffusion from each open cluster, the opening probability of those still closed is enhanced. This suggests spatial coupling to be a good indicator for spiking. In order to quantify spatial coupling, we define its strength as the probability C_{12} that the first open cluster opens another one before reclosing itself (see Eq. **3.2** in Section 3.1). To obtain a value relating to coupling, we have to subtract the probability C_{12}^{∞} that two uncoupled clusters very far apart open incidentally at the same time: $C_{12} - C_{12}^{\infty}$. The channel closing rate γ is the most important parameter determining T_{sl}, rendering it also a good spike regime indicator.

Indeed, the spiking regime is essentially determined by the cluster coupling $C_{12} - C_{12}^{\infty}$, as shown in Fig. 4.3. However, to obtain that graph, we first need sound criteria for the possible regimes of cluster dynamics in the model (Fig. 4.1). Since we are dealing with a stochastic system, the transitions between the four regimes local events, spiking, bursting and overstimulation (Fig. 4.1) are continuous, and

we cannot expect to find sharp criteria separating them. An intuitive definition of spiking is that the average interspike interval T_{av} is larger than the average spike length T_{sl}, with not too many local events per spike – a realistic value would be in the order of 20 [67]. Since we are more interested in the transitions to the extreme cases puffs and over-stimulation, the transition from spiking to bursting is not considered in detail here, but rather a general spiking regime. An appropriate criterion to separate spiking and bursting would be something similar to $T_{av} < T_{sl}$.

At over-stimulation, T_{av} tends to zero. The condition applied here is $T_{av} < 0.01\ T_{sl}$. The boundary from spiking towards local events can be defined by a maximal average number of local events in between two spikes. With the DeYoung-Keizer model at resting $[Ca^{2+}]$ c_0, opening of the first cluster is governed by an exponential waiting-time distribution (Appendix A.1). That means, puffs are generated by a process well described by a single puff-rate $\lambda_0 = \lambda_0([IP_3],N_{ch},c_0)$. The average interpuff interval of the cell is then $T_0 = (N_{cl}\lambda_0)^{-1}$. The average interspike interval is proportional to T_0, i.e., $T_{av}=\tilde{T}_{av}T_0$ and $\tilde{T}_{av}$ does not depend on λ_0. We limit spiking towards long T_{av} (i.e., towards local events) by the condition $\tilde{T}_{av}<50$.

The ranges of γ and $C_{12} - C_{12}^{\infty}$ for which spiking occurs are shown in Figs. 4.3 and 4.4. Fig. 4.4A shows spiking conditions with 4 clusters on a tetrahedron and 8 clusters on a cube. The red symbols show the critical values for the long-T_{av} criterion C_l, the black ones the values for the short-T_{av} criterion C_s. The C_l-values with 4 and 8 clusters are all quite close to each other. Spiking disappears for 4 clusters, 8 clusters and a large range of γ-values within a narrow range of coupling, because T_{av} increases steeply there with decreasing $C_{12} - C_{12}^{\infty}$.

The short-T_{av} criterion entails different C_s-values for the 4- and 8-cluster systems. C_s is smaller for 8 clusters than for 4 clusters. The essential dependence on the number of clusters N_{cl} seems to be exponential, since the N_{cl} th root of the critical values ${C_s}^{1/N_{cl}}$ is very similar for 4 and 8 clusters, as shown in Fig. 4.4B. The experimentally relevant γ values are about 60 s^{-1} [196]. Hence, about 0.8 is the short-T_{av} critical value for ${C_s}^{1/N_{cl}}$ and about 0.18 is the long-T_{av} critical value C_l. Note that these values do not depend on how we change coupling. The critical values are very similar for different numbers of channels per cluster N_{ch}, particularly for $\gamma > 1$ s^{-1}, which includes the range of realistic values around 60 s^{-1} (Fig. 4.4C). In this sense, ${C_s}^{1/N_{cl}}$ and C_l are universal for the systems investigated

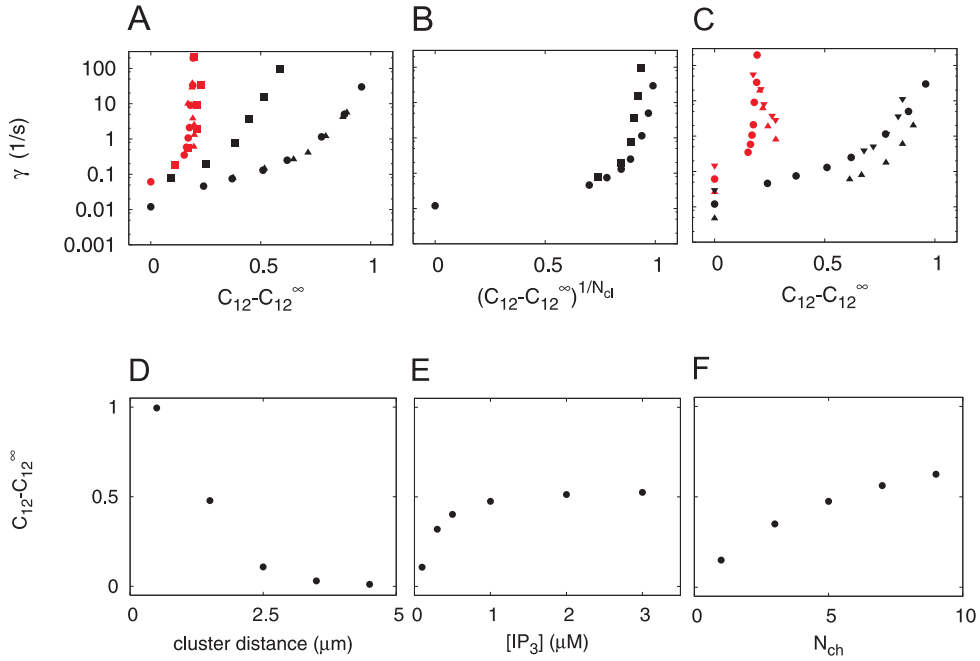

Figure 4.4: Detailed analysis of the spiking regime. (A) Spiking occurs for values of the coupling $C_{12} - C_{12}^{\infty}$ and channel closing rate γ between the red and black symbols (cf. Fig. 4.3). Both the four cluster model (squares) and the eight cluster model (circles) are investigated here. Spiking is defined by a long-T_{av} criterion (red) and a short-T_{av} criterion (black), respectively (see text). Each pair of squares and circles indicates the critical $(\gamma, C_{12} - C_{12}^{\infty})$, while coupling was changed by varying cluster distance (values range from 0.5 μm to ∞). The triangles show the critical values for the four cluster model obtained when we varied $C_{12} - C_{12}^{\infty}$ by changing $[IP_3]$. That leads to very similar results. (B) C_s depends essentially exponentially on N_{cl}, since the $N_{cl}th$ root of C_s is similar for the four cluster model (squares) and the eight cluster model (circles). (C) The spiking criterion is not much effected by the number of channels per cluster N_{ch}, at least for $\gamma > 1$ s^{-1}. Shown is the four cluster model with N_{ch}=3 (upper triangles), N_{ch}=5 (squares) and N_{ch}=9 (lower triangles). (D-F) The cluster coupling $C_{12} - C_{12}^{\infty}$ depends on various system parameters like cluster distance, $[IP_3]$ and the number of channels in a cluster N_{ch}.

here. It can be expected that this universality applies beyond these systems – how far has to be elucidated by future research.

The main conclusion from the preceding analysis is that the spiking regime is essentially determined by the cluster coupling (Fig. 4.3 – an emergent parameter that itself is controlled by system parameters like cluster distance, $[IP_3]$ or N_{ch}. The spike pattern also depends on the channel closing rate γ, but that is a molecular property of the IP_3R : γ should merely depend on the ratio of different IP_3R isotypes expressed in the cell, which is rather constant for a given cell type [211]. Thus, it seems that the cell can control the spiking regime in many different ways, another possibility not considered here are Ca^{2+} buffers – but they all converge to a single macroscopic variable, the cluster coupling.

4.2 The σ-T_{av} Relation Reveals Functional Robustness and Adaptivity

Because we are dealing with a stochastic system, it is not sufficient to consider average values only. We need to include higher moments of the Interspike Interval (ISI) distribution in the description. The average ISI decreases upon stimulation. But the standard deviation needs to decrease also in order for a typical frequency to exist. That is warranted for Ca^{2+} spiking by the existence of a relation between the average ISI T_{av} and the standard deviation σ and its course from large σ and T_{av} to small σ and T_{av}. That relation is a property of the Ca^{2+} spiking mechanism. It does not exist for all spike-generating systems (see below). As a main result of this thesis, this section will show that the σ-T_{av} relation of the hierarchic stochastic model is functionally robust and adaptive to specific needs at the same time. These model predictions will be verified by single-cell experiments presented in Chapter 5.

Biological function can be studied with the σ-T_{av} relation of interspike intervals

Ca^{2+} signalling uses a variety of modes of information transmission (see Section 2.1). Frequency encoding [57, 121, 175] is the mode which is relevant in the context here. How can stochastic sequences comply with this function of the pathway? What determines the information content of a random sequence of spikes, and how should interspike interval (ISI) distributions respond to a stimulus?

Ca^{2+} spike-sequences are random [67, 195], and they are part of carefully regulated signal transduction pathways depending on reliable signals at each step [27]. Therefore, we need to consider the conditions for the ability of Ca^{2+} spikes to transmit information. The maximal information content of a given spike sequence is a measure for how statistically different it is from the 'most random sequence', i.e., a pure Poisson Process. If the maximal information content is larger than 0, downstream parts of the Ca^{2+} pathway have in principle the possibility to distinguish the given sequence from a Poisson Process. The Kulback Entropy of the given sequence relative to a Poisson Process is a measure for the statistical difference [82].

The Kulback Entropy for spike-sequences obeying linear σ-T_{av} relations was calculated in ref. [192]. It depends essentially only on the slope of that relation, which equals 0 for a slope of 1 and increases for decreasing slope. Cells exhibiting stimulated spike trains have a smaller slope and larger maximal information content than spontaneously spiking cells [192, 195]. We conclude that the slope of the σ-T_{av} relation is one of its properties relevant for biological function.

ISI distributions should respond to a stimulus by moving to smaller average ISIs in order to obtain a change of the average frequency. The stimulated signal should also be detectable, i.e., there should be a typical frequency at which the spectrum of the stimulated ISI sequence should have a peak as sharp as possible. That requires a small standard deviation of the ISI sequences. *A priori*, a stochastic system with as many parameters as Ca^{2+} signalling could respond in different ways to stimulation, as sketched in Fig. 4.5. But only the response along the black arrow from large T_{av} and large σ to smaller T_{av} and smaller σ meets both requirements that T_{av} and σ decrease upon stimulation. A series of earlier

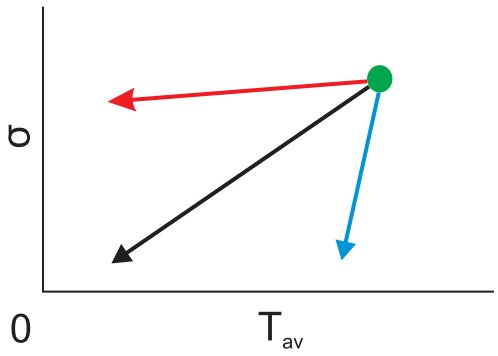

Figure 4.5: Caricature of different responses of a cell to stimulation. Before stimulation, the cell has values of σ and T_{av} as indicated by the green dot. The arrows indicate the transitions to the values assumed upon stimulation. The red transition would provide for a change of the average ISI, but would not decrease the standard deviation σ. The spectrum of that stimulated ISI sequence would be very broad and the spike train would not have a typical frequency anymore. The blue transition would correspond to a typical frequency after stimulation, but would not change the average ISI substantially. The black transition does change the average ISI and leads to a typical frequency. A response of the cell to stimulation along the black arrow corresponds to σ-T_{av} relation of Ca^{2+} signaling and the requirements for frequency encoding.

experimental studies [195] and single-cell measurements contained in this thesis (see Fig. 5.4) show that Ca^{2+} signalling exhibits this response, and that warrants its biological function.

The described response of Ca^{2+} signalling to stimulation does only live up to the requirements for a universal signalling mechanism if it is a property of the mechanism and not only of individual cells. Stimulation is, in mathematical terms, a change of parameter values. One way of guaranteeing a specific response of T_{av} and σ to parameter changes is the existence of a well-defined σ-T_{av} relation for the mechanism. If such a relation exists, changes of parameters only shift the position of the cell on the relation and do not move it to a position in the σ-T_{av} plane away from it. In experiments, the existence of such a relation means that all cells using the mechanism align along the relation, independent of their individual parameter values, and do not scatter all over the σ-T_{av}-plane. It is also obvious that the most robust case, where changes of the values of all parameters do not move a cell away from the relation, will not exist in general. Changes of the values of some

parameters will do so, and changes of the values of others will not.

Hence, the fact of the existence of a well-defined σ-T_{av} relation is important for pathway function. The experimental relations shown in ref. [195] and Fig. 5.4 are obtained by plotting the average and standard deviation from many different cells (population relation). The individual cells are different with respect to the value of many parameters like number of clusters, spatial cluster arrangement, concentrations of Ca^{2+}-binding proteins, volume, ER content, etc. but nonetheless they align along a linear function. Individual σ-T_{av} relation have been obtained in earlier studies by conducting two or more different experiments with the same cell [195]. They showed agreement between the slope of the individual σ-T_{av} relation and the population relation. Therefore, the experiments proof the existence of a well-defined σ-T_{av} relation.

Although the existence of a well-defined σ-T_{av} relation is not guaranteed in general, it might be a property of all spiking systems. That is not the case, however, as could be illustrated by calculations of σ and T_{av} for the perfect integrate and fire model, which is one of the prototypical spike-generating systems in neuronal membrane dynamics [193]. Upon variation of parameters in that model, the data points occupy an area in the σ-T_{av}-plane and do not align along a single curve as they do for the Ca^{2+} signalling model (see Fig. 4.6 below). Consequently, there are spike generating mechanisms which exhibit a σ-T_{av} relation, and there are mechanisms which do not.

In summary, the existence of a σ-T_{av} relation, the slope of the relation and the fact that its course is from large σ and T_{av} to small σ and T_{av} are all relevant for the biological function of the pathway. An important research objective of this thesis is to investigate the robustness of these properties.

The σ-T_{av} relation has more useful properties. It reveals the general type of the stochastic process: The linear relation obtained here means that signals become more precise at higher stimulation. Further, it indicates the existence of feedbacks (see below) and the information content. Thus, simple spike train measurements with a group of cells can provide information on the pathway properties. Last but not least, the σ-T_{av} relation is a good representation of experimental results with groups of cells of the same cell type. Typically, the spread of T_{av} values obtained from one sample of cells in a single experiment is large [195], since T_{av}

depends on the details of cluster size, dynamics and arrangement (see Fig. 4.2). The same applies to the relation between stimulation strength and spiking frequency. Both characteristics are strongly affected by cell variability, and therefore they are sample specific to some degree. The σ-T_{av} relation does not have that drawback.

The σ-T_{av} relation of the hierarchic stochastic model is robust to changes of cluster coupling

The σ-T_{av} relation can be calculated analytically for the tetrahedron model and by stochastic simulations for larger cluster arrangements, as described in Chapter 3. The relation is almost linear (Fig. 4.6), as expected from experimental observations (see Chapter 5 and ref. [195]). Apart from a small range at small T_{av}, the slope of the σ-T_{av} relation is always 1 in the Ca^{2+} model presented in Chapter 3.

The cluster distance affects the minimal interspike interval T_{min}, which was defined as the smallest T_{av} observed in a set of simulations (Inset of Fig. 4.6). It is in the range of the average interpuff interval of about 10 s for strong coupling at cluster distance $a = 1.5$ µm and about 80 s for weak coupling at $a = 5$ µm. This range is similar to values measured in astrocytes, microglia, PLA and HEK cells [195], SH-SY5Y cells [197], pancreatic acinar cells and airway smooth muscle cells [200]. Remarkably, we observe a T_{min} larger than 0 although the model did not assume an absolute refractory period. That suggests that refractoriness can be achieved simply by the geometry of the cluster arrangement, without a strict inhibitory state of Ca^{2+} channels, which is assumed in many Ca^{2+} models [67].

Nevertheless, neither the cluster distance, nor any other of the model parameters, could change the slope of the σ-T_{av} relation. The model presented here describes the properties of individual clusters and their coupling in its current state. Remarkably, the model generates a slope equal to 1 for all parameter values in the spiking regime – that also holds for larger cluster arrangements like the cube model and even for the irregular cube model (Fig. 4.6). That means, the slope is robust with respect to changes of cluster coupling, since the model parameters act by regulation of the cluster coupling (Fig. 4.4). However, it was shown experimentally that the slope of the σ-T_{av} relation can be smaller than 1 even for

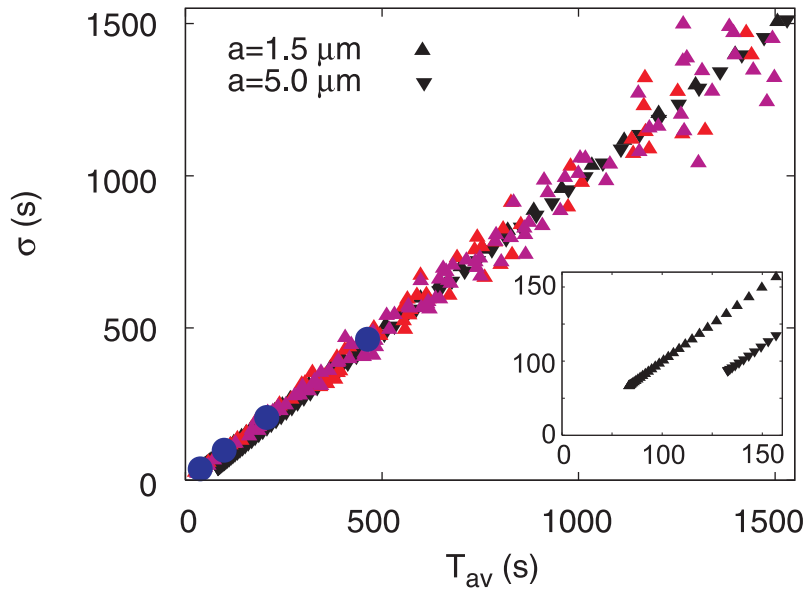

Figure 4.6: The slope of the σ-T_{av} relation is robust to changes of cluster coupling. Each symbol represents a single model simulation with a specific set of system parameters. Upper triangles: cluster distance $a = 1.5$ µm; lower triangles: $a = 5$ µm ; black symbols: tetrahedron model; red symbols: regular cube model; pink symbols: irregular cube model; blue circles: analytical solution of the full model (see Section 3.3) for the tetrahedron model with $a = 1.5$ µm. σ-T_{av} relations were obtained by variation of the channel closing rate γ, parameters not mentioned here are given in Tab. 3.1. The slope of the relation is always one, regardless which model parameters are varied. The inset shows that variation of the cluster distance changes the minimal interspike interval T_{min}.

large values of T_{av} [195]. Therefore, a realistic Ca^{2+} model should reproduce a slope smaller than one in a realistic parameter regime – it seems that something is missing in the model presented so far.

Global feedback tunes the σ-T_{av} relation for specific needs of the signalling pathway

Measured ISI-distributions have been successfully described by the ansatz of a delayed exponential distribution [192, 195]. It introduces a process of recovery from a global negative feedback upon a spike. The feedback is imposed on all clusters in difference to coupling between clusters by Ca^{2+} diffusion, the spatial range of which is much shorter than the cell size. The negative feedback might be realised *in vivo* by desensitisation G-protein coupled receptors (Fig. 2.4 and ref. [216]), by depletion of the endoplasmic reticulum, via the Ca^{2+}-dependence of IP_3-3-kinase [27, 60], or by other feedbacks [104, 216] decreasing puff probability or amplitude.

In order to be consistent with these experimental studies, the same description of recovery from global negative feedbacks is used here. It is introduced in the model as a slow rise of the opening probability for the first cluster opening from 0 just after a global spike to an asymptotic value λ_0 (see Section 3.5):

$$\lambda(t - t_{\mathrm{sp}}) = \lambda_0(1 - e^{-\xi(t-t_{\mathrm{sp}})}), \tag{4.1}$$

with t_{sp} denoting the time of the last spike and ξ the recovery rate. Figure 4.7A shows that the slope of the σ-T_{av} relation decreases for decreasing values of ξ, and that the non-linear behavior at small T_{av} is more pronounced. It can be concluded that global negative feedback can change the slope of the σ-T_{av} relation, while properties of individual clusters and their coupling can not. Slopes smaller than 1 are a result of emergent behavior, or in other words a property of the whole pathway, but not a consequence of properties of individual clusters.

The σ-T_{av} relation is robust against a wide range of changes of the values of parameters describing the properties of clusters, their spatial arrangement and the coupling strength. These entail for instance the rates of channel closing and

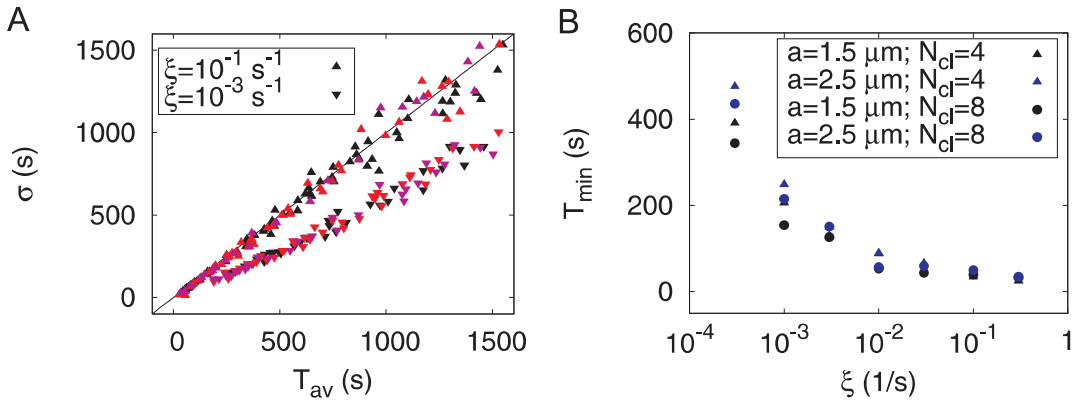

Figure 4.7: The σ-T_{av} relation can be adapted by global feedback. (A) Modification of the σ-T_{av} relation by the delayed puff rate given by Eq. **4.1**. For moderate values of T_{av}, the slope of the σ-T_{av} relation decreases with ξ (upper triangles: $\xi = 0.1$ s^{-1}; lower triangles: $\xi = 10^{-3}$ s^{-1}). The relations are identical for the four cluster model (black), the eight cluster model (red) and the eight cluster model with randomly shifted vertex positions (pink). (B) The minimal ISI T_{min} increases with decreasing ξ. The four cluster model has longer T_{min}s than the eight cluster model. T_{min} has been identified with the smallest observed T_{av} when γ is modified in simulations.

puff nucleation, and the cluster distance, the position of clusters, the number of clusters, the number of channels per cluster and the buffer concentration (see Fig. 4.7 and ref. [194]). Varying the values of these parameters does not change the curve describing the dependence of σ on T_{av}. But they determine T_{av}, as we have seen above. Hence, they determine the position of a cell on the σ-T_{av} relation and can be used to control the average spiking frequency.

If the position on the σ-T_{av} relation of the cell without stimulation is at large or infinitely large T_{av}, it can move to smaller T_{av} by stimulation or by other reasons like rearranging channels and clusters. Indeed, clustering in cells is a dynamic process [71, 209, 210, 242]. During this control of spiking, the positive slope of the σ-T_{av} relation and the existence of the minimal interspike interval guarantee that faster spiking is also more regular despite the stochastic character of spike generation. The minimal interspike interval T_{min} is another property of the σ-T_{av} relation affected by the global recovery process (Fig. 4.7B). It increases with decreasing recovery rate ξ.

We have seen that the slope is controlled by global feedback (Fig. 4.7). In

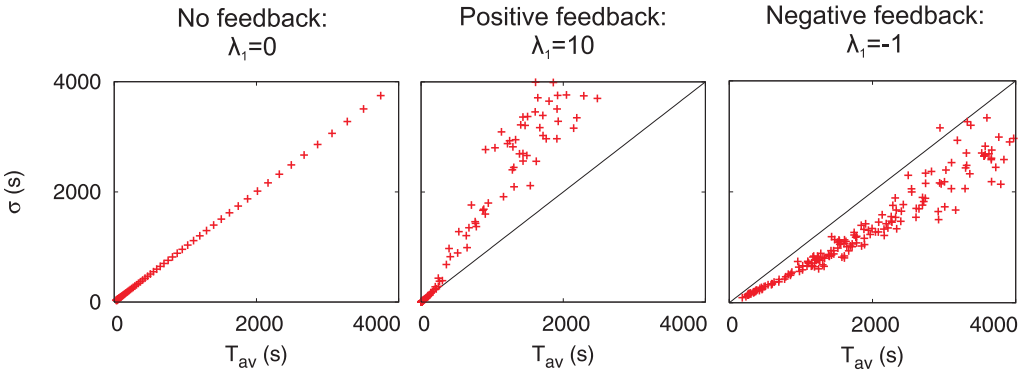

Figure 4.8: The type of global feedback shapes the σ-T_{av} relation. Symbols are single calculations of the tetrahedron model (Section 3.4) with global feedback according to Eq. **4.2** (see text for details). σ-T_{av} relations were obtained by variation of the channel closing rate γ, the recovery rate was $\xi = 10^{-3}$ s^{-1}, other parameters are given in Tab. 3.1.

those calculations, only negative feedback was considered, because that results in the slope smaller than 1 typically observed in experiments (see Chapter 5 and ref. [195]). A more genereal form of Eq. **4.1** is

$$\lambda(t - t_{sp}) = \lambda_0(1 + \lambda_1 e^{-\xi(t-t_{sp})}), \tag{4.2}$$

where λ_1 sets the type of the feedback. $\lambda_1 > 0$ means positive feedback, resulting in a slope larger than one (Fig. 4.8). As mentioned earlier, such a signal with slope larger than one in the σ-T_{av} relation can also transmit information.

Conclusion

The analysis presented in this section has shown that the σ-T_{av} relation of Ca^{2+} signals is robust to changes of cluster coupling and that it can be adapted to specific needs by global feedback. Robustness of the σ-T_{av} relation corresponds to *functional robustness* of the system: Parameters which modify T_{av} and therewith the transmitted signal do not determine the general statistical properties contained in the σ-T_{av} relation. That guarantees system function, which in this case is signal transmission with well-defined noise characteristics. Adaptivity by global feedback processes illustrates a way how system function can be fine-tuned to the specific needs of the cell-type. Robustness of function and adaptivity are key properties

that can be expected from a versatile signalling mechanism like Ca^{2+} dynamics – the present analysis shows that they are by no means contradictive to a stochastic mechanism with large variability (see Chapter *Discussion*).

4.3 Analytic Approximations of Model-Dependencies on Cellular Parameters

The hierarchic stochastic model presented in this thesis was designed to employ probability density distributions for cluster opening $\psi_o(c, t-\tau)$ as input data (cf. Chapter 3). While the closing probabilities ψ_c can be assumed to be governed by a simple formular for our purposes, the opening probabilities ψ_o need to be computed from single-channel models (or can potentially be measured directly), and are subsequently fitted to γ-distributions or exponential distributions (see Section 3.2). That procedure is rather laborious for parameter-scans like those shown in Fig. 4.2, especially when dealing with large systems like the irregular cube model (Section 3.5). Moreover, it lacks an analytic dependence of the input data on cellular parameters, which would be needed to integrate the hierarchic stochastic model into larger signalling cascades. Therefore, this section seeks to develop an analytic approximation for the dependence of ψ_o on the cellular parameters cluster distance, IP_3 concentration and number of channels per cluster.

As mentioned before, the input data have the form of γ-distributions or exponential distributions, and therefore an analytical description is required for the parameters α and β of the γ-distributions or the parameter λ of the exponential distributions (see Section 3.2). We found that the α-dependence on all parameters can be described by a Hill equation,

$$\alpha(x) = \frac{V_x x^{n_x}}{K_x^{n_x} + x^{n_x}} + 1, \quad x{=}Ca^{2+}, \text{ } IP_3 \text{ or } N_{ch}. \tag{4.3}$$

The second term in Eq. **4.3** ('+1') reflects the fact that γ-distributions change shape at $\alpha < 1$. For β, a power-law-like dependence on the parameters up to a

base-level was observed, which can be approximated by the function

$$\beta(x) = \frac{1}{A_x x^{m_x}} + B_x, \quad x{=}\mathrm{Ca}^{2+},\ \mathrm{IP_3}\ \text{or}\ \mathrm{N_{ch}}. \tag{4.4}$$

Variation of the cluster distance only causes variation in the Ca^{2+} concentration arising by opening of adjacent clusters, while the base-level $[Ca^{2+}]$ is unaffected, and with it the puff-rate λ. Thus, λ only changes if $[IP_3]$ or N_{ch} are modulated. We find that the behaviour of λ differs between the two types of stimuli: The dependence of the puff-rate on the IP_3 concentration has the form of another Hill plot, and λ is proportional to the number of channels per cluster:

$$\lambda(p) = \frac{V_{p,\lambda} p^{n_{p,\lambda}}}{K_{p,\lambda}^{n_{p,\lambda}} + p^{n_{p,\lambda}}}, \quad \lambda(N) = a_{N,\lambda} N, \tag{4.5}$$

where p and N denote $[IP_3]$ and N_{ch}, respectively.

Figure 4.9 shows fits to α, β and λ computed for several values of each of the system parameters Ca^{2+}, IP_3 and N_{ch}, while the other parameters are kept constant. The fits are surprisingly good, with exception of the β-dependence on the Ca^{2+} concentration, which cannot reflect the slow decay for high values of Ca^{2+} , since Eq. **4.4** tends to the constant B_x for $x \to \infty$. But this is not too problematic, since $[Ca^{2+}] > 1$ µM appears only at very small cluster distances of ≤ 1 µm (see Eq. **3.7** and ref. [221]).

Variation of the cluster distance requires only the set of fitting parameters needed to approximate the $[Ca^{2+}]$-dependence of ψ_o at standard parameters, which are given as an example in in Tab. 4.1. Modulation of $[IP_3]$ or N_{ch} causes variation of ψ_o at all system configurations with at least one channel cluster yet to be opened. The configurations differ in the local Ca^{2+} concentration at which ψ_o is computed, and therefore also the fitting parameters are different in each configuration and have to be determined separately. Appendix A.3 provides the information needed for variation of the puff-rates λ and of the parameters α and β in response to modulation of $[IP_3]$ and N_{ch}, at all configurations of the tetrahedron model (see Section 3.4).

The described fittings of analytical functions to computed opening probabilities ψ_o at verying cellular parameters provide all the information needed to perform

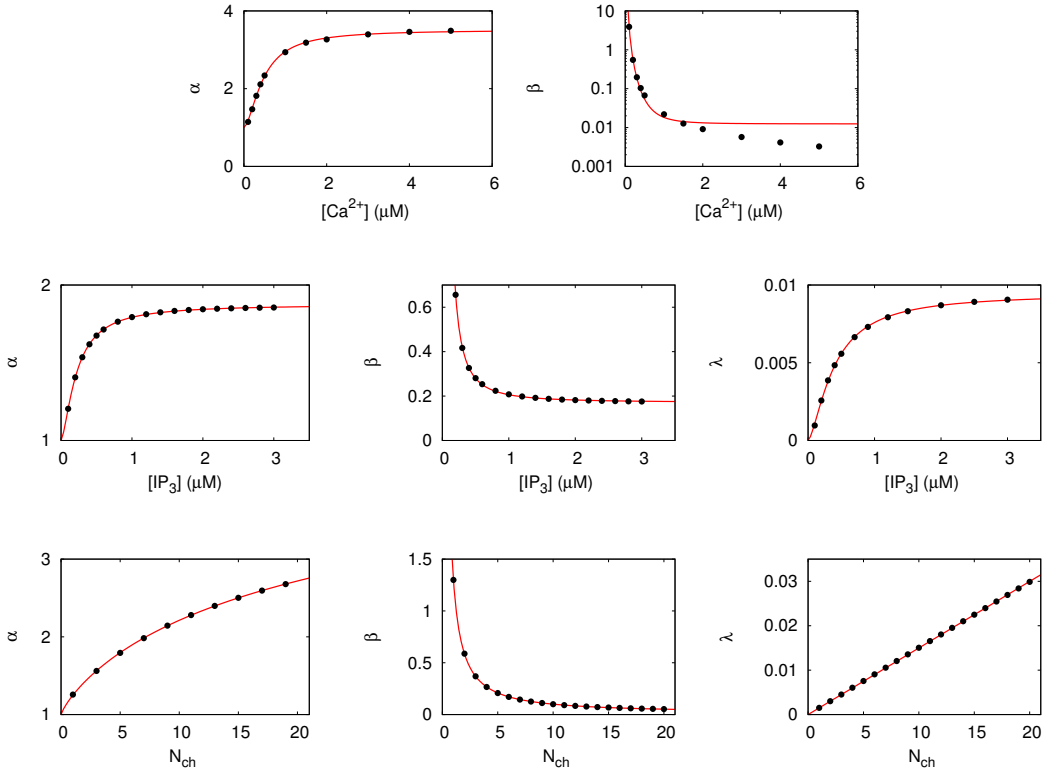

Figure 4.9: Analytic approximations of parameter dependencies of the opening probabilities ψ_o. Circles are fittings of results from the De Young-Keizer model to γ-distributions with parameters α and β or to exponential distributions with parameter λ (see Section 3.2). The calculations were performed at standard parameter values (Tab. 3.1) and the value indicated at the x-axis. Concerning the Ca^{2+} concentration in the curves with IP_3 and N_{ch}, the γ-distributions were computed at $[Ca^{2+}]$ resulting from the standard cluster distance (see Eq. 3.7), and the exponential distributions were computed with the standard base-level $[Ca^{2+}]$. Lines are nonlinear fits to Eqs. 4.3-4.5, determining the fitting parameters shown in Tab. 4.1 and Appendix A.3. Those relations and fitting parameters serve as analytic approximations of the hierarchic stochastic model, which might be applied to simulate larger signalling cascades in future research (see text for details).

Table 4.1: Fitting parameters for approximated analytic opening probabilities ψ_o near standard parameter values (Tab. 3.1). Values are shown with the standard error resulting from curve fitting with the software package gnuplot. This table shows only the values of fitting parameters approximating the Ca^{2+}-dependence of the hierarchic stochastic model, which can be used for simulations with varying cluster distance (the index c stands for $[Ca^{2+}]$). Parameters needed for variation of $[IP_3]$ and N_{ch} are given in Appendix A.3.

Parameter	**Symbol**	**Value**	**Unit**
α at saturating $[Ca^{2+}]$	V_c	2.41 ± 0.030	
half-saturation constant for $\alpha([Ca^{2+}])$	K_c	0.45 ± 0.010	μM
hill coefficient for $\alpha([Ca^{2+}])$	n_c	1.78 ± 0.049	
power-law coefficient of $\beta([Ca^{2+}])$	A_c	226.3 ± 5.67	μM^{-1} s
base-level of $\beta([Ca^{2+}])$	B_c	0.031 ± 0.010	s^{-1}
scaling exponent of $\beta([Ca^{2+}])$	m_c	2.94 ± 0.008	

calculations of the hierarchic stochastic model with approximative analytic input data. Fig. 4.10 shows that the accuracy of the analytic approximation is quite convincing near standard parameter values. Therefore, Eqs. **4.3**-**4.5** can serve as analytical approximations of ψ_o as computed from the De Young-Keizer model, in dependence on the parameters that appear therein (Ca^{2+}, IP_3 and N_{ch}) – at least if we are not too much interested in the effect of simultaneous changes of them. Computation of the dependence of T_{av} on parameters for small intervals, e.g., is much more convenient by Eq. **4.3** than by individual fits of all required opening probabilities to γ-distributions.

Analytic dependencies of input data on cellular parameters are not only more appropriate for analyses of parameter spaces than discrete computations of input data for every set of cellular parameters – especially when dealing with larger models and more complicated cluster arrangements than the tetrahedron model (see Section 3.5). Most importantly, analytic dependencies are required to integrate the hierarchic stochastic model into larger signalling cascades. There, cellular parameters like the IP_3 concentration are not constant input data, but rather intermediate model variables, which are subject to feedback processes controlling pathway properties (see Sections 2.1 and 4.2).

It is intended to perform such integrated model simulations in future research, and for that purpose the described approximative analytic dependeces of input data on cellular parameters are an important first step.

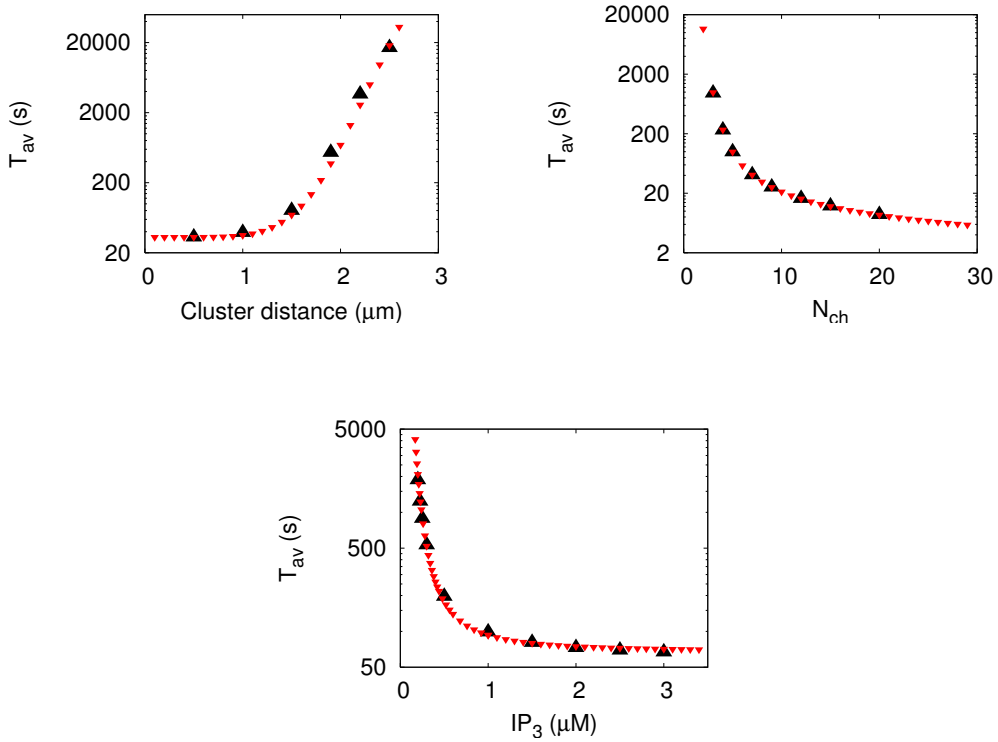

Figure 4.10: Comparison of T_{av} computed with the De Young-Keizer model and with approximated analytical opening probabilities ψ_o. Upper triangles are replotted from Fig. 4.2. Lower triangles are computed by the analytic expressions of the hierarchic stochastic model (see Section 3.4), with opening probabilities ψ_o computed by Eqs. **4.3**-**4.5**, with fitting parameters given in Tab. 4.1 and Appendix A.3. The plots show that in model simulations near standard parameter values (Tab. 3.1), the analytic approximations are in good agreement with the originally used opening probabilities ψ_o described in Section 3.2.

4.4 Summary

The first part of this thesis presents a theory which is able to calculate the characteristics of cellular Ca^{2+} signals from puff property distribution functions, cluster arrangement and - if it applies - an additional description of a global feedback process. That theory reproduces spike patterns arising at quite different experimental conditions despite the rather simple mechanisms (Ca^{2+}-induced Ca^{2+} release and Ca^{2+} diffusion) it is based on. The spike pattern is solely controlled by the spatial coupling of clusters, which is determined by the combined action of system properties ($[IP_3]$, N_{ch}, N_{cl}, etc.).

Most importantly, the σ-T_{av} relation, a new description of cellular systems with huge cell-to-cell variability, is robust to changes of spatial coupling, but can be adapted by global feedback. Such feedbacks from cellular Ca^{2+} release events (Ca^{2+} spikes) to Ca^{2+} channel dynamics are realised by pathway elements like phosphorylation of IP_3Rs by PKC, IP_3 degradation or store depletion (see Section 2.1). A well-defined σ-T_{av} relation is an important element of pathway function (see Section 4.2). Therefore, robustness of the σ-T_{av} relation implies *functional robustness* in a stochastic system – that is a major topic of this thesis and further substantiated in Chapter 5. Moreover, the mentioned findings imply that the signal-to-noise ratio can be tuned cell-type specific by details of the upstream signalling pathway – independent of the strength of the input signal, which is usually the IP_3 concentration (see Chapter *Discussion*).

In the last section, the simple form of the parameter dependencies of the opening transition times computed from the De Young-Keizer model was exploited to propose analytical functions of these dependencies. Those functions can potentially be used to integrate the hierarchic stochastic model into larger signalling cascades, where cellular parameters like $[IP_3]$, N_{ch} or cluster distance are subject to feedback regulation rather than being constant system properties.

Part II

Experiments

5 Live Cell Imaging in HEK Cells

The main results in Chapter 4 were concerned with the robustness properties of the hierarchic stochastic model presented in Chapter 3: It predicts, on one hand, that the average interspike interval T_{av} is highly sensitive to stimulation and other variables regulating cluster coupling. On the other hand, the model predicts that the relation of T_{av} and the standard deviation of interspike intervals σ is robust with respect to such modifications, and can only be modulated by global feedback. Interspike intervals (ISIs) encode a major part of the information carried by the Ca^{2+} signal, and so ISI distributions are an important characteristic of Ca^{2+} signalling pathways, which can be compared to mathematical models [57, 175, 192]. This chapter presents measured Ca^{2+} spikes from HEK293 cells, which support the predictions that T_{av} is sensitive to cluster coupling, but the σ-T_{av} relation is robust. As mentioned in the Introduction, the data result from a collaboration with Prof Colin Taylor and Dr Stephen Tovey, most of the shown spike-sequences were recorded by the author under their supervision.

5.1 Materials and Methods

Materials. Cell culture media, Fura-2 AM, Fluo-4 AM and Pluronic F-127 were from Invitrogen. Human parathyroid hormone (PTH) fragments were obtained from Bachem (Saffron Walden, UK), where 'PTH' denotes PTH(1-34) that has been shown to have full biological activity. Other chemicals were from Sigma-Aldrich.

Cell Culture. HEK 293 cells stably transfected with human type 1 PTH receptor (HEK-PR1 cells) [187] were cultured in Dulbecco's modified Eagle's medium/ Ham's F-12, supplemented with L-glutamine (2mM), foetal calf serum (10 %) and

G-418 (800 μg ml^{-1}). The cells were grown in an incubator (95 % air, 5 % CO_2, 37° C) and passaged every 3rd day.

Single Cell Imaging. All experiments were performed at 20° C in Hepes buffered saline (HBS). HBS had the following composition: 135 mM NaCl, 5.9 mM KCl, 1.2 mM $MgCl_2$, 1.5 mM $CaCl_2$, 11.6 mM HEPES, 11.5 mM glucose, pH 7.3. For recording the Sr^{2+} spikes shown by the end of Section 5.2, $CaCl_2$ was replaced by $SrCl_2$ (cf. [142]). For imaging, cells were plated onto 22-mm round glass coverslips coated with 0.1 % poly-L-lysine. Then, cells were loaded with Fura-2 AM (2 μM) for 45 min at 20° C, followed by a period of 45 min in HBS for deesterification of the indicator. Single cell fluorescence measurements were performed as previously described [187]. Ratios of Fura-2 fluorescence with excitation at 340 nm and 380 nm wavelength were collected at intervals of 5 s. Agonists were added by solution exchange at time points and concentrations indicated in the figure captions.

Statistical Analysis of Spike-Sequences. After correction for background fluoresence, ratios of Fura-2 emission were evaluated as previously described [191, 195]. Briefly, after cutting initial transients, data were normalised by a running average, and spikes were identified with an increase of at least 20 % from baselevel. Since it was intended to determine standard deviations of interspike intervals, which converge relatively slowly with the number of events [48], long stationary spike sequences are required. It was chosen to accept data with at least 12 spikes, which are not too noisy. From those, linear trends were removed by subtraction of a linear fit to the plot of ISIs against time (see Fig. 5.1), and averages (T_{av}) and standard deviations (σ) of the ISI sequences were determined. Slopes and intercepts of σ-T_{av} relations were obtained from linear fits to the function $y = m(x - x_0)$.

Statistical Tests. To test the signficance of quantitative results, two types of tests were employed: Differences in T_{av} values of individual spike-sequences before and after addition of a pharmaceutical agent or a change in stimulation strength were tested by a paired student's t-test. Equivalence of slopes of σ-T_{av} relations

was tested by an appropriate F-test comparing populations of spike-sequences. All statistical tests were performed with the software package Graphpad Prism.

5.2 Pharmacological Study of Ca^{2+} Spike-Sequences

Human embryonic kidney (HEK) cells are a cell line that has been widely used in cell biology for several decades. Ca^{2+}-signals in HEK cells have been studied previously and are in fact a well established model system for the analysis of intracellular Ca^{2+} dynamics [31, 134, 187, 195, 227, 228]. However, only the study by Skupin *et al* [195] performed a detailed statistical analysis of long Ca^{2+} spike-sequences. The study presented in this chapter sought to extend that work to the investigation of different experimental conditions. In particular, it was intended to compare spike statistics arising after application of different pharmacological agents and to relate the findings to the model predictions obtained from the mathematical analyses presented in Chapter 4.

HEK cells exhibit long repetitive Ca^{2+} spikes under appropriate conditions

HEK cells are particularly well suited for the statistical analysis of Ca^{2+} spikes, because they exhibit long stationary IP_3-mediated Ca^{2+} signals [195]. Importantly, they can persist in buffer for several hours, which is a necessary condition for the long-term measurements required for this investigation. Furthermore, they express IP_3Rs that can be sensitised by cAMP [228], which was exploited in the present analysis, and they are easy to culture.

Ca^{2+}-signals in HEK cells can be recorded after stimulating the cells with carbachol (CCH), an agonist of the endogenous muscarinic M_3 receptor [188]. This G-Protein coupled receptor induces activation of Phospholipase C (PLC) and subsequent production of IP_3 [21, 188]. IP_3 molecules activate IP_3Rs in the endoplasmic reticulum (ER), which act as channels releasing Ca^{2+} ions from the ER lumen into the cytosol (see Section 2.1). After reclosing of the Ca^{2+} channels, Ca^{2+} is

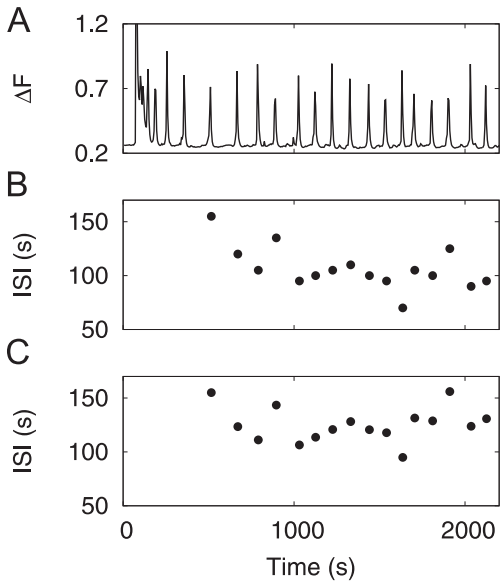

Figure 5.1: Spike-sequences from measured Ca^{2+} signals exhibit large variations. (A) Typical Ca^{2+} signal of an individual HEK cell upon stimulation with 30 μM CCH (see Section 5.1). After an initial transient with very fast spikes, the signal exhibits a seemingly stationary and regular spiking pattern. (B) Interspike intervals (ISIs) extracted from the spike-sequence shown in A without the initial transient. (C) ISIs shown in B after correction for linear trends (see Section 5.1). This analysis shows that the ISI sequence exhibits a small trend, and that even after removing that trend, the variation between individual ISIs of a single cell has the order of magnitude of the ISIs.

pumped back into the ER by SERCA pumps [21] (cf. Fig. 2.1).

Measured Ca^{2+}-signals have the typical form of repetitive increases in the cytosolic Ca^{2+} concentration (Ca^{2+} spikes), if cells are stimulated by moderate concentrations of CCH (see Fig. 5.1A and refs. [31, 134, 195]). Over-stimulation (> 100 μM CCH) causes a sustained increase in cytosolic $[Ca^{2+}]$, and very weak stimulation (< 1 μM CCH) results in essentially only local events (not shown). That cascade of Ca^{2+} signalling regimes is very similar to the pattern derived from the mathematical model (Fig. 4.3).

The frequency, but not the amplitude of Ca^{2+} spikes in HEK cells, depends on the concentration of CCH [31], as originally shown for Hepatocytes [246]. Since the spiking stops after a few minutes if Ca^{2+} is depleted from the extracellular

medium [31], it is generally assumed that the sustained oscillations require store-operated Ca^{2+} entry across the plasma membrane (see Section 2.1). Nevertheless, downstream targets like Protein Kinase C are not affected if store-operated Ca^{2+} entry is inhibited [31], showing that IP_3R -mediated intracellular Ca^{2+} dynamics are the mechanism that drives physiologic Ca^{2+} signals in HEK cells.

CCH-induced Ca^{2+} spikes typically start with an initial transient of several minutes. In that time frame, spikes have a higher frequency and amplitude than in the following phase, which shows a more stationary pattern and can persist for more than an hour (Fig. 5.1A and ref. [31]). Nevertheless, spike-sequences often show small trends over longer time-frames, and therefore it is appropriate to remove linear trends for the purposes of this study (Section 5.1 and Fig. 5.1B). Notably, even after removing linear trends, the individual ISIs show large variations (Fig. 5.1B) – in contrast to the regular oscillation frequency obtained in deterministic mathematical models (Section 2.1).

T_{av} is sensitive to application of pharmacological agents

The stochastic mathematical model presented in this thesis (Section 3.1) predicted that the average interspike interval T_{av} is set by processes regulating the sensitivity of individual Ca^{2+} channels or their local interaction (Section 4.1). To test that prediction, HEK cells were stimulated by moderate concentrations of CCH (30 μM) and treated with additional pharmacological agents that modify the signalling pathway (Fig. 5.2A): Parathyroid hormone (PTH) induces cyclic Adenosine-Monophosphate (cAMP) mediated sensitisation of IP_3 receptors [228]. U73122 (U7) and cyclopiazonic acid (CPA) are inhibitors of Phospholipase C and sarco-endoplasmic reticulum Ca^{2+} ATPase (SERCA), respectively [143, 161, 250]. We used CPA instead of the more commonly used thapsigargin as a SERCA inhibitor, because CPA binds reversibly and does not completely disable store refilling [161] –that is necessary to obtain the long-lasting repetitive spikes we wish to investigate.

All tested conditions provide long spike-sequences suitable for statistical analysis (Fig. 5.2B). CPA induces a longer initial transient and therefore requires longer recordings. Visual inspection of Fig. 5.2B suggests that PTH reduces T_{av}, and that

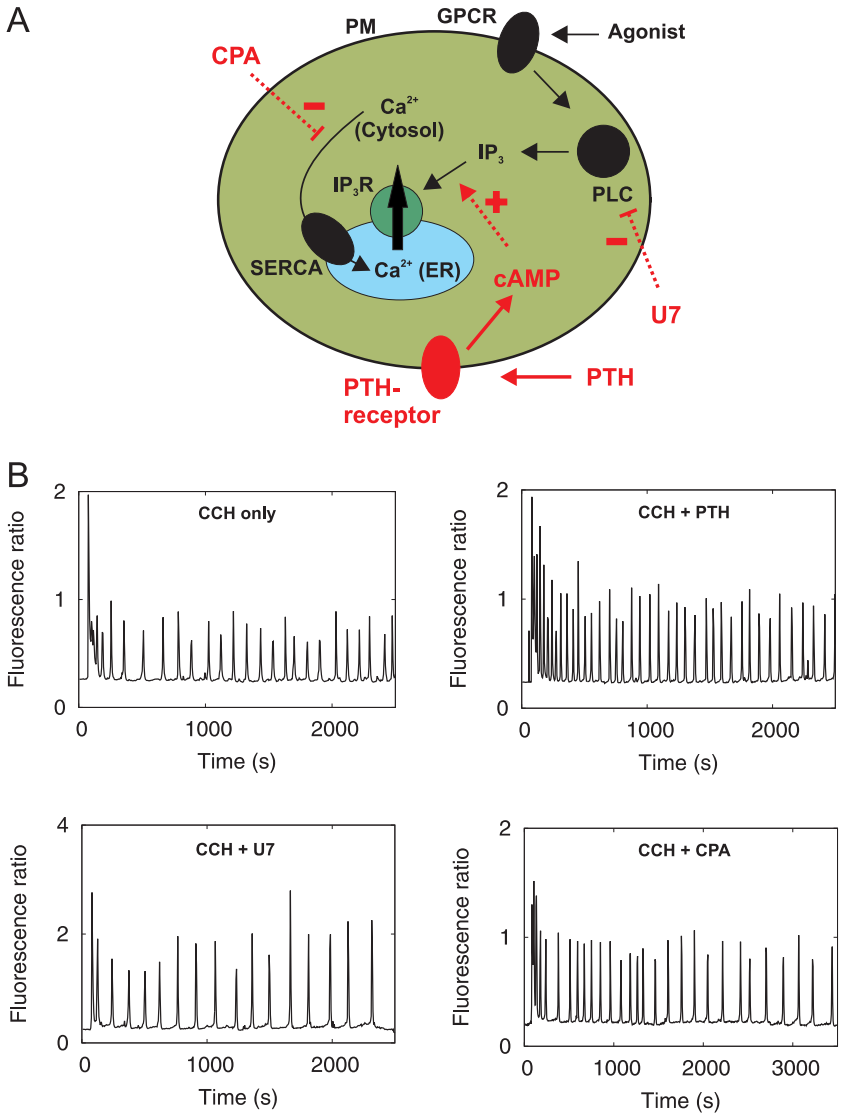

Figure 5.2: The Ca^{2+} signalling machinery can be manipulated by pharmacological agents. (A) The applied agents modify the Ca^{2+}-signalling pathway depicted in Fig. 2.1 as illustrated here (see text for details): Parathyroid hormone (PTH) induces cAMP-mediated sensitisation of IP_3 receptors, U73122 (U7) and Cyclopiazonic Acid (CPA) are inhibitors of PLC and SERCA pumps, respectively. (B) Fura-2 emission of single cells was recorded after stimulation with 30 µM CCH and addition of 10 nM PTH, 1 µM U73122 or 10 nM CPA as indicated (see Section 5.1). The interspike intervals are shorter with PTH and longer with U7 or CPA (cf. Fig. 5.3). All spikes-sequences exhibit initial transients, which are removed for statistical analysis – the longest transients appear after addition of CPA, because CPA requires additional time to enter the cells.

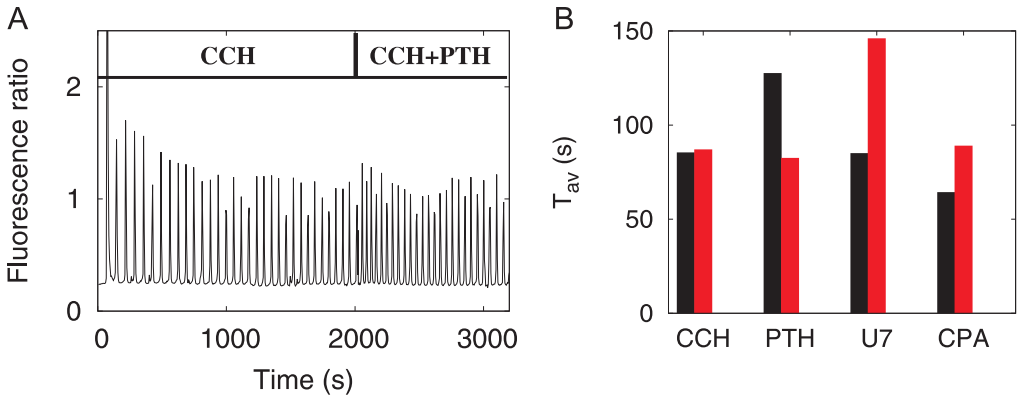

Figure 5.3: Pharmacological agents significantly modulate T_{av}. (A) Long spike-sequences with PTH added after $\approx$ 30 min revealed a fast modification of the typical interspike interval. (B) Statistical analysis: T_{av} was determined for the time before (black bars) and the time after (red bars) addition of the agent. Shown are population averages, but statistical analysis was performed pair-wise for single-cell data like shown in A. T_{av} decreased when PTH was added, and it increased when U7 or CPA were added ($n \geq 28$ and $P < 0.0001$ with paired t-test, for each of the agents). CCH only was also examinated as a control, and showed that T_{av} does not change without addition of pharmacological agents (bar labeled 'CCH').

U7 and CPA enhance T_{av}. To verify these results, we monitored spike-sequences in individual cells before and after addition of the pharmacological agents (Fig. 5.3). Indeed, statistical analysis of the ISIs before and after addition of the agents showed that T_{av} is significantly modified ($P < 0.0001$) upon application of PTH, U7 or CPA. These changes were not a result of systematic slowing-down of the interspike intervals, since the ISI sequences became shorter with PTH, remained stationary with CCH only, and became slower with CPA and U7.

The different behaviours of T_{av} in response to the different pharmacological agents (Figs. 5.2 and 5.3) can be explained by their action on different elements of the Ca^{2+} signalling machinery (Fig. 5.2A): PTH induces formation of cAMP, which causes IP_3R sensitisation enhancing Ca^{2+} release, while U7 inhibits PLC, reducing IP_3 supply and thus reducing IP_3R activity. Since IP_3R sensitisation is an instance of cluster coupling (see Section 4.1), the result that T_{av} decreases when IP_3R sensitisation increases is in good agreement with the mathematical model.

The action of CPA is not as easy to interpret, since inhibition of SERCA pumps generally has two effects: It leads to slower refilling of intracellular Ca^{2+} stores in the ER and to a higher cytosolic Ca^{2+} concentration. A higher cytosolic Ca^{2+} concentration can be expected to increase cluster coupling and therefore to result in faster spiking activity – such a correlation was indeed suggested by an earlier study, where pump activity was enhanced by increasing the temperature [178, 191]. However, the finding that SERCA inhibition increases T_{av} (Fig. 5.3) suggests that in our case of a dramatic slowing-down of pump-activity, the consequences of slow store-refilling are dominating, resulting in slower spiking activity (see Section 2.1). As mentioned above, we observed a prolonged initial transient with CPA, which also points towards an incomplete refilling of the ER between release spikes. Nevertheless, that interpretation should be verified by an independent experiment in future research.

Although the nature of the impact of CPA on Ca^{2+} dynamics still needs to be verified, it is known that spiking in HEK cells causes store-operated Ca^{2+} entry [31]. Refilling is therefore one of the processes of recovery of the cell from the previous spike in the meaning of Eq. **4.1**. Since the filling state of the ER determines the strength of the release current, it is also a global coupling variable. Thus, it can be expected that manipulation of store-refilling modulates global feedback, and therewith the σ-T_{av} relation (see Section 4.2).

The σ-T_{av} relation measured in HEK cells is robust to changes in IP_3R sensitivity but sensitive to SERCA pump activity

Spike-sequences can be characterised by the relation of standard deviation (σ) and average (T_{av}) of interspike intervals (ISIs): That relation reveals important properties of a stochastic signal like the maximal information content and the signal-to-noise ratio [192, 193, 195] (cf. Section 4.2 and Chapter *Discussion*). The mathematical analysis presented in Section 4.2 predicted that the σ-T_{av} relation of Ca^{2+} spikes is robust to changes of cluster coupling but sensitive to modulation of global feedback.

The pharmacological agents PTH and U7 modify cluster coupling by manipu-

lating elements of the Ca^{2+} signalling pathway (Fig. 5.2), and they indeed affect T_{av} (Fig. 5.3). The finding that the SERCA inhibitor CPA induced an increase in T_{av} (Fig. 5.3) suggested that the main effect of CPA is to slow-down refilling of intracellular Ca^{2+} stores (see above). Slow store-refilling has the effect of a global negative feedback from a cellular Ca^{2+} spike to the probability of the next spike: A Ca^{2+} spike is much less likely when the stores are not completely refilled. Therefore, slowing-down of store-refilling corresponds to smaller recovery rates ξ from global negative feedback (see Section 4.2, particularly Eq. **4.1** and Fig. 4.7).

To test for robustness of the σ-T_{av} relation in HEK cells, T_{av} and σ were obtained from ISI sequences like those shown in Fig. 5.1 (see Section 5.1). The relation was linear with a small intercept of less than 40 s and a slope smaller than one (Fig. 5.4). In these properties, it is very similar to the relations measured in other cell types and predicted from the hierarchic stochastic model (see ref. [195] and Section 4.2, respectively). The main difference between the ISIs measured in HEK cells and Astrocytes is the slope of the relation (Fig. 5.4). Therefore, the main issue of this investigation was to elucidate which properties of the signalling pathway determine the slope *in vivo*.

The slope was quantified by a linear fit of the data to the function $\sigma = m(T_{av} - x_0)$, where the fitting parameters x_0 and m are the intercept and the slope of the relation, respectively. As a main result of this thesis, the analysis showed that the slope of the σ-T_{av} relation did not change significantly when the agents modifying cluster coupling (PTH and U7) where applied, but it did change upon addition of the SERCA inhibitor CPA (Fig. 5.5 and Tab. 5.1). Since a possible interpretation of Fig. 5.3 was that CPA induces slower store-refilling and thus slower recovery from negative feedback (see above), these results strongly support the model predictions that the σ-T_{av} relation is robust to changes of cluster coupling, but can be adapted by global feedback. Note that the minimal interspike interval T_{min} (Tab. 5.1) is similar to the value predicted from the mathematical model for a moderate global feedback (cf. Fig. 4.7B).

Addition of CPA not only reduces the slope of the σ-T_{av} relation, it also resulted in a smaller intercept, in comparison to the other agents (Tab. 5.1). That is somewhat counter-intuitive: If the main effect of CPA was slower store-refilling, that should rather enhance the deterministic time (or recovery time) between

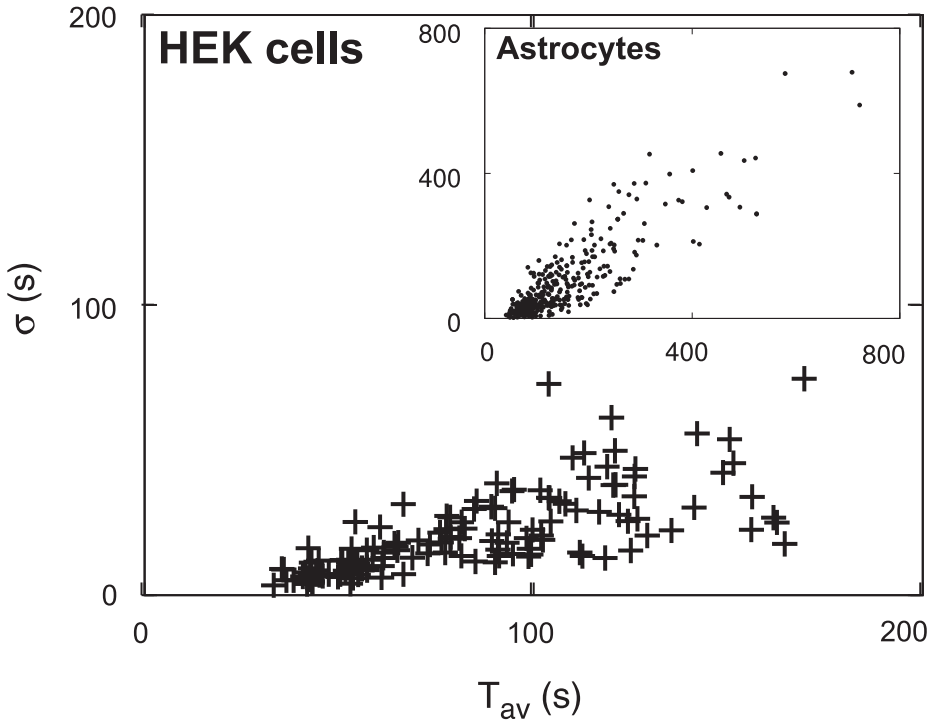

Figure 5.4: σ-T_{av} relations of ISIs from different cell lines are different. Each symbol represents a single cell. Data were recorded and processed as shown in Fig. 5.1, subsequently standard deviation (σ) and average (T_{av}) of the ISI-sequences were calculated. The inset shows the σ-T_{av} relation recorded in Astrocytes by Alexander Skupin (reprinted from ref. [191] with permission from the author). The relations from HEK cells and Astrocytes are both linear, but they are different with respect to the slope and the intercept of that linear curve, as suggested in ref. [195].

successive ISIs, which was identified with the intercept of the relation in earlier studies [192, 195]. However, note that the difference in the observed T_{min} (the smallest measured ISI) is much smaller than the difference in the fitted value x_0. Taking into account that T_{min} is generally rather small in HEK cells [195], it could be that the slightly smaller T_{min} is just a consequence of the smaller slope.

Conclusion

The presented analysis of Ca^{2+} spike-sequences in HEK cells confirmed the model predictions that T_{av} is controlled by cluster coupling, while the σ-T_{av} relation

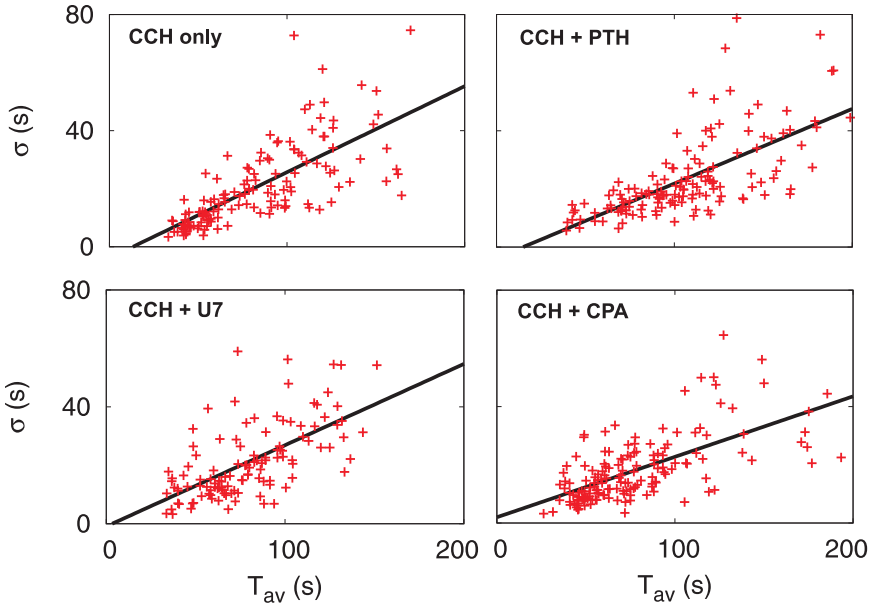

Figure 5.5: The pharmacological study of σ-T_{av} relations of ISIs in HEK cells supports model predictions. Each symbol represents a single cell, see Fig. 5.2 for a description of the applied pharmacological agents. The lines refer to the linear fit $y = m(x - x_0)$ with slope m and intercept x_0 (see text). The slope of the σ-T_{av} relation did not significantly change when PTH and U7 were added, but it did change significantly upon application of CPA (see Tab. 5.1).

Table 5.1: Linear fitting and minimal interspike interval T_{min} of the σ-T_{av} relations shown in Fig. 5.5. The P-value refers to a significance test of the linear fit in relation to the 'only CCH' experiment (see Section 5.1). It indicates the probability that a random sample generates a slope this different.

Condition	slope	P-value	x_0 (s)	T_{min} (s)
only CCH	0.30	–	13.25	33.1
CCH+PTH	0.26	0.254	15.94	39.3
CCH+U7	0.28	0.671	3.33	35.0
CCH+CPA	0.21	0.005	-9.50	25.6

is robust to it. Furthermore, the experiments with the SERCA inhibitor CPA provide support for the prediction that negative feedback, in this case mediated by slow store-refilling, reduces the slope of the relation – however, that proposal should be verified by future research. Those properties of the σ-T_{av} relation reveal sensitivity to control, functional robustness and adaptivity of the Ca^{2+} signalling toolkit (see Chapter *Discussion*). The demonstrated agreement of measured spike-sequences with model predictions also provides evidence for the stochastic model of intracellular Ca^{2+} dynamics (Section 3.1).

5.3 Analysis of Sr^{2+} Spike-Sequences

Earlier studies have reported that the Ca^{2+} signalling machinery can also run with Sr^{2+} instead of Ca^{2+}, and repetitive Sr^{2+} spikes can be recorded in the same way as Ca^{2+} spikes [86]. That is intriguing, since Sr^{2+} has a much less pronounced inhibitory effect on the IP_3R than Ca^{2+} [142]. Thus, the observation of repetitive Sr^{2+} spikes suggests that Ca^{2+}-mediated inhibition is not a necessary condition for spiking, a fact often neglected, especially in deterministic Ca^{2+} models [67, 182]. Although Sr^{2+} spikes have been investigated earlier, a statistical analysis of Sr^{2+} interspike intervals has not been published before. Here, apart from characterisation of Sr^{2+} spikes at different stimulation strengths, the focus was on determination of the σ-T_{av} relation of Sr^{2+} ISIs.

Interestingly, after an initial transient, in which supposedly the intracellular medium still contained Ca^{2+}, the Sr^{2+} spikes appear more regular than the Ca^{2+} spikes (Fig. 5.6A). Further, they have larger spike widths and spike periods than Ca^{2+} spikes, and they do not increase the spike frequency with stronger stimulation (Fig. 5.6B). The last fact is astonishing, because at the applied concentration of 1 mM CCH, we still record slow and rather regular Sr^{2+} spikes, while with Ca^{2+}, that concentration already causes the regime of over-stimulation (data not shown, see also ref. [31]). That can be interpreted as follows: The spiking frequency cannot increase with the stimulation strength, because IP_3R sensitisation is already saturated. Therefore, the large T_{av} values have a different reason: T_{av} is dominated by the time required for store-refilling, which is dramatically slower with Sr^{2+} than with Ca^{2+}. If that interpretation was correct, the effect would be similar to the

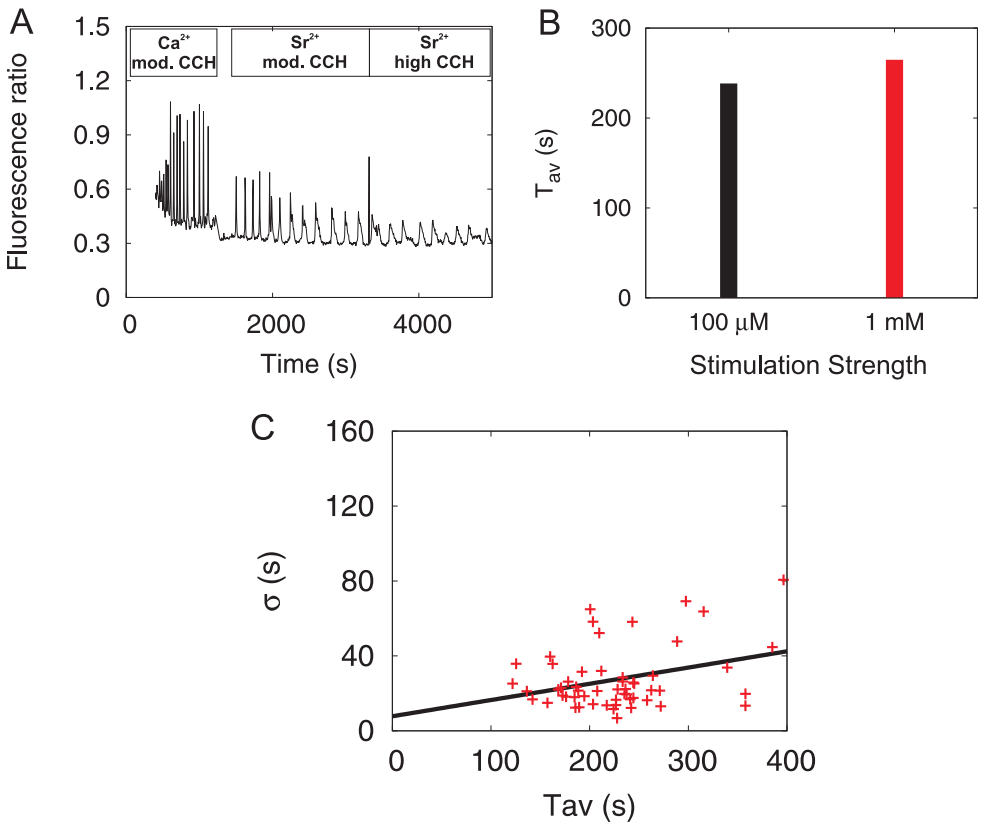

Figure 5.6: Sr^{2+}-spikes exhibit saturation of IP_3Rs and a σ-T_{av} relation with very small slope. (A) At the beginning of the experiment, cells were stimulated moderately (mod.) with 100 µM CCH. After 15 min, the extracellular medium was replaced by HBS containing Sr^{2+} instead of Ca^{2+} (see Section 5.1), and Sr^{2+}-spikes were recorded. After 30 min, the stimulation strength was increased from 100 µM to 1 mM CCH. (B) T_{av} of Sr^{2+}-spikes did not significantly change at higher stimulation strength (n=24, P=0.42). Like in Fig. 5.3, shown are population averages, but statistical analysis was performed pair-wise with data like the example shown in (A). (C) The σ-T_{av} relation of Sr^{2+}-spikes stimulated with 100 µM CCH had slope $m = 0.087$, intercept $x_0 = -89.5$ s, and minimal ISI $T_{min} = 121.9$ s. The small slope and large T_{min} (cf. Fig. 5.5 and Tab. 5.1) suggest the occurence of strong negative feedback mediated by very slow store-refilling (see text).

case of Ca^{2+} spikes manipulated by the SERCA inhibitor CPA (see Fig. 5.2), but even more dramatic.

The hypothesis of slow store-refilling in Sr^{2+} spikes fits well with the σ-T_{av} relation obtained for Sr^{2+} spike-sequences (Fig. 5.6C): It exhibits a very small slope and a large minimal ISI T_{min}, and therefore, model predictions would entail the occurence of strong global negative feedback in the Sr^{2+} spikes (Section 4.2). Slow store-refilling could account for such a feedback (see above). Note that although very small, the slope of the Sr^{2+} σ-T_{av} relation is still significantly ($P < 0.01$) different from zero.

Although the presented results are encouraging, Sr^{2+} spikes are not sufficiently investigated to draw final conclusions. Also other processes than store-refilling could account for the slowness and regularity of Sr^{2+} spikes, and also for the small slope of the σ-T_{av} relation. Nevertheless, the fact that a manipulation as drastic as replacing the messenger ion still results in a linear σ-T_{av} relation, with properties that can eventually be rationalised on the basis of the mathematical model, underlines the power of that theory. It also emphasises the value of the σ-T_{av} relation for the interpretation of population experiments with large variation (see Chapter *Discussion*).

5.4 Summary

This chapter presented long-term single-cell measurements in HEK cells, which were recorded to investigate spike-statistics in relation to the model predictions obtained in Chapter 4.

In particular, spike measurements with the pharmacological agents PTH and U73122 verified the predictions that the average interspike interval T_{av} depends on cluster coupling, but the relation of T_{av} and the standard deviation of interspike intervals σ is robust to changes of cluster coupling (Section 5.2). This finding has direct biological implications, because the σ-T_{av} relation reveals important properties of stochastic systems and facilitates interpretation of single-cell data with large variability (see Section 4.2). In addition to the experiments concerning cluster coupling, Ca^{2+} spike recordings with CPA and Sr^{2+} spike recordings provided support for the prediction that negative feedback reduces the slope of the σ-T_{av}

relation (Sections 5.2 and 5.3). However, these results still have to be taken with caution, as mentioned in the respective sections.

The model predictions outlined above were a direct consequence of the stochastic spike generating mechanism proposed in this thesis, which is based on channel clustering and Ca^{2+}-induced Ca^{2+} release (Section 3.1). Therefore, verification of those predictions also strongly support the hypothesis that repetitive Ca^{2+} spikes arise from such a stochastic mechanism, and not from limit-cycle oscillations (cf. Section 2.1 and Chapter *Discussion*).

6 TIRF Measurements of Ca^{2+} Puffs

Chapter 5 provided experimental evidence verifying a major prediction concerning the output from the theoretical analysis in Chapter 4, the robustness of the σ -T_{av} -relation of interspike intervals. This chapter considers the input data to the hierarchic stochastic model, which were probability distribution functions for opening and closing of Ca^{2+} channel clusters (Chapter 3). The local cluster dynamics described by such data are an important indication for the nature of the spike-generating mechanism: If Ca^{2+} spikes result from a reaction-diffusion oscillator, which has long been the standard assumption in mathematical modelling (see Section 2.1), the local dynamics (called Ca^{2+} puffs) should exhibit the typical time-scale of the system [105, 150]. Furthermore, if the global dynamics are regular periodic oscillations, this should also be true for the local dynamics. This chapter will study such questions by analysing high-resolution puff-data from two mammalian cell lines, SH-SY5Y cells and HEK cells, which were obtained by collaborations with the labs of Prof Ian Parker and Prof Colin Taylor (see Introduction). Furthermore, this chapter will relate the measured puff-distributions to the computed opening probabilities used in model simulations (Chapter 3), demonstrating the power of the model to relate local and global dynamics of intracellular Ca^{2+} signalling.

6.1 Materials and Methods

Experimental procedures. Puff-data from SH-SY5Y cells were recorded by Dr Ian Smith in the lab of Prof Ian Parker (see Introduction). The data were collected by methods previously described [197], see Appendix B.1 for a brief description.

For *Materials* and *Cell culture* of HEK cells, see corresponding paragraphs in Section 5.1.

In preparation of puff recordings, HEK cells were loaded 45 min with 1 μM cell-permeant caged IP_3 ($ciIP_3$-AM from SiChem, Bremen, Germany) and 45 min with 1 μM $ciIP_3$-AM supplemented by 5 μM Fluo-4-AM (Invitrogen, Carlsbad, CA) as Ca^{2+} dye. In order to prevent cellular Ca^{2+} spikes, which would impair statistical analysis of puff dynamics, cells were further treated with the slow Ca^{2+} chelator ethylene glycol tetraacetic acid (EGTA, see ref. [197]). For that purpose, cells were loaded for another 45 min with 5 μM EGTA-AM (Invitrogen, Carlsbad, CA). To induce Ca^{2+} puffs, $ciIP_3$-AM was uncaged with a flash of ultraviolet light (UV flash) generated by a JML-C2 Xenon Flash lamp (Rapp Opto) using a capacitance of ≈3000 microF with a pulse length of around 1 ms.

To record puff-sequences, several movies were taken on an Olympus IX81 microscope equipped with a TIRF objective (magnification ×60, N.A. 1.49). Excitation of the dye was via a 488 nm solid state diode-based laser. Images were captured with a high-speed Andor iXon 860 camera (128×128 pixels, 100 frames/s) and Andor Solis software. Recorded movies were processed and analysed on a 64 bit personal computer with the open source software package ImageJ. After background subtraction, the function FdivF0 was used to normalise fluoresence intensity and make puff-sites more obvious for subsequent visual inspection of the movies. Regions of interest were selected (circles of a diameter of about 1 μm), from which time-series of average fluorescence intensity were extracted to a data-file.

Statistical analysis. The obtained puff traces were analysed as previously described for spike train analysis [195]. Briefly, after choosing a sufficiently long and not too noisy data set, data were normalised by a running average, and puffs were identified by an increase of at least 20 % from base-level (see Fig. 6.1). Linear trends were removed, because they would bias the statistical analysis, which requires stationary data sets. Then, standard deviation and average of interpuff intervals (IPIs) were determined, similar to the analysis of Ca^{2+} spike-sequences (Chapter 5). Histograms of individual puff-sequences and fitting to probability distributions (see Section 6.2) were computed with the software package Matlab (Mathworks).

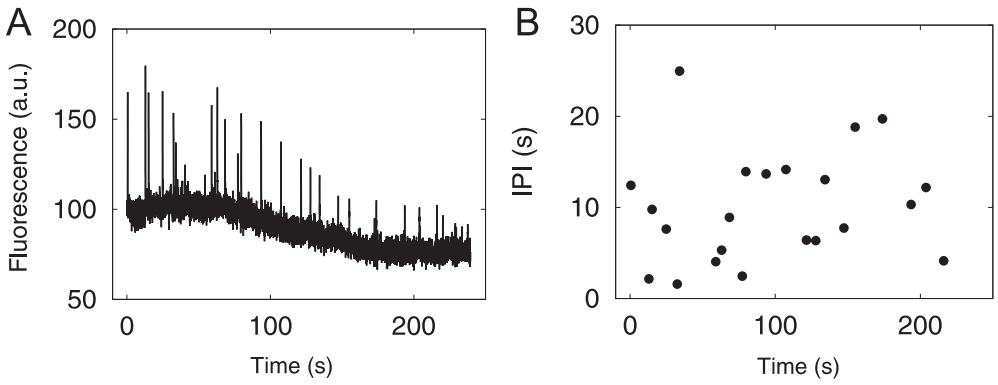

Figure 6.1: Puff-data from SH-SY5Y cells obtained by flash photolysis of caged IP_3. From the raw data (A), interpuff intervals (IPIs) were extracted after removing unstationary tails and linear trends (B). See Section 6.1 for details.

Probability distribution functions. We used two types of probability distributions: First, the exponential distribution with parameter λ,

$$\psi(t) = \lambda e^{-\lambda t}, \tag{6.1}$$

which is the waiting time distribution of the Poisson Process and has a coefficient of variation (CV=standard deviation over mean) of 1. Second, a time-dependent exponential distribution, which can be derived from Eq. **6.1** by introduction of a time-dependence to the parameter λ [195]:

$$\psi(t) = \lambda_0 \left(1 - e^{-\xi t}\right) \exp\left[-\int_0^t \lambda_0 (1 - e^{-\xi \tau}) d\tau\right], \tag{6.2}$$

where the integral can be evaluated to obtain an analytical formula. The puff-rate λ_0 is a measure for the typical interpuff interval, similar to the inverse of T_{av}. To determine the recovery rate ξ, we set $\lambda_0 = 1/T_{av}$ and obtain ξ from nonlinear fitting to the measured IPI distributions.

6.2 Characterisation of Interpuff Interval Distributions

Elementary Ca^{2+} release events (puffs) precede cellular Ca^{2+} spikes in many cell types [23, 33, 137, 227, 248] (see also Section 2.1). This section presents a quantitative analysis of experimentally measured Ca^{2+} puffs and relates the findings to a mechanistic view of intracellular Ca^{2+} dynamics [193, 224]. Puff-data were obtained from total internal reflection fluorescence (TIRF) microscopy measurements in human neuroblastoma SH-SY5Y cells and HEK cells, where Ca^{2+} puffs were evoked by flash photolysis of caged IP_3 (see Section 6.1).

Figure 6.1 exhibits a typical puff-sequence from SH-SY5Y cells and the extracted interpuff intervals (IPIs). In contrast to those data, in HEK cells, puff-activity typically started 30 to 60 s after flash photolysis (Fig. 6.2A-C). Further, it often persisted not longer than a minute (Fig. 6.2A) and sometimes consisted of rare singular events rather than sequences (Fig. 6.2B). The initiation of global Ca^{2+} waves was inhibited with the slow Ca^{2+} chelator EGTA (Section 6.1), but could not always be excluded (Fig. 6.2D).

IPI distributions are non-Poissonian delayed exponentials

First insights about local puff dynamics can be obtained by computing histograms of the measured IPIs from individual puff sites (Fig. 6.3). Some of the distributions are monotonously decreasing curves (Fig. 6.3A-B) and are well fit by exponential distributions (Eq. **6.1**). But remarkably, in both SH-SY5Y cells and HEK cells, most of the distributions exhibit a pronounced maximum at an IPI larger than zero (Fig. 6.3C-D), consistent with earlier measurements of Ca^{2+} puffs in *Xenopus Laevis* oocytes [248]. That means, they are not generated by a simple Poisson Process – that would be the natural expectation for a stochastic sequence of rare events – because the Poisson Process obeys an exponential waiting time distribution.

The maximum implies that negative feedback renders reactivation of the puff-site immediately after the preceding puff unlikely – similar to Ca^{2+}-mediated inhibition at global Ca^{2+} spikes (see Section 2.1). However, since the data are well fit by distribution functions starting at time point 0 (see below), we do not observe an

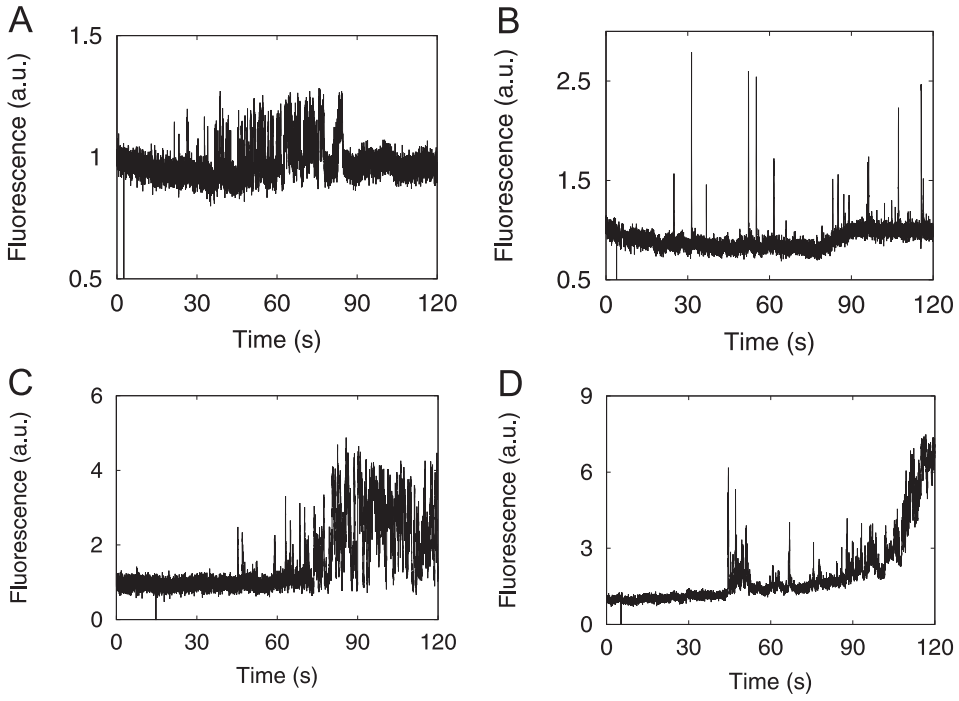

Figure 6.2: Typical puff recordings from HEK cells. Ca^{2+} puffs were evoked by a UV flash at 5 to 15 sec (vertical line below base-level) and recorded for 2 min. In HEK cells, puff-activity often persisted not longer than a minute (A), could exhibit singular events rather than sequences suitable for statistical analysis (B), and started 60 s after flash photolysis (C). Sometimes global waves were initiated despite EGTA-loading (D).

absolute refractory period, during which puffs do not occur with certainty. That is different from global spikes, for which we can observe a well-defined minimal interspike interval T_{min}, in theory and experiments (Sections 4.2 and 5.2).

Recovery from inhibition can be accounted for by a time-dependent Poisson Process [195]. 'Time-dependent' means that the parameter λ of the distribution is itself a function of time, $\lambda(t) = \lambda_0(1 - \exp[-\xi t])$, with an additional parameter ξ, which is the recovery rate (see Eq. **6.2**). $\xi = 0$ means infinitely slow recovery, and for $\xi \to \infty$, the Poisson Process is approached. That formalism is very similar to the way we introduced negative feedback to the hierarchic stochastic model (Eq. **4.1**). Indeed, the measured IPIs with positive maxima are well fit by Eq. **6.2** (Fig. 6.3C-D). For both cell types, relations of average interpuff intervals T_{av} and typical recovery times $1/\xi$ resemble linear curves (Fig. 6.3E-F).

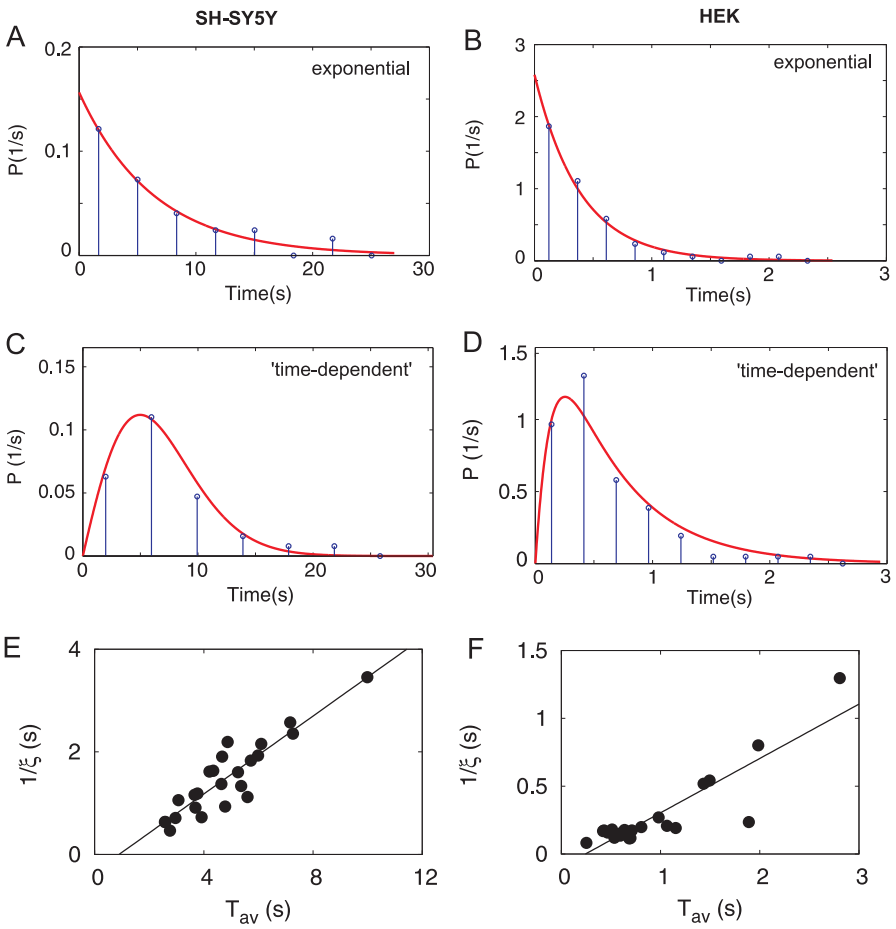

Figure 6.3: Interpuff intervals are generated by a Poisson Process with short additional recovery times. Data were obtained from SH-SY5Y cells (A,C,E) or HEK cells (B,D,F). (A-D) Stem plots are histograms from individual stationary IPI sequences as shown in Figs. 6.1 and 6.2. The number of bins is set to the square root of the number of IPIs in the sequence (between 13 and 100). Red lines are fits to the exponential distribution (Eq. **6.1**) or the time-dependent exponential distribution (Eq. **6.2**), as indicated. Histograms of most traces with SH-SY5Y cells (24 out of 30) and HEK cells (23 out of 40) exhibit a pronounced maximum for IPIs larger than zero and are well fit by Eq. **6.2**, and not by Eq. **6.1**, indicating the occurrence of a recovery process. For comparison with theoretical IPI distributions, see also Fig. 6.4. (E-F) Relations of the average interpuff interval T_{av} and the typical recovery time $1/\xi$. Each data point represents a single puff-site, the recovery rate ξ was obtained by non-linear fitting (see Section 6.1). The relations of both cell types resemble linear curves with slopes 0.38 (SH-SY5Y) and 0.40 (HEK). The plots show that T_{av} and $1/\xi$ are both well below 10 s (SH-SY5Y) and 3 s (HEK). Thus, local dynamics cannot explain the period of global Ca^{2+} spikes, which is in the range of 100 s (see Fig. 5.4 and ref. [232]).

Relation to computed opening probabilities

The hierarchic stochastic model of intracellular Ca^{2+} dynamics presented in Chapter 3 requires opening probability distributions of Ca^{2+} channel clusters as input data. The model simulations shown in Chapter 4 employed opening probabilities computed from the De Young-Keizer model (see Section 3.2). That means, they are based on *in vitro* data and on certain assumptions concerning the dynamics of individual Ca^{2+} channels in an internally strongly coupled cluster (cf. Section 2.1). Since the local Ca^{2+} release events investigated in this chapter reflect cluster dynamics, the computed cluster opening probability distributions, in principle, can be compared to the experimentally measured IPI distributions shown in Fig. 6.3.

Indeed, both the computed and the measured IPI distributions are single-peaked and have long non-zero tails (Figs. 6.3 and 6.4). Although the computed opening probabilities were fit by γ-distibutions in Section 3.2, Fig. 6.4 shows that they equally well fit the time-dependent exponential distribution, Eq. **6.2**. γ-distributions were used mainly because they are more convenient in mathematical computations, but here, time-dependent exponential distributions are more useful, because their parameters λ and ξ have a more direct biological interpretation (see above).

Statistical moments and fitting parameters of the computed IPI distributions are shown in Tab. 6.1. They can be compared to the values obtained from experimental measurements of λ and ξ (Fig. 6.3) and σ and T_{av} (Fig. 6.5 below), respectively. For higher Ca^{2+} concentrations, the theoretical distributions are similar to HEK cell data, and for lower $[Ca^{2+}]$, they are closer to SH-SY5Y puffs. In both cases, the ξ-values tend to be too large. Thus, the experimental and theoretical distributions are in qualitative, but not in quantitative, agreement. That is not surprising, since theoretical distributions were computed independently, without fitting of parameters to the data: A correct adjustment of single-channel models to puff-data would require data for varying values of the local Ca^{2+} and IP_3 concentrations (see Section 3.2), which are not experimentally accessible.

Since single-channel models cannot be optimised by *in vivo* data from Ca^{2+} puffs, the structure of the hierarchic stochastic model (Section 3.1) suggests using measured IPI distributions directly as input data. For that purpose, we would

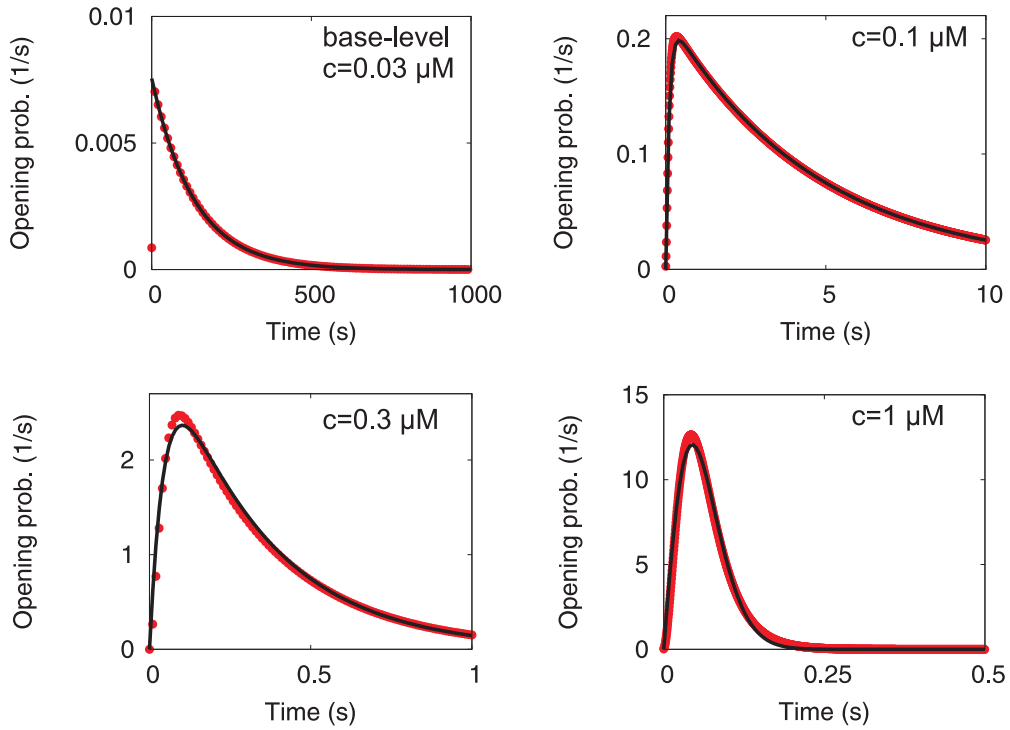

Figure 6.4: Computed IPI distributions are well fit by the time-dependent exponential distribution. Red circles are computed opening probability distributions at standard parameters (Tab. 3.1) and indicated local Ca^{2+} concentration c (cf. Section 3.2). Black lines are fits to the exponential distribution, Eq. **6.1**, at base-level Ca^{2+}, or fits to the time-dependent exponential distribution, Eq. **6.2** (see Tab. 6.1).

Table 6.1: Statistics and fitting parameters of computed IPI distributions (Fig. 6.4).

c (μM)	T_{av} (s)	σ (s)	λ_0 (s^{-1})	ξ (s^{-1})
0.03	131.45	130.05	0.00755	∞
0.1	3.00	2.65	0.217	9.18
0.3	0.35	0.32	3.27	20.74
1.0	0.065	0.040	63.34	7.89

need measured distributions with different strength of cluster coupling to reflect Ca^{2+}-induced Ca^{2+} release. Puff-data were obtained by decoupling of channel clusters with the slow Ca^{2+} buffer EGTA, which in most cases prevents the initiation of cellular Ca^{2+} spikes (see Section 6.1). Therefore, it should in principle be possible to obtain such data by variation of the EGTA concentration. However, that approach is technically difficult, because it is not possible to directly control the intracellular EGTA concentration that results from EGTA loading. Thus, direct application of measured input data to the hierarchic stochastic model remains a task for future research.

6.3 Specification of the Spike-Generating Mechanism

The mechanism generating cellular Ca^{2+} spikes is still under discussion: While the classic theory explains Ca^{2+} spikes on the basis of reaction-diffusion dynamics, newer results suggest that spiking emerges from coupling of stochastic excitable elements, so-called array-enhanced coherence resonance (see Section 2.1 and below). This section investigates whether the local dynamics of IP_3-induced Ca^{2+} release – the cluster dynamics – exhibit properties of oscillatory behaviour and the time scales of the global dynamics. Alternatively, the long time scales may arise from processes, which are only manifest in the transition from local events (puffs) to global events (cellular concentration spikes), or are initiated by global events only. IPI distributions are analysed with respect to their average value, a refractory period and periodic IPI modulation and correlation. The analysis shows that the cluster dynamics do not exhibit the long time scales of the global dynamics. Neither IPI distributions nor IPI correlations show properties of oscillatory behaviour.

Cell behaviour emerging from local subsystems can be characterised by statistical analysis of local events

Cell behaviour arises from the dynamic interaction of individual molecules [145]. It may exhibit spiking like the membrane potential of neurons [105] and oscillations like glycolysis in yeast [243] or circadian rhythms [46], but also bi-stability like in cytokine signalling in T cells [42] and hypersensitisation in intracellular signalling cascades [124] (see refs. [105, 150] for further examples of dynamic interaction). The behaviour of the single molecule does not typically exhibit these dynamic regimes or even the time scales of cellular behaviour. They are the result of interactions and self-organisation among all the molecules forming the corresponding cellular pathway or subsystem. While typically cell behaviour and molecular behaviour are well characterised, we know little about how one turns into the other. Does cell behavior arise on the level of protein complexes or on the cell level only? How are molecular dynamics coordinated across the whole cell?

Intracellular Ca^{2+} signalling is particularly interesting in that respect, since cell behaviour arises from the interaction of essentially identical elements, which are the Inositol 1,4,5-trisphosphate receptor channels IP_3Rs (Section 2.1). They control Ca^{2+} release from the endoplasmic reticulum. The system is ideal to study the role of spatial structure and self-organisation for the emergence of cell behaviour, since it exhibits the structural hierarchy of channels, channel clusters and cluster array on the cell level. Openings of single Ca^{2+} channels (blips) are followed by collective openings of channels in a cluster (puffs). Ca^{2+} from a puff-site diffusing to neighbouring clusters can activate them by Ca^{2+}-induced Ca^{2+} release (CICR, see Fig. 2.2), eventually leading to a global Ca^{2+} spike. Sequences of these concentration spikes form the Ca^{2+} signal in many different cell types.

Ca^{2+} dynamics are often perceived as a deterministic reaction-diffusion system [67, 105, 150]. These systems have local dynamics resulting from chemical reactions and spatial coupling by diffusion of the reactants. The local dynamics in our case are the opening and closing of channel clusters, the local Ca^{2+} release and the feedback of the local Ca^{2+} concentration to channel state dynamics. The spatial coupling is the diffusion of free Ca^{2+} and its modulation by buffers. According to the theory of reaction diffusion systems [129, 150], the local dynamics

set the dynamic regime of the system – oscillatory or stationary – and exhibit the typical time scales of the global dynamics. The minimal interspike interval would correspond to the duration of release plus a refractory period within this concept. In particular, we should observe the same time scales in the cluster dynamics as in the cellular dynamics, if the concept applies.

IPI distributions and σ-T_{av} relations of interpuff intervals show that puffs are irregular and much faster than Ca^{2+} spikes

Section 6.2 presented IPI distributions obtained from measured puff-data in HEK and SH-SY5Y cells. Beside experimental verification of the assumed opening probabilities, these data also show that IPI distributions have maxima at less than 5 s, and that recovery times are faster than 8 s (Fig. 6.3E-F). That means, recovery takes less than 10 s at the weak flash durations used here, while the time-scale of global oscillations approaches such values only for very strong stimulation [197]. Average interspike intervals (ISIs) of SH-SY5Y cells and HEK cells at low stimulation with carbachol (CCH) are in the range of 100 s (see ref. [232] and Fig. 5.4, respectively). It was shown also in *Xenopus* oocytes that IPIs are shorter than ISIs [138]. Therefore, these results strongly suggest that the global period of Ca^{2+} spikes is not set by the local dynamics for a broad range of experimental systems.

The σ-T_{av} relation is a tool to quantify populations of stochastic events (cf. Section 4.2). The relation of the measured IPI sequences is clearly linear, with a slope smaller than 1 and an intercept about zero (Fig. 6.5A). In this linear relation, the intercept represents an absolute refractory time, and the slope may be interpreted as a population-averaged coefficient of variation ($CV=\sigma/T_{av}$), which is a measure of noise in the underlying stochastic process: CV=1 indicates the Poisson process, which has maximal noise, while CV=0 would be a completely deterministic process [233]. Thus, the relation indicates a stochastic process which shows no absolute refractory time, but which contains recovery processes that reduce its CV. This finding is in agreement with the recovery rates obtained by fitting of single IPI distributions (cf. Fig. 6.3).

In addition to the σ-T_{av} relation of a group of puff-sites, the puff statistics can

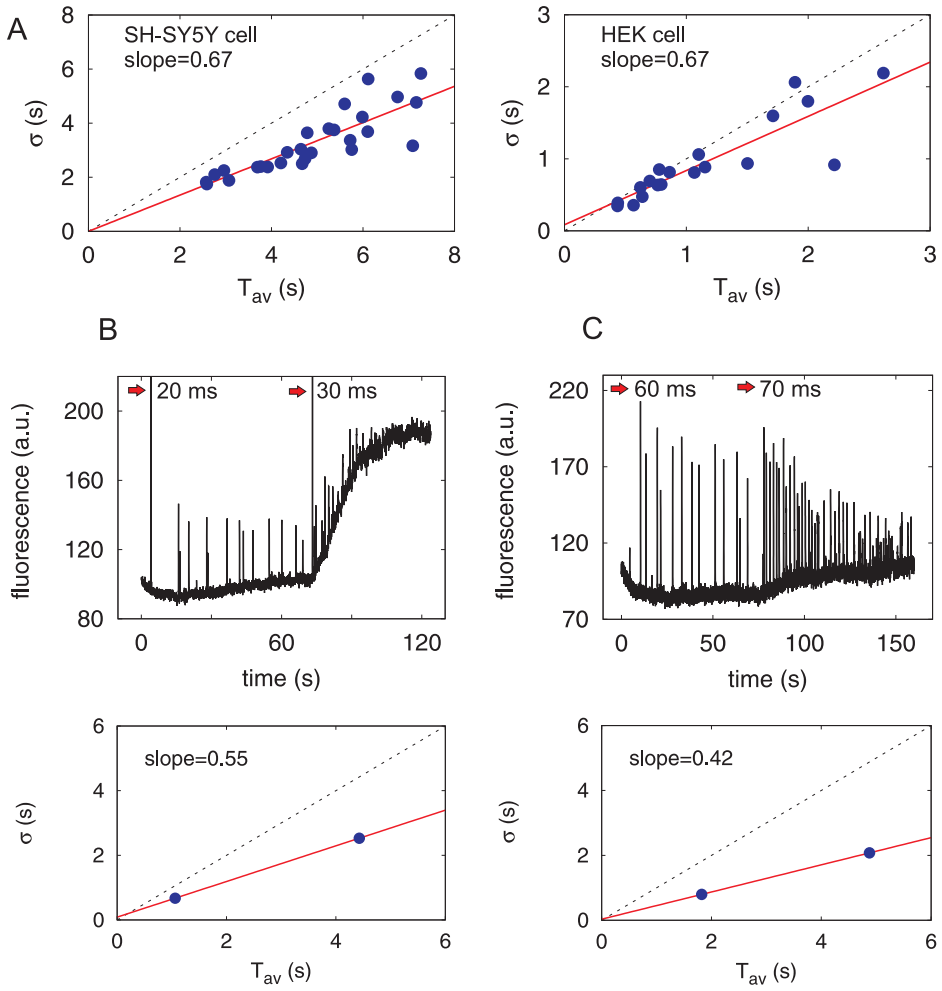

Figure 6.5: The relation of standard deviation (σ) and average (T_{av}) of interpuff intervals is linear with zero intercept and slope smaller than one. Dashed lines mark the identity function, and red solid lines are linear fits with indicated slope (see Section 6.1). (A) Population relations obtained from SH-SY5Y cells and HEK cells, as indicated. Each data point represents a single experiment. The intercepts are 0 s ± 0.6 s (SH-SY5Y) and -0.16 s ± 0.12 s (HEK). (B-C) Single puff-site σ-T_{av} relations from SH-SY5Y cells. Data were obtained by stimulation of one puff-site with two successive UV-flashes at indicated time points and flash durations, resulting in two data points with σ and T_{av} for the site. Apart from T_{av}, also the base-level fluorescence intensity increased in response to stronger stimulation, and therefore running averages are subtracted for statistical analysis (Section 6.1). In B, but not in C, the UV flash is visible in the data as a large increase in fluorescence intensity. The average slope of single-site σ-T_{av} relations was 0.49 ± 0.14, the average intercept -0.11 s ± 0.73 s (n=7). In both the population and the single puff-site experiments, the intercept is almost zero and the slope is smaller than one, indicating recovery processes without an absolute refractory period.

be further characterised by the σ-T_{av} relations of individual puff-sites. For this purpose, it is necessary to perform two successive experiments with different flash durations in the same field of view, in order to obtain two data points of the relation from the same puff-site. Two values of σ and T_{av} from these sequences are sufficient to completely determine a linear relation. It is then the relation of the individual puff-site (Fig. 6.5B-C). We obtained single-site σ-T_{av} relations with a slope slightly smaller than in the population relation. Therefore we conclude that in difference to cellular Ca^{2+} signals [195], we cannot derive the individual relation from population relations, demonstrating the necessity of single puff-site analysis. The intercept of the individual relations is close to zero like in the population relation, which confirms the absence of an absolute refractory period in the local dynamics.

Successive IPIs are uncorrelated and IPI sequences show no sign of periodicity

The large slope of the σ-T_{av} relation and the absence of absolute recovery times, which were confirmed by measurements at individual puff sites, indicate a highly irregular stochastic process generating cluster dynamics. Another test for the regularity of oscillations is the analysis of correlations between successive events (return maps, see Fig. 6.6). If the puff sequences were to represent noisy oscillations, the plot of the nth vs. the n+1th IPI would have the geometry of an ellipse, the width being a measure for the number of puffs per period (Fig. 6.6A-B). Such an analysis was performed for all traces containing more than 40 successive puffs (Fig. 6.6C-D shows typical examples), and the pattern is clearly distinct from a regular ellipse.

Not only the return maps, also the shape of the IPI distributions (Fig. 6.3A-D) indicate the absence of periodicity: They never exhibited more than one maximum. That shows that the sequences are not periodic, with a period in the range of the average IPI, since a noisy periodic process would show a multimodal distribution, i.e., maxima at the period and at multitudes of it [234]).

Other methods to test for periodicity like time correlation or Fourier Transform are not applicable here, since they require much longer sequences to give meaningful results [48]. However, the complete picture with IPI distributions, σ-T_{av}

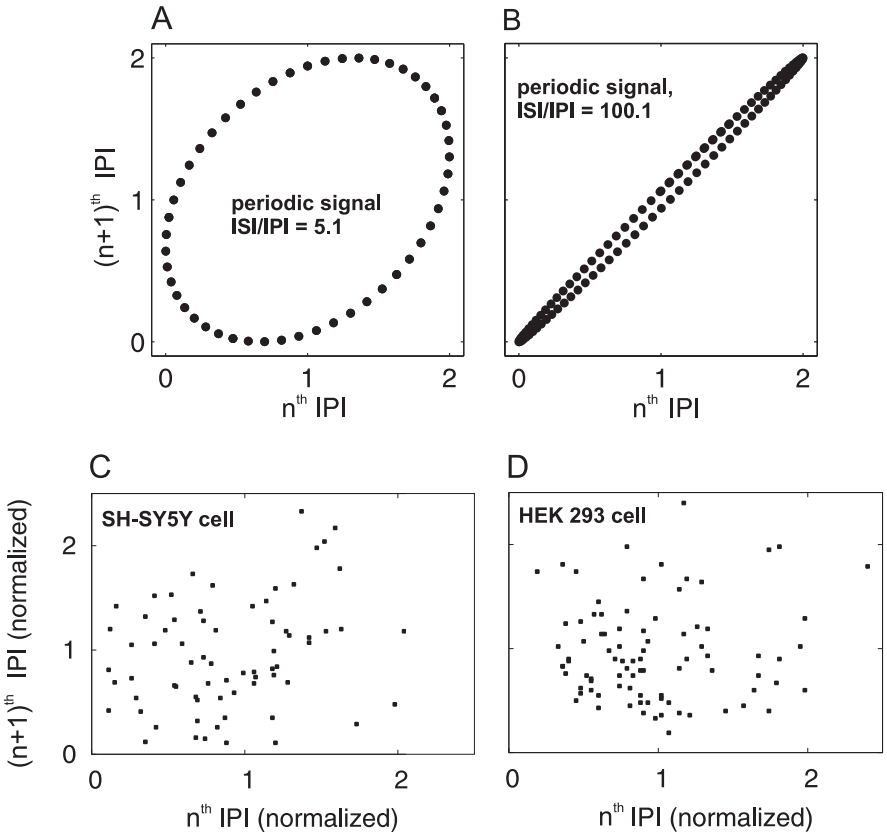

Figure 6.6: Successive inter-puff intervals are uncorrelated. (A,B) Return plot for the pure periodic process $f = Asin(2\pi n/N) + B$, where $A = 1$ is the amplitude, $B = 1$ shifts the process to positive values, n indexes the IPI, and N is the number of IPIs per ISI. The ratio of IPIs to ISIs is 5.1 (A) or 100.1 (B). In this periodic process, the relation of the nth vs. the n+1th IPI resembles an ellipse, and the width depends on the number of IPIs per ISI. (C,D) Return maps of typical puff sites in SH-SY5Y cells (C) and HEK 293 cells (D). IPIs have been normalized to the average IPI of the site. The obvious lack of an elliptical relationship suggests that there is no periodic relationship between successive IPIs.

relations and return maps provides evidence for the hypothesis that Ca^{2+} puffs are non-periodic and exhibit recovery times much faster than global spikes (see Chapter *Discussion*).

6.4 Summary

Since it is known that Ca^{2+} spikes emerge from the interaction of clusters of IP_3Rs in a stochastic and irregular way, this chapter sought to investigate and quantify puff dynamics in more detail.

The measured puff-distributions are similar to the opening probabilities computed from single-channel models. The presented results demonstrate that puff dynamics are governed by a stochastic process with average IPI much faster than cellular Ca^{2+} spikes. Furthermore, puff-sites are subject to refractoriness, which however does not result in absolute refractory periods (intercept in the σ-T_{av} relation), but generates a maximum in the IPI distribution at < 8 s. This is much faster than recovery times of typical global signals [195]. The puff-data did not provide any evidence for oscillatory dynamics of individual puff-sites with a period in the range of the average ISI.

These findings suggest that the long time-scales and repetitive spikes on the cell level are a result of global processes – that means, a result of emergent behaviour (see Introduction). In particular, they provide support for the stochastic mechanism for cellular Ca^{2+} dynamics proposed in this thesis (Fig. 2.5) on the basis of *in vivo* measurements of the microscopic dynamics (see Chapter *Discussion*).

Part III

Discussion

7 Discussion

Any living cell carries with it the experiences of a billion years of experimentation by its ancestors.

(Max Delbrück, quoted from ref. [158])

Ca^{2+} is an important second messenger providing a toolkit to transmit information from the plasma membrane to the nucleus, which is used by a large number of signalling cascades in eukaryotic cells (Section 2.1). The main purpose of cell signalling systems is reliable information processing, and that is continuously challenged by intrinsic and extrinsic fluctuations and by a changing environment (Section 2.2). To persist in evolution, biological systems must be robust and adaptive at the same time. In a complex, spatially resolved stochastic cell signalling mechanism like Ca^{2+} dynamics, those properties can only be resolved by a systems perspective. That means that the pathway is considered as a whole, with all possible interactions of its constituents (see Chapter 1).

This thesis investigates that systems perspective by a multidisciplinary approach, ranging from mathematical modelling over data analysis to live cell imaging. Chapter 3 presents a new modelling framework suitable for analysis of spatially resolved stochastic systems. There is now increasing evidence that such a mechanism applies to Ca^{2+} dynamics (Section 2.1) – that proposition is further substantiated by theoretical analyses and single cell experiments contained in this thesis (see below). Chapter 4 derives important properties of the investigated Ca^{2+} model. Those lead to predictions concerning sensitivity, robustness and adaptivity of spiking statistics, which to a large extent could be directly tested and verified by live cell imaging in HEK cells (Chapter 5). Finally, Chapter 6 contains statistical analyses of the local Ca^{2+} release events, which were detected by high-resolution

fluorescence micoscopy. Those data show that the variability of the global dynamics does not stem from the local fluctuations but arises by coupling.

Most of the theoretical work contained in this thesis was recently published in *PNAS* [225]. The experimental measurements were obtained by collaborations with Prof Colin Taylor and Prof Ian Parker and were to a large extent performed by the author (see Chapter 1). Manuscripts containing the results of Chapters 5 and 6 are in preparation.

Hierarchic stochastic modelling - a new technique building the bridge between local and global events in stochastic systems

The first goal of this thesis was to develop a theory which is able to calculate the characteristics of cellular Ca^{2+} signals from puff property distribution functions and cluster arrangement (Chapter 3). The theory is based on the principle of emergent behaviour. That means, system dynamics are perceived as a result of the interaction of subsystems at the next lower level, rather than being a direct consequence of first principles (see Chapter 1). The presented theory follows emergent behaviour from single subsystems over clusters to interaction of clusters in a cellular environment, deriving simple distribution functions for emergent properties on each level (Fig. 1.1).

The full theory is formulated in terms of integro-differential equations describing time-dependent statistics on the cell level. Analytical expressions are derived for stationary statistical properties in simplified test cases. An efficient delayed stochastic simulation algorithm reveals cluster dynamics and can be applied to more complex cluster arrangements. That algorithm can be further extended to account for an additional description of a global feedback process (Section 3.5).

The main advantages of the presented approach in comparison to standard methods are a huge reduction in the number of considered system states and the focus on measurable quantities. That implies that we are liberated from the duty of determining kinetic parameters describing microscopic state-changes, which often is a serious challenge in systems biology [114, 115, 128, 176, 177, 241]. Rather, the

probability distributions for macroscopic state-changes considered as input data here can often be computed from known constraints or even measured *in vivo*, as demonstrated in this thesis for Ca^{2+} dynamics (Sections 6.2 and 3.2).

Measured and computed probability distribution functions are also available for other cellular systems like gene expression [132, 184, 247, 249], autocatalytic reactions [53, 54] or kinetic proofreading [17, 149]. Therefore, the presented modelling framework can be applied to a wide range of systems consisting of coupled clusters of subsystems.

Importantly, although the new theory does not consider microscopic dynamics in detail, microscopic dynamics are considered by computing statistical properties emerging from strongly coupled microscopic entities (Fig. 1.1). They determine the shape of the distribution functions describing macroscopic state changes. In these respects, the theory is similar to a recent approach from Kholodenko and co-workers to the description of scaffold proteins [35, 36]. However, they assume that clusters are independent, while cluster coupling is an important element of the modelling concept presented here.

The theory as presented in Chapter 3 has the property that the input data do not depend analytically on parameters of the entire signalling pathway like the stimulation strength: IP_3 enters the model only indirectly as a parameter in the single-channel models, from which the opening probabilities ψ_o are computed (see Section 3.2). As mentioned before, that type of input data is advantageous for the analysis of the stochastic Ca^{2+} signalling mechanism (see below), because in contrast to ψ_o, cellular parameters and microscopic dynamics cannot be measured *in vivo* – therefore, considering them only implicitly leads to a more reliable description.

However, integration of the hierarchic stochastic model into models of larger signalling cascades requires analytic dependencies on cellular parameters. Therefore, in Section 4.3, analytic approximations of the dependencies of the opening transition probabilities on the cellular parameters $[IP_3]$, N_{ch} and cluster distance are investigated. We found that Hill Equations and power-laws describe those dependencies with high precision, and model calculations based on the originial opening probabilities ψ_o and on the analytic approximations are in good agreement.

These encouraging results can be used to compute model variables like the av-

erage interspike interval from cellular parameters by closed-form analytic expressions. That approach will be used to integrate realistic stochastic Ca^{2+} models into simulations of larger signalling cascades in future research.

The new theory predicts that pathway function is robust against cell variability, sensitive for control and adaptive to changing environments

As mentioned above, signalling mechanisms in eukaryotic cells are confronted with various sources of intrinsic and extrinsic fluctuations and with continuously changing environmental conditions (see Section 2.2). Therefore, key properties expected from a versatile and evolutionarily conserved signalling toolkit like intracellular Ca^{2+} dynamics [28] are robustness to noise and adaptivity. In fact, those properties, together with the known modularity and universality of Ca^{2+} signalling [27, 212], would qualify that mechanism as a core module in the sense of the 'theory of facilitated variation' from Gerhart and Kirschner [75, 110] (Section 2.2).

The biological function of Ca^{2+} signals is information transmission from the plasma membrane to the nucleus (see Section 2.1). That information is encoded in the frequency of interspike intervals [57, 121, 127, 175, 252], or more precisely, in their distribution [192, 193]. Analysis of the stochastic model showed that the pathway function of frequency encoding and information transmission is robust with respect to cell variability despite the sensitivity of interspike intervals (ISIs) to all cellular details (Chapter 4). Such robustness of function arises from the robustness of the relation between moments of ISI distributions, i.e., it is specific to stochastic systems. This strongly suggests that one of the biological functions of stochasticity is to render Ca^{2+} signalling functionally robust – which is a new aspect of the use of fluctuations by cells. The functional robustness is closely related to the convergence of control by many biological parameters onto a few distribution parameters, and both can be imagined as arising from the time-scale separation between interpuff intervals (IPIs) and interspike intervals (ISIs) (see below).

Robustness of function is compatible with control of signalling, since the average

interspike interval T_{av} and the signal type depend sensitively on channel properties, cluster arrangement, buffering conditions, and other details. Control is possible, since not specific values of the average ISI, but pathway function is robust against cell variability. Control of T_{av} shifts the cell's position on the relation of T_{av} and the standard deviation of ISIs σ. Since it obeys that relation, stimulated spike trains will be as regular as possible and will exhibit a typical frequency. And as long as a slope smaller than 1 is maintained, spike trains can transmit information by frequency encoding [192]. Therefore, robustness of the σ-T_{av} relation biologically means robustness of these two functionally important properties.

Thus, the pathway meets the requirement of robustness against cell variability and component tolerances necessary for biological networks [3]. This functional robustness is not the result of feedback and control, but it is a property of the stochastic spike generation mechanism.

In mathematical terms, functional robustness is independence of the σ-T_{av} relation from parameters, which vary between individual cells of the same cell type. Which mathematical structure causes this independence? By the calculations presented here (Section 4.2) and in experiments [195], it was shown that interspike intervals can often be described by two parameters, e.g. $P_{ISI}(T_{av}, \xi)$ – in some cell types, also a recovery period T_{min} needs to be considered [195]. The few distribution parameters are controlled by many biological parameters like $[IP_3]$, cluster distance, channel state transition rates, etc. That is an enormous reduction of complexity, since all biological feedbacks and control circuits converge on only two distribution parameters.

Those findings imply that the cluster parameters do not control the recovery rate ξ. Consequently, the relation $\sigma(T_{av},\xi)$ does not depend on the cluster parameters, since the recovery rate ξ does not depend on them. It is robust against changes of these parameters. Robustness with respect to buffer concentration, stimulation strength and IP_3R sensitivity was also established experimentally (see Chapter 5 and refs. [192, 195]). The calculations presented here (Section 4.2) and recently published multiple-scale simulations [194] suggest that $\sigma(T_{av},\xi)$ is also robust with respect to changes of the number of channels per cluster, the channel closing rate, the spatial arrangement of clusters and the pump rate. They change T_{av} and σ, but they do not change the relation between them.

These theoretical results are strongly supported by the experimental finding that the slope of the individual σ-T_{av} relation is essentially the same as the slope of the population relation within one cell type [192], while the same group of cells exhibits a wide range of average ISIs. The differences between individual cells of the same cell type affect T_{av} but not the relation $\sigma(T_{av},\xi)$.

The probability for a Ca^{2+} spike is the product of the probability for a local Ca^{2+} release event (Ca^{2+} puff) and the probability for a puff to set off a wave. As mentioned before, the latter factor, which is determined by cluster coupling, does not shape the σ-T_{av} relation. Therefore, without global feedback, the slope of the σ-T_{av} relation is always one (Fig. 4.6), indicating that completely decoupled local events are generated by a Poisson Process with exponentially distributed waiting-times (see Section 3.2). The slope of the relation, and therefore the maximal information content of spike sequences, can however be modulated by the global recovery rate ξ (see Fig. 4.7).

There is a variety of Ca^{2+} signalling pathways. They differ in the feedback upon a Ca^{2+} spike, i.e., with respect to the value of ξ. That agrees with the experimental finding that the recovery rate ξ is cell type specific [195] and with experimental results in this thesis (see below). Hence, cells can tune the spiking pattern by adjusting global feedback processes in the course of evolution (see below). Recovery from negative feedback is described in its most simple form only here. It can be expected that non-linear recovery dynamics lead to qualitatively similar σ-T_{av} relations [238].

We gain a mechanistic understanding of functional robustness by considering time-scales. In the hierarchic stochastic model, the ISI distribution is determined by the probability for a puff to set off a wave and by global feedback. Since not each puff initiates a wave, IPIs are shorter than ISIs – that is confirmed experimentally in Section 6.3 (see below). Cluster properties and the whole complexity of channel state dynamics determine the IPI and the time course of a puff, but only the statistics of the occurrence of many puffs on longer time-scales shape the ISI distribution and the σ-T_{av} relation. Distributions generated that way are often described by a few parameters only [233], as is also illustrated by examples from other signalling systems, cell mechanics or gradient and quorum sensing [6, 11, 120, 132, 251, 253].

Measured spike-sequences confirm sensitivity to control and functional robustness as well as adaptivity of the Ca^{2+} signalling pathway

After building and analysing the stochastic model, another aim of the thesis was experimental validation of important model predictions. For that purpose, long-term measurements of Ca^{2+} spike-sequences in the presence of pharmacological agents were performed and analysed (Chapter 5).

A first result was that the agents Parathyroid Hormone (PTH) and U73122 (U7) act on the average interspike interval T_{av} in opposite directions: PTH decreased and U7 increased T_{av}. That is in excellent agreement with the model prediction that T_{av} is controlled by cluster coupling, because the agents act on IP_3R sensitisation, an instance of cluster coupling (Section 4.1), in opposite directions: PTH induces formation of cAMP, which enhances IP_3R sensitisation, and U7 inhibits Phospholipase C, thus reducing formation of IP_3, the soluble factor activating IP_3Rs (see Fig. 5.2).

Second, the theoretical analysis suggested that although T_{av} is controlled by a number of processes converging to the emergent parameter cluster coupling, the general properties of pathway statistics encoded in the σ-T_{av} relation are robust to such changes (Section 4.2). The finding that PTH and U7 did manipulate T_{av}, but not the σ-T_{av} relation (Fig. 5.5), is a direct verification of that model prediction based on *in vivo* data.

The third model prediction relevant to the analysis of spike-sequences stated that the σ-T_{av} relation can be adapted by global feedback (Section 4.2). In particular, the slope of the relation can be reduced by a negative feedback ranging from a cellular Ca^{2+} spike to IP_3R sensitivity or to other system properties setting the probability for the next spike (Fig. 4.7). The feedback could be mediated by degradation of IP_3 or by phosphorylation of the IP_3R via Protein Kinase C (PKC), but also by store depletion (see Section 2.1). Such drastic changes in pathway function cannot be expected to occur spontaneously in a living organism, but they could accumulate in the course of evolution – and in fact different cell lines differ by the slopes of their σ-T_{av} relations [195].

Experiments with the SERCA inhibitor CPA and records of spikes mediated by

Sr^{2+} instead of Ca^{2+} (Sections 5.2 and 5.3) indicated that indeed drastic slowing-down of refilling of intracellular stores could account for a smaller slope of the σ-T_{av} relation. Although independent control experiments still have to be performed, that finding would be in agreement with the proposition of Michael Berridge [25] that "the frequency of Ca^{2+} oscillations (could) depend upon how quickly the store can be loaded". Further research is also required to verify adaptivity of the σ-T_{av} relation by manipulation of more specific pathways like global feedback provided by Protein Kinase C. However, the data obtained so far from the CPA and Sr^{2+} experiments provide further support for the significance of predictions from the hierarchic stochastic model and for the utility of the σ-T_{av} relation for the analysis of cell-population experiments.

Since the pathways determine the feedback and the recovery process, via the σ-T_{av} relation, they also determine the signal-to-noise ratio and the information content that can be transmitted by the ISI sequence (see above). Hence, cells can optimise spiking statistics by adjusting negative feedback. Such tunability of the σ-T_{av} relation by global feedback enhances *evolvability* of the pathway (see Section 2.2): The signal-to-noise ratio can be optimised individually for the specific pathway making use of the Ca^{2+} signalling toolkit. Because of the *functional robustness*, that property is independent of the input signal, which is the stimulation strength triggering cluster coupling.

It can be hypothesised that pathways including negative feedback can control targets requiring more regular spiking, and pathways without it are more eligible for targets with weak frequency dependence. Functional studies of that kind would be an exciting task for future research.

In summary, the data analysis presented in Chapter 5 verifies the model prediction that Ca^{2+} dynamics, though emerging from a complex spatially resolved mechanism with large cell-to-cell variability, have favourable properties in respect to signal statistics: They exhibit sensitivity to control by stimulation strength, robustness in respect to cluster coupling, and adaptivity of the signal-to-noise ratio by feedback control. Such *functional robustness* supplemented by *rapid evolvability* (Section 2.2) of important properties – here, the signal-to-noise-ratio – qualifies the Ca^{2+} signalling toolkit as a core unit of cell signalling [75].

TIRF recordings of local Ca^{2+} release events strongly support the stochastic spike-generating mechanism

After the discovery that Ca^{2+} spikes emerge from the interaction of clusters of IP_3Rs in a stochastic and irregular way, this work intended to investigate and quantify the local dynamics in more detail. In particular, it was an open question wether the observed stochasticity on the cell level [195] stems from intrinsic or extrinsic noise (see Section 2.2). In the definition from Elowitz *et al.* [63], intrinsic noise is the noise contribution that remains if we "consider a population of cells identical not just genetically, but also in the concentrations and states of their cellular components". Applied to Ca^{2+} dynamics, that means that the stochastic model proposed in this thesis and in earlier studies by the Falcke group (see Section 2.1) corresponds to an intrinsically noisy mechanism, while a deterministic reaction-diffusion mechanism with additive noise can be classified as extrinsically noisy.

The presented results (Chapter 6) demonstrate that puff dynamics are governed by a stochastic process with average interpuff interval (IPI) much faster than cellular Ca^{2+} spikes. Furthermore, puff-sites are subject to refractoriness, which however does not result in absolute refractory periods (intercept in the σ-T_{av} relation), but generates a maximum in the IPI distribution at 3 to 5 s. In the data, there is no evidence for oscillatory dynamics of individual puff-sites with a period in the range of the average ISI. Therefore, the shown data reject the assumption of a reaction-diffusion mechanism with extrinsic noise for intracellular Ca^{2+} dynamics.

That outcome was theoretically predicted based on realistic simulations of local cytosolic Ca^{2+} concentrations and a channel state model with half maximum values of the Ca^{2+} feedback to channel state dynamics in the range of measured values [221, 222]. Channel cluster dynamics are non-oscillatory (except in very small parameter ranges), since local concentrations saturate feedback [221].

Earlier studies in frog oocytes [138, 248] came to similar conclusions with respect to refractoriness on the basis of IPI distributions averaged across populations of puff-sites. The high-resolution data presented here permit statistical analysis of IPIs of individual sites and thus give a more complete picture. The finding that puff

statistics are very similar in experimental systems as distinct as frog oocytes and mammalian cell lines demonstrates universality of the Ca^{2+} signalling toolkit [28] throughout species.

If Ca^{2+} oscillations do not arise from the local oscillatory dynamics, how can we explain the regular spiking patterns observed in experimental data? Previous theoretical studies in the Falcke group showed that despite the stochastic character of spike initiation, apparently regular Ca^{2+} oscillations can emerge as a direct consequence of coordinated release on the cell level (refs. [67, 194] and Section 4.1). Regular oscillations arise when the spike probability after an absolute or almost absolute refractory period becomes very large and spikes arise very soon after it has elapsed.

A natural explanation for the emergence of the ISI time scale and the time scale separation between IPI and ISI arises from the wave nucleation mechanism for spike generation (Fig. 2.5). It perceives global spikes as arising from a puff which managed to set off sufficiently many neighbouring puff-sites to initiate a global release spike. As mentioned earlier, the probability for a global spike is the product of the probability for a puff and the probability that this puff activates sufficiently many neighbours. The latter factor causes the time scale separation between IPI and ISI. Consequently, the ratio of IPI to ISI is a measure for the strength of coupling between clusters in a cell.

The ISI of cellular dynamics may also exhibit negative feedbacks prolonging the ISI or causing an absolute refractory period (Section 4.2). The results presented in Chapter 6 strongly suggest this absolute refractoriness to arise from global processes, since we could not find it in the local dynamics.

Relation of data from live cell imaging to the hierarchic stochastic model

A major advantage of the hierarchic stochastic model is that it does not depend on cellular parameters like $[IP_3]$ or N_{ch}, which cannot be measured *in vivo*. Rather, the most important input data to the model are probability distribution densities for opening events of Ca^{2+} channel clusters. The shown puff-recordings obtained by TIRF microscopy (Section 6.2) confirm the shape of the distributions used as

input data in model simulations (Section 3.2). They further provide evidence for the most important model assumption, which is the wave-nucleation mechanism for the generation of Ca^{2+} spikes (see above).

The Ca^{2+} spike-sequences obtained by single-cell fluorescence microscopy show that the hierarchic stochastic model generates spiking statistics which are in excellent agreement with *in vivo* data (Section 5.2). More importantly, the data strongly support conclusions derived from the model, demonstrating the predictive power of hierarchic stochastic modelling: The robustness properties of the Ca^{2+} signalling pathway, which are a major result of this thesis, would hardly have been discovered without the modelling – but they would not be as convincing without the experimental validation.

Summary and outlook

Classic mathematical models describe Ca^{2+} spikes as nonlinear but deterministic limit-cycle oscillations [67, 182]. However, recent studies have suggested that they are actually governed by a stochastic process emerging from coupled clusters of Ca^{2+} channels (see Section 2.1). This thesis provides further evidence for such a mechanism in several ways: First, spike statistics are characterised for different experimental conditions, and results are in agreement with stochastic models (Section 5.2). Second, local dynamics are shown to disagree with the assumption of deterministic reaction-diffusion dynamics (Section 6.3). And third, model simulations reveal that the stochastic model reproduced experimentally observed Ca^{2+} signals, starting from experimentally verified distribution functions describing cluster dynamics (Section 4.2).

A major goal of this thesis was providing a framework to formulate theory in terms of measurable quantities. The experiments needed to determine input data required for the presented Ca^{2+} model and to verify predictions partly were performed previously, partly they contributed to this thesis, and partly they still need to be performed.

Concerning the input data, the cluster closing time distribution has been measured *in vivo* [196]. Cluster opening probabilities were measured as part of this thesis (Section 6.2), but their dependence on cluster coupling has not been deter-

mined yet. When that has been done, modelling of cellular Ca^{2+} dynamics will no longer need to rely on channel state models derived from patch clamp records. That paves the road to realistic models of Ca^{2+} signaling pathways, which rely on *in vivo* data.

Predictions derived from the presented theory include sensitivity to control, *functional robustness* and *evolvability* of the mechanism generating stochastic intracellular Ca^{2+} spikes (see above). All these properties were addressed by a pharmacologic study of spike-sequences in this thesis (Chapter 5), but the last point, feedback control of the σ-T_{av} relation, should be substantiated by further independent experiments. That could be done by manipulating one of the many reported feedbacks from Ca^{2+} to IP_3R activity, e.g. via Protein Kinase C (see Fig. 2.4 and refs. [152, 216]).

The findings presented in this thesis also suggest investigating in detail how the Ca^{2+} signal is read by downstream parts of the pathway. Fluctuations of ISIs might be substantial in the range of frequencies relevant for Ca^{2+}-controlled gene expression [57, 127, 195, 252]. Since studies on frequency decoding used artificial regular signals [57, 127, 252], it is not known how frequency-sensitive processes respond to random sequences. In that context, it would be particularly interesting to investigate how the σ-T_{av} relation, the frequency sensitivity of the down-stream parts of the pathway and the decoding mode relate to each other in functional *in vivo* assays.

Conclusions

What could be the reasons for a cell to prefer a stochastic mechanism for Ca^{2+} spiking over a deterministic one? A deterministic mechanism requires sufficient synchronization and large molecule numbers. The minimal error of such a mechanism decreases only with the quartic root of signalling events for arbitrarily complex feedback regulation [126]. Is it worth the effort? The linear and robust σ-T_{av} relation of the stochastic mechanism (Fig. 4.7) implies a signal-to-noise ratio which is equal to or larger than the inverse of its slope, independent of the input signal (the IP_3 concentration). The signal-to-noise ratio can be controlled by a simple negative feedback. Such a well-defined and adaptive signal-to-noise ratio could be

as effective as a more regular 'deterministic' mechanism, but at much lower costs in terms of copy numbers of proteins; and the mechanism is robust with respect to cell variability. It seems that it suffices to be random.

This thesis presents a multidisciplinary approach to investigate Ca^{2+} signalling in particular and properties of stochastic signalling mechansims in general. Special emphasis was placed on emergent properties of such systems like *sensitivity to control*, *functional robustness* and *evolvability*, on developing a new modelling framework formulated in measurable quantities, and on experimental validation of the model and the most important model predictions. The presented work employed a systems view on a spatially resolved stochastic signalling pathway. In theory and experiment, it followed emergent behaviour over three levels of molecular organisation in a living system, which are single channels, channel clusters and arrays of channel clusters.

The obtained results could never have been achieved by only investigating the single channels. Therefore, this thesis underpins the statements (page XV) that "one can analyse any number of compounds (in a cell) but one will never get a living bacterium out of it, unless one introduces totally new and complementary points of view" (Max Delbrück), and that "the central task (...) is to catalogue and understand emergent behaviour in its many guises, including potentially life itself" (Laughlin and Pines).

A Theoretical Appendix

A.1 Computation of the Opening Probability Densities ψ_o

The opening probability densities $\psi_o(c, t-\tau)$ introduced in Chapter 3 depend on the local Ca^{2+} and IP_3 concentrations as well as on the number of channels in the cluster N_{ch}. It is only necessary to index the Ca^{2+} concentration c, because it provides for the spatial coupling (see Section 3.1) and therefore drives the spatiotemporal dynamics. ψ_o and ψ_c can be measured, and indeed the measured closing time distribution given by Eq. **3.3** is used in simulations. But since ψ_o has only been measured for resting $[Ca^{2+}]$, and not for a range of concentrations yet, it needs to be calculated from models as described in the following.

Opening transition times are obtained by a method developed in an earlier study in the Falcke lab [94, 223, 224]. The method uses the De Young-Keizer model [51] (see also Fig. 2.3) for the description of the individual IP_3Rs with the parameter values given in Tab. A.1. On the basis of that model, ψ_o can be computed from the Master Equation describing the random channel state changes. Briefly, the DeYoung-Keizer model assumes that a channel is open when three out of the four subunits of the IP_3R are bound by IP_3 and activating Ca^{2+}, but not by inhibiting Ca^{2+}. The transition rates between the states could be determined by experiments to some extent.

Table A.1: Parameter values for the De Young-Keizer model (Fig. 2.3) used to compute the opening transition times ψ_o (see Fig. 3.2).

Parameter	**Value**	**Unit**
a1	20	$(\mu\text{M s})^{-1}$
a2	0.001	$(\mu\text{M s})^{-1}$
a3	20	$(\mu\text{M s})^{-1}$
a4	0.025	$(\mu\text{M s})^{-1}$
a5	10	$(\mu\text{M s})^{-1}$
d1	2.6	μM
d2	0.03077	μM
d3	2.6	μM
d4	0.1	μM
d5	12.25	μM

A.2 Multi-Scale Simulations of Ca^{2+} Currents

Skupin and Falcke developed a detailed stochastic model of intracellular Ca^{2+} dynamics, which has recently been published [194]. That model explicitly simulates single-channel and buffer dynamics and uses more realistic equations for Ca^{2+} diffusion than the model presented in Chapter 3. It cannot be solved analytically and needs parallel computing to run efficiently. The Ca^{2+} currents obtained from that model show that fluctuations in the number of open channels during a puff smooth out by diffusion to nearby clusters (Fig. A.1). This is in fact a property of the Green's function that governs diffusive propagation [14], and it legitimates the assumption of a constant Ca^{2+} current in the cluster during a puff (Chapter 3).

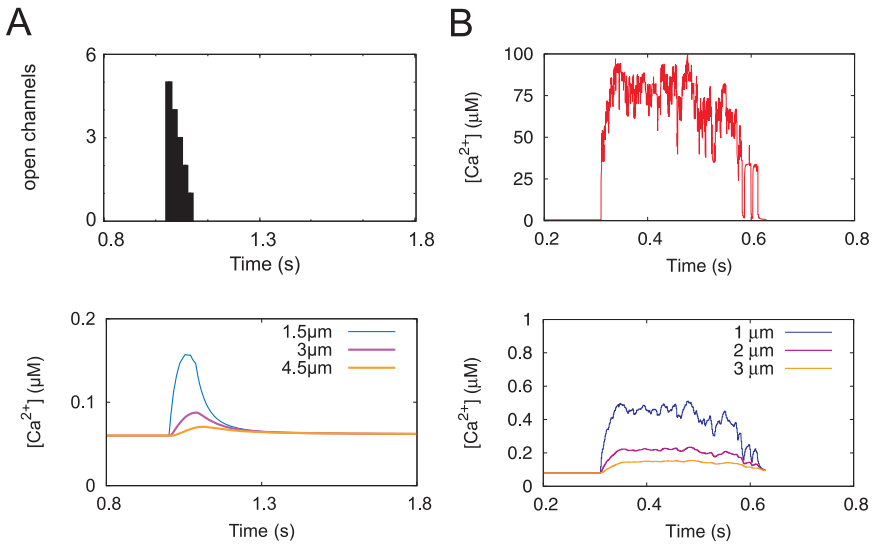

Figure A.1: Simulation of the rise of free $[Ca^{2+}]$ due to an open cluster. This figure was kindly provided by Alexander Skupin and prepared by the method published in ref. [194]. (A) The time course of channel closing was chosen according to the average measured rate in reference [196]. Top: number of open channels in the open cluster. Bottom: $[Ca^{2+}]$ at typical distances to neighboured clusters. (B) Simulation of a random and very long puff. Top: $[Ca^{2+}]$ at the open cluster. Bottom: $[Ca^{2+}]$ at typical distances to neighboured clusters. The simulations show that the assumption of a constant $[Ca^{2+}]$ at neighboured clusters during a puff is a good approximation, because the Ca^{2+} currents smooth out by diffusion, as referred to in Section 3.1. To obtain the shown graphs, linearized buffer and pump dynamics like described in [194] were used, with a total concentration of stationary buffer of 100 µM (dissociation constant 2 µM). Other parameter values are: Concentration of mobile buffer of 20 µM (A) and 100 µM (B) with dissociation constant 0.16 µM and diffusion coefficient 95 $\mu m^2 s^{-1}$; diffusion coefficient of free Ca^{2+} 220 $\mu m^2 s^{-1}$; pump flux coefficient 100 s^{-1}; 10 channels per cluster; single channel current 0.12 pA (A) and 0.11 pa (B); cell radius 10 µm.

A.3 IP_3- and N_{ch}- Dependencies of the Approximated ψ_o

Section 4.3 describes how the input data to the hierarchic stochastic model (see Section 3.2) can be approximated by analytic dependencies on the parameters $[Ca^{2+}]$, $[IP_3]$ and N_{ch}. In practice, instead of varying the Ca^{2+} concentration, it is more appropriate to do simulations with varying cluster distance, which causes different Ca^{2+} concentrations arising by opening of adjacent clusters. For that purpose, the fitting parameters given in Tab. 4.1 are sufficient. However, modulation of $[IP_3]$ and N_{ch} causes different opening probabilities ψ_o at each configuration with at least one closed cluster. In the case of the tetrahedron model (Section 3.4), those are the system states with 0, 1, 2 or 3 open clusters. The base-level configuration with all clusters closed is described by exponential distributions, which are approximated according to Eq. **4.5**, while the other configurations are described by γ-distributions and approximated by Eqs. **4.3-4.4**. The fitting parameters for the mentioned system configurations are given in Tabs. A.2 and A.3 for the dependences on $[IP_3]$ and N_{ch}, respectively.

Table A.2: Fitting parameters determining approximated dependence of ψ_o on $[IP_3]$(indicated by the index p). The second index indicates the number of open clusters N_{cl} in the tetrahedron model, for which the fittings to γ-distributions were performed, or relation to the puff-rate λ. Parameters needed to compute $[Ca^{2+}]$ in the respective system configurations are given in Tab. 3.1.

Parameter	**Value**	**Fitting Error**	**Unit**
$V_{p,1}$	0.874	0.001	
$K_{p,1}$	0.221	0.000	μM
$n_{p,1}$	1.504	0.005	
$A_{p,1}$	37.70	1.24	μM^{-1} s
$B_{p,1}$	0.177	0.001	s^{-1}
$m_{p,1}$	1.822	0.001	
$V_{p,2}$	1.609	0.001	
$K_{p,2}$	0.192	0.001	μM
$n_{p,2}$	1.612	0.010	
$A_{p,2}$	206.9	9.9	μM^{-1} s
$B_{p,2}$	0.044	0.000	s^{-1}
$m_{p,2}$	1.903	0.021	
$V_{p,3}$	1.975	0.003	
$K_{p,3}$	0.180	0.001	μM
$n_{p,3}$	1.627	0.016	
$A_{p,3}$	437.2	25.0	μM^{-1} s
$B_{p,3}$	1.913	0.025	s^{-1}
$m_{p,3}$	0.023	0.000	
$V_{p,\lambda}$	0.00940	0.00008	s^{-1}
$K_{p,\lambda}$	0.383	0.006	μM
$n_{p,\lambda}$	1.510	0.034	

Table A.3: Fitting parameters determining approximated dependence of ψ_o on N_{ch}(indicated by the index N). The second index indicates the number of open clusters N_{cl} in the tetrahedron model, for which the fittings to γ-distributions were performed, or relation to the puff-rate λ. Parameters needed to compute $[Ca^{2+}]$ in the respective system configurations are given in Tab. 3.1.

Parameter	**Value**	**Fitting Error**	**Unit**
$V_{N,1}$	3.610	0.024	
$K_{N,1}$	22.52	0.36	
$n_{N,1}$	0.838	0.004	
$A_{N,1}$	0.778	0.001	s
$B_{N,1}$	0.0138	0.0000	s^{-1}
$m_{N,1}$	1.712	0.001	
$V_{N,2}$	3.821	0.012	
$K_{N,2}$	8.558	0.074	
$n_{N,2}$	0.813	0.003	
$A_{N,2}$	3.786	0.008	s
$B_{N,2}$	0.008	0.000	s^{-1}
$m_{N,2}$	1.147	0.005	
$V_{N,3}$	3.969	0.015	
$K_{N,3}$	5.948	0.063	
$n_{N,3}$	0.781	0.004	
$A_{N,3}$	8.260	0.026	s
$B_{N,3}$	0.005	0.000	s^{-1}
$m_{N,3}$	1.088	0.007	
$a_{N,\lambda}$	0.00150	0.00000	s^{-1}

B Experimental Appendix

B.1 Materials and Methods for Puff Recordings in SH-SY5Y Cells

Measurements of puff-sequences in SH-SY5Y cells were performed by Dr Ian Smith in the lab of Prof Ian Parker (see Introduction). The experimental procedures were published in ref. [197] and are recapitulated here in brief. Puff-recordings in HEK cells are described in Section 6.1.

Cell Culture and loading. Human neuroblastoma SH-SY5Y cells were cultured as previously described [197] in a mixture (1:1) of Ham's F12 medium and Eagle's minimal essential medium, supplemented with 10 % (v/v) foetal calf serum and 1 % nonessential amino acids. Cells were incubated at 37° C in a humidified incubator gassed with 95 % air and 5 % CO_2, passaged every 7 days and used for up to 20 passages. Four days prior to imaging, cells were harvested in phosphate-buffered saline (PBS) without Ca^{2+} or Mg^{2+} and sub-cultured in Petri dishes with glass coverslips as the base (MatTek) at a seeding density of 3×104 cells/ml. Cells were then loaded a few hours before use by incubation with HEPES-buffered saline (HBS: in mM; NaCl 135, KCl 5, $MgSO_4$ 1.2, $CaCl_2$ 2.5, HEPES 5, glucose 10) containing 1 μM ciIP_3/PM (SiChem, Bremen, Germany) at room temperature for 45 mins, followed by incubation with 1 μM caged ciIP_3PM plus 5 μM fluo-4AM (Invitrogen, Carlsbad, CA) at room temperature for 45 min, and finally 45 min with 5 μM EGTA-AM (Invitrogen, Carlsbad, CA).

Total Internal Reflection Fluorescence (TIRF) Microscopy. Imaging of changes in the Ca^{2+} concentration was accomplished using a home-built TIRF

microscope system based around an Olympus IX 70 microscope equipped with an Olympus X60 TIRFM objective (NA 1.45). Fluorescence of cytosolic Fluo-4 was excited within the $\approx$ 100 nm evanescent field formed by total internal reflection of a 488 nm laser beam incident through the microscope objective at the cover-glass/aqueous interface. Images of emitted fluorescence ($>$ 510 nm) were captured at a resolution of 128×128 pixels (1 pixel = 0.33 μm) at a rate of 500 frames/s by a Cascade 128 electron multiplied CCD camera (Roper Scientific). Photorelease of iIP_3 from a caged precursor was evoked by flashes of UV (350-400nm) light derived from a fiber-optic arc lamp source introduced via a UV reflecting dichroic mirror in the upper side-port of the microscope. The UV light was adjusted to uniformly irradiate a region slightly larger than the imaging frame, and any given imaging field was exposed to only a single flash.

Bibliography

[1] M. Acar, J. T. Mettetal, and A. van Oudenaarden. Stochastic switching as a survival strategy in fluctuating environments. *Nat Genet*, 40(4):471–5, 2008.

[2] L. Alberghina, T. Höfer, and M. Vanoni. Molecular networks and system-level properties. *J Biotechnol*, 144(3):224–33, 2009.

[3] U. Alon. Biological Newtworks: The Tinkerer as an Engineer. *Science*, 301, 2003.

[4] U. Alon. *An Introduction to Systems Biology: Design Principles of Biological Circuits*. Chapman and Hall, 2006.

[5] U. Alon. Network motifs: theory and experimental approaches. *Nat Rev Genet*, 8(6):450–61, 2007.

[6] U. Alon, M. G. Surette, N. Barkai, and S. Leibler. Robustness in bacterial chemotaxis. *Nature*, 397(6715):168–71, 1999.

[7] V. S. Anishenko, V. Astakhov, A. Neiman, T. Vadivasova, and L. Schimansky-Geier. *Nonlinear Dynamics of Chaotic and Stochastic Systems: Tutorial and Modern Developments*. Springer, 2007.

[8] A. Atri, J. Amundson, D. Clapham, and J. Sneyd. A single-pool model for intracellular calcium oscillations and waves in the Xenopus laevis oocyte. *Biophys J*, 65(4):1727–39, 1993.

[9] N. Q. Balaban, J. Merrin, R. Chait, L. Kowalik, and S. Leibler. Bacterial persistence as a phenotypic switch. *Science*, 305(5690):1622–5, 2004.

[10] M. Barberis, E. Klipp, M. Vanoni, and L. Alberghina. Cell size at S phase initiation: an emergent property of the G1/S network. *PLoS Comput Biol*, 3(4):e64, 2007.

[11] N. Barkai and S. Leibler. Robustness in simple biochemical networks. *Nature*, 387(6636):913–7, 1997.

[12] N. Barkai and B. Z. Shilo. Variability and robustness in biomolecular systems. *Mol Cell*, 28(5):755–60, 2007.

[13] M. Barrio, K. Burrage, A. Leier, and T. Tian. Oscillatory Regulation of Hes1: Discrete Stochastic Delay Modelling and Simulation. *Plos Comput Biol*, 2(9):1017–1030, 2006.

[14] G. Barton. *Elements of Green's Functions and Propagation: Potentials, Diffusion, and Waves*. Oxford University Press, Oxford, 1989.

[15] A. Becskei, B. Seraphin, and L. Serrano. Positive feedback in eukaryotic gene networks: cell differentiation by graded to binary response conversion. *EMBO J*, 20(10):2528–35, 2001.

[16] A. Becskei and L. Serrano. Engineering stability in gene networks by autoregulation. *Nature*, 405(6786):590–3, 2000.

[17] G. Bel, B. Munsky, and I. Nemenman. The simplicity of completion time distributions for common complex biochemical processes. *Phys Biol*, 7(1):016003, 2010.

[18] K. Bentele and M. Falcke. Quasi-steady approximation for ion channel currents. *Biophys J*, 93(8):2597–608, 2007.

[19] H. C. Berg. *Random Walks in Biology, expanded edition*. Princeton University Press, 1993.

[20] H. C. Berg and E. M. Purcell. Physics of chemoreception. *Biophys J*, 20(2):193–219, 1977.

[21] M. J. Berridge. Inositol trisphosphate and calcium signalling. *Nature*, 361(6410):315–25, 1993.

[22] M. J. Berridge. The AM and FM of calcium signalling. *Nature*, 386(6627):759–60, 1997.

[23] M. J. Berridge. Elementary and global aspects of calcium signalling. *J Physiol*, 499 (Pt 2):291–306, 1997.

[24] M. J. Berridge. Lymphocyte activation in health and disease. *Crit Rev Immunol*, 17(2):155–78, 1997.

[25] M. J. Berridge. Inositol trisphosphate and calcium signalling mechanisms. *Biochim Biophys Acta*, 1793(6):933–40, 2009.

[26] M. J. Berridge, M. D. Bootman, and P. Lipp. Calcium–a life and death signal. *Nature*, 395(6703):645–8, 1998.

[27] M. J. Berridge, M. D. Bootman, and H. L. Roderick. Calcium signalling: dynamics, homeostasis and remodelling. *Nat Rev Mol Cell Biol*, 4(7):517–29, 2003.

[28] M. J. Berridge, P. Lipp, and M. D. Bootman. The versatility and universality of calcium signalling. *Nat Rev Mol Cell Biol*, 1(1):11–21, 2000.

[29] I. Bezprozvanny, J. Watras, and B. E. Ehrlich. Bell-shaped calcium-response curves of Ins(1,4,5)P3- and calcium-gated channels from endoplasmic reticulum of cerebellum. *Nature*, 351(6329):751–4, 1991.

[30] U. S. Bhalla and R. Iyengar. Emergent properties of networks of biological signaling pathways. *Science*, 283(5400):381–7, 1999.

[31] G. S. Bird and J. Putney, J. W. Capacitative calcium entry supports calcium oscillations in human embryonic kidney cells. *J Physiol*, 562(Pt 3):697–706, 2005.

[32] W. J. Blake, K. A. M, C. R. Cantor, and J. J. Collins. Noise in eukaryotic gene expression. *Nature*, 422(6932):633–7, 2003.

[33] M. Bootman, E. Niggli, M. Berridge, and P. Lipp. Imaging the hierarchical Ca^{2+} signalling system in HeLa cells. *J Physiol*, 499 (Pt 2):307–14, 1997.

[34] M. D. Bootman, M. J. Berridge, and P. Lipp. Cooking with calcium: the recipes for composing global signals from elementary events. *Cell*, 91(3):367–73, 1997.

[35] N. M. Borisov, A. S. Chistopolsky, J. R. Faeder, and B. N. Kholodenko. Domain-oriented reduction of rule-based network models. *IET Syst Biol*, 2(5):342–51, 2008.

[36] N. M. Borisov, N. I. Markevich, J. B. Hoek, and B. N. Kholodenko. Signaling through receptors and scaffolds: independent interactions reduce combinatorial complexity. *Biophys J*, 89(2):951–66, 2005.

[37] D. Bratsun, D. Volfson, L. S. Tsimring, and J. Hasty. Delay-induced stochastic oscillations in gene regulation. *Proc Natl Acad Sci U S A*, 102(41):14593–8, 2005.

[38] D. Bray. Signaling complexes: biophysical constraints on intracellular communication. *Annu Rev Biophys Biomol Struct*, 27:59–75, 1998.

[39] D. Bray, M. D. Levin, and C. J. Morton-Firth. Receptor clustering as a cellular mechanism to control sensitivity. *Nature*, 393(6680):85–8, 1998.

[40] F. J. Bruggeman, N. Blüthgen, and H. V. Westerhoff. Noise management by molecular networks. *PLoS Comput Biol*, 5(9):e1000506, 2009.

[41] A. Brummer, C. Salazar, V. Zinzalla, L. Alberghina, and T. Hofer. Mathematical modelling of DNA replication reveals a trade-off between coherence of origin activation and robustness against rereplication. *PLoS Comput Biol*, 6(5):e1000783, 2010.

[42] D. Busse, M. de la Rosa, K. Hobiger, K. Thurley, M. Flossdorf, A. Scheffold, and T. Höfer. Competing feedback loops shape IL-2 signaling between helper and regulatory T lymphocytes in cellular microenvironments. *Proc Natl Acad Sci U S A*, 107(7):3058–63, 2010.

[43] T. Cagatay, M. Turcotte, M. B. Elowitz, J. Garcia-Ojalvo, and G. M. Suel. Architecture-dependent noise discriminates functionally analogous differentiation circuits. *Cell*, 139(3):512–22, 2009.

[44] L. Cai, C. K. Dalal, and M. B. Elowitz. Frequency-modulated nuclear localization bursts coordinate gene regulation. *Nature*, 455(7212):485–90, 2008.

[45] C. Cardenas, R. A. Miller, I. Smith, T. Bui, J. Molgo, M. Muller, H. Vais, K. H. Cheung, J. Yang, I. Parker, C. B. Thompson, M. J. Birnbaum, K. R. Hallows, and J. K. Foskett. Essential regulation of cell bioenergetics by constitutive InsP3 receptor Ca^{2+} transfer to mitochondria. *Cell*, 142(2):270–83, 2010.

[46] S. Clodong, U. Duhring, L. Kronk, A. Wilde, I. Axmann, H. Herzel, and M. Kollmann. Functioning and robustness of a bacterial circadian clock. *Mol Syst Biol*, 3:90, 2007.

[47] D. Cox. *Renewal Theory*. Methuen & Co, 1970.

[48] D. Cox and P. Lewis. *The Statistical Analysis of Series of Events*. Chapman and Hall, 1966.

[49] P. C. da Fonseca, S. A. Morris, E. P. Nerou, C. W. Taylor, and E. P. Morris. Domain organization of the type 1 inositol 1,4,5-trisphosphate receptor as revealed by single-particle analysis. *Proc Natl Acad Sci U S A*, 100(7):3936–41, 2003.

[50] B. C. Daniels, Y. J. Chen, J. P. Sethna, R. N. Gutenkunst, and C. R. Myers. Sloppiness, robustness, and evolvability in systems biology. *Curr Opin Biotechnol*, 19(4):389–95, 2008.

[51] G. W. De Young and J. Keizer. A single-pool inositol 1,4,5-trisphosphate-receptor-based model for agonist-stimulated oscillations in Ca^{2+} concentration. *Proc Natl Acad Sci U S A*, 89(20):9895–9, 1992.

[52] E. Dekel and U. Alon. Optimality and evolutionary tuning of the expression level of a protein. *Nature*, 436(7050):588–92, 2005.

[53] M. Delbrück. Statistical Fluctuations in Autocatalytic Reations. *J Chem Phys*, 8:120–124, 1940.

[54] M. Delbrück. The burst size distribution in the growth of bacterial viruses (bacteriophages). *J Bacteriol*, 50:131–5, 1945.

[55] M. Delbrück. What is Life? and What is Truth? *Quart Rev Biol*, 20(4):370–372, 1945.

[56] T. Dobzhansky. Nothing in biology makes sense except in the light of evolution. *Am Biol Teach*, 35:125–129, 1973.

[57] R. E. Dolmetsch, K. Xu, and R. S. Lewis. Calcium oscillations increase the efficiency and specificity of gene expression. *Nature*, 392(6679):933–6, 1998.

[58] G. Dupont, A. Abou-Lovergne, and L. Combettes. Stochastic aspects of oscillatory Ca^{2+} dynamics in hepatocytes. *Biophys J*, 95(5):2193–202, 2008.

[59] G. Dupont and L. Combettes. What can we learn from the irregularity of Ca^{2+} oscillations? *Chaos*, 19(3):037112, 2009.

[60] G. Dupont and C. Erneux. Simulations of the effects of inositol 1,4,5-trisphosphate 3-kinase and 5-phosphatase activities on Ca^{2+} oscillations. *Cell Calcium*, 22(5):321–31, 1997.

[61] G. Dupont, O. Koukoui, C. Clair, C. Erneux, S. Swillens, and L. Combettes. Ca^{2+} oscillations in hepatocytes do not require the modulation of InsP3 3-kinase activity by Ca^{2+} . *FEBS Lett*, 534(1-3):101–5, 2003.

[62] A. Eldar and M. B. Elowitz. Functional roles for noise in genetic circuits. *Nature*, 467(7312):167–73, 2010.

[63] M. B. Elowitz, A. J. Levine, E. D. Siggia, and P. S. Swain. Stochastic gene expression in a single cell. *Science*, 297(5584):1183–6, 2002.

[64] C. Espinosa-Soto and A. Wagner. Specialization can drive the evolution of modularity. *PLoS Comput Biol*, 6(3):e1000719, 2010.

[65] M. Falcke. Buffers and oscillations in intracellular Ca^{2+} dynamics. *Biophys J*, 84(1):28–41, 2003.

[66] M. Falcke. On the role of stochastic channel behavior in intracellular Ca^{2+} dynamics. *Biophys J*, 84(1):42–56, 2003.

[67] M. Falcke. Reading the patterns in living cells – the physics of Ca^{2+} signaling. *Advances in Physics*, 53(3), 2004.

[68] M. Falcke, J. L. Hudson, P. Camacho, and J. D. Lechleiter. Impact of mitochondrial Ca^{2+} cycling on pattern formation and stability. *Biophys J*, 77(1):37–44, 1999.

[69] M. Falcke, L. Tsimring, and H. Levine. Stochastic spreading of intracellular Ca(2+) release. *Phys Rev E*, 62(2 Pt B):2636–43, 2000.

[70] O. Feinerman, J. Veiga, J. R. Dorfman, R. N. Germain, and G. Altan-Bonnet. Variability and robustness in T cell activation from regulated heterogeneity in protein levels. *Science*, 321(5892):1081–4, 2008.

[71] M. Ferreri-Jacobia, D. O. Mak, and J. K. Foskett. Translational mobility of the type 3 inositol 1,4,5-trisphosphate receptor Ca^{2+} release channel in endoplasmic reticulum membrane. *J Biol Chem*, 280(5):3824–31, 2005.

[72] S. Feske. Calcium signalling in lymphocyte activation and disease. *Nat Rev Immunol*, 7(9):690–702, 2007.

[73] E. P. Fischer. Max Delbrück. *Genetics*, 177(2):673–6, 2007.

[74] H. B. Fraser, A. E. Hirsh, G. Giaever, J. Kumm, and M. B. Eisen. Noise minimization in eukaryotic gene expression. *PLoS Biol*, 2(6):e137, 2004.

[75] J. Gerhart and M. Kirschner. The theory of facilitated variation. *Proc Natl Acad Sci U S A*, 104 Suppl 1:8582–9, 2007.

[76] A. M. Gilfillan and C. Tkaczyk. Integrated signalling pathways for mast-cell activation. *Nat Rev Immunol*, 6(3):218–30, 2006.

[77] D. T. Gillespie. Exact stochastic simulation of coupled chemical reactions. *J Phys Chem*, 81:2340–2361, 1977.

[78] D. T. Gillespie. Transition time statistics in simple bi-stable chemical systems. *Physica A*, 101, 1980.

[79] D. T. Gillespie. *Markov Processes – An Introduction for Physical Scientists*. Academic Press, 1992.

[80] A. Goldbeter. *Biochemical Oscillations and Cellular Rhythms: The Molecular Bases of Periodic and Chaotic Behaviour*. Cambridge University Press, 1997.

[81] A. Goldbeter, G. Dupont, and M. J. Berridge. Minimal model for signal-induced Ca^{2+} oscillations and for their frequency encoding through protein phosphorylation. *Proc Natl Acad Sci U S A*, 87(4):1461–5, 1990.

[82] I. Goychuk and P. Hänggi. Stochastic resonance in ion channels characterized by information theory. *Phys Rev E Stat Phys Plasmas Fluids Relat Interdiscip Topics*, 61(4 Pt B):4272–80, 2000.

[83] D. Greenfield, A. L. McEvoy, H. Shroff, G. E. Crooks, N. S. Wingreen, E. Betzig, and J. Liphardt. Self-organization of the Escherichia coli chemotaxis network imaged with super-resolution light microscopy. *PLoS Biol*, 7(6):e1000137, 2009.

[84] M. Hafner, H. Koeppl, M. Hasler, and A. Wagner. 'Glocal' robustness analysis and model discrimination for circadian oscillators. *PLoS Comput Biol*, 5(10):e1000534, 2009.

[85] G. Hajnoczky, L. D. Robb-Gaspers, M. B. Seitz, and A. P. Thomas. Decoding of cytosolic calcium oscillations in the mitochondria. *Cell*, 82(3):415–24, 1995.

[86] G. Hajnoczky and A. P. Thomas. Minimal requirements for calcium oscillations driven by the IP3 receptor. *EMBO J*, 16(12):3533–43, 1997.

[87] P. Hammerstein. Darwinian adaptation, population genetics and the streetcar theory of evolution. *J Math Biol*, 34(5-6):511–32, 1996.

[88] P. Hammerstein, E. H. Hagen, A. Herz, and H. Herzel. Robustness: A Key to Evolutionary Design. *Biol Theory*, 1(1):90–93, 2005.

[89] C. J. Hanson, M. D. Bootman, and H. L. Roderick. Cell signalling: IP3 receptors channel calcium into cell death. *Curr Biol*, 14(21):R933–5, 2004.

[90] L. Hartwell. Theoretical biology. A robust view of biochemical pathways. *Nature*, 387(6636):855, 857, 1997.

[91] L. H. Hartwell, J. J. Hopfield, S. Leibler, and A. W. Murray. From molecular to modular cell biology. *Nature*, 402(6761 Suppl):C47–52, 1999.

[92] R. Heinrich, S. M. Rapoport, and T. A. Rapoport. Metabolic regulation and mathematical models. *Prog Biophys Mol Biol*, 32(1):1–82, 1977.

[93] R. Heinrich and S. Schuster. *The regulation of cellular systems*. Chapman and Hall, 1996.

[94] E. R. Higgins, H. Schmidle, and M. Falcke. Waiting time distributions for clusters of IP_3 receptors. *Journal of Theoretical Biology*, 259(2):338–349, 2009.

[95] D. Holowka and B. Baird. Antigen-mediated IGE receptor aggregation and signaling: a window on cell surface structure and dynamics. *Annu Rev Biophys Biomol Struct*, 25:79–112, 1996.

[96] M. Huse, L. O. Klein, A. T. Girvin, J. M. Faraj, Q. J. Li, M. S. Kuhns, and M. M. Davis. Spatial and temporal dynamics of T cell receptor signaling with a photoactivatable agonist. *Immunity*, 27(1):76–88, 2007.

[97] T. Höfer, A. Politi, and R. Heinrich. Intercellular Ca^{2+} wave propagation through gap-junctional Ca^{2+} diffusion: a theoretical study. *Biophys J*, 80(1):75–87, 2001.

[98] F. Ichas, L. S. Jouaville, and J. P. Mazat. Mitochondria are excitable organelles capable of generating and conveying electrical and calcium signals. *Cell*, 89(7):1145–53, 1997.

[99] Q. X. Jiang, E. C. Thrower, D. W. Chester, B. E. Ehrlich, and F. J. Sigworth. Three-dimensional structure of the type 1 inositol 1,4,5-trisphosphate receptor at 24 Å resolution. *EMBO J*, 21(14):3575–81, 2002.

[100] L. M. John, M. Mosquera-Caro, P. Camacho, and J. D. Lechleiter. Control of IP(3)-mediated Ca^{2+} puffs in Xenopus laevis oocytes by the Ca^{2+}-binding protein parvalbumin. *J Physiol*, 535(Pt 1):3–16, 2001.

[101] M. Kaern, T. C. Elston, W. J. Blake, and J. J. Collins. Stochasticity in gene expression: from theories to phenotypes. *Nat Rev Genet*, 6(6):451–64, 2005.

[102] N. Kashtan and U. Alon. Spontaneous evolution of modularity and network motifs. *Proc Natl Acad Sci U S A*, 102(39):13773–8, 2005.

[103] N. Kashtan, M. Parter, E. Dekel, A. E. Mayo, and U. Alon. Extinctions in heterogeneous environments and the evolution of modularity. *Evolution*, 63(8):1964–75, 2009.

[104] N. N. Kasri, A. M. Holmes, G. Bultynck, J. B. Parys, M. D. Bootman, K. Rietdorf, L. Missiaen, F. McDonald, H. De Smedt, S. J. Conway, A. B. Holmes, M. J. Berridge, and H. L. Roderick. Regulation of InsP3 receptor activity by neuronal Ca^{2+}-binding proteins. *EMBO J*, 23(2):312–21, 2004.

[105] J. Keener and J. Sneyd. *Mathematical Physiology*. Springer, 2009.

[106] B. N. Kholodenko. Cell-signalling dynamics in time and space. *Nat Rev Mol Cell Biol*, 7(3):165–76, 2006.

[107] B. N. Kholodenko. Spatially distributed cell signalling. *FEBS Lett*, 583(24):4006–12, 2009.

[108] B. N. Kholodenko and W. Kolch. Giving space to cell signaling. *Cell*, 133(4):566–7, 2008.

[109] M. Kirschner and J. Gerhart. Evolvability. *Proc Natl Acad Sci U S A*, 95(15):8420–7, 1998.

[110] M. Kirschner and J. Gerhart. *The Plausibility of Life: Resolving Darwin's Dilemma*. Yale University Press, 2006.

[111] H. Kitano. Computational systems biology. *Nature*, 420(6912):206–10, 2002.

[112] H. Kitano. Systems biology: a brief overview. *Science*, 295(5560):1662–4, 2002.

[113] H. Kitano. Biological robustness. *Nat Rev Genet*, 5(11):826–37, 2004.

[114] E. Klipp and R. Heinrich. Evolutionary optimization of enzyme kinetic parameters; effect of constraints. *J Theor Biol*, 171(3):309–23, 1994.

[115] E. Klipp, W. Liebermeister, C. Wierling, A. Kowald, H. Lehrach, and R. Herwig. *Systems Biology: A Textbook*. Wiley VCH, 2009.

[116] M. Kollmann, L. Lovdok, K. Bartholome, J. Timmer, and V. Sourjik. Design principles of a bacterial signalling network. *Nature*, 438(7067):504–7, 2005.

[117] E. Korobkova, T. Emonet, J. M. Vilar, T. S. Shimizu, and P. Cluzel. From molecular noise to behavioural variability in a single bacterium. *Nature*, 428(6982):574–8, 2004.

[118] M. Krantz, D. Ahmadpour, L. G. Ottosson, J. Warringer, C. Waltermann, B. Nordlander, E. Klipp, A. Blomberg, S. Hohmann, and H. Kitano. Robustness and fragility in the yeast high osmolarity glycerol (HOG) signal-transduction pathway. *Mol Syst Biol*, 5:281, 2009.

[119] E. Kussell and S. Leibler. Phenotypic diversity, population growth, and information in fluctuating environments. *Science*, 309(5743):2075–8, 2005.

[120] Y. Lan, P. G. Wolynes, and G. A. Papoian. A variational approach to the stochastic aspects of cellular signal transduction. *J Chem Phys*, 125(12):124106, 2006.

[121] A. Z. Larsen, L. F. Olsen, and U. Kummer. On the encoding and decoding of calcium signals in hepatocytes. *Biophys Chem*, 107(1):83–99, 2004.

[122] R. B. Laughlin. *A Different Universe: Reinventing Physics from the Bottom Down*. Basic Books, New York, 2005.

[123] R. B. Laughlin and D. Pines. The theory of everything. *Proc Natl Acad Sci U S A*, 97(1):28–31, 2000.

[124] S. Legewie, N. Blüthgen, R. Schäfer, and H. Herzel. Ultrasensitization: switch-like regulation of cellular signaling by transcriptional induction. *PLoS Comput Biol*, 1(5):e54, 2005.

[125] R. E. Lenski, J. E. Barrick, and C. Ofria. Balancing robustness and evolvability. *PLoS Biol*, 4(12):e428, 2006.

[126] I. Lestas, G. Vinnicombe, and J. Paulsson. Fundamental limits on the suppression of molecular fluctuations. *Nature*, 467(7312):174–8, 2010.

[127] W. Li, J. Llopis, M. Whitney, G. Zlokarnik, and R. Y. Tsien. Cell-permeant caged InsP3 ester shows that Ca^{2+} spike frequency can optimize gene expression. *Nature*, 392(6679):936–41, 1998.

[128] W. Liebermeister, U. Baur, and E. Klipp. Biochemical network models simplified by balanced truncation. *FEBS J*, 272(16):4034–43, 2005.

[129] S. Lin and L. Segel. *Mathematics applied to deterministic problems in the natural sciences*. SIAM, Philadelphia, 1988.

[130] H. Lodish, A. Berk, C. Kaiser, M. Krieger, M. Scott, and A. Bretscher. *Molecular Cell Biology*. Palgrave Macmillan, 6th edition, 2007.

[131] R. Losick and C. Desplan. Stochasticity and cell fate. *Science*, 320(5872):65–8, 2008.

[132] T. Lu, T. Shen, C. Zong, J. Hasty, and P. G. Wolynes. Statistics of cellular signal transduction as a race to the nucleus by multiple random walkers in compartment/phosphorylation space. *Proc Natl Acad Sci U S A*, 103(45):16752–7, 2006.

[133] C. H. Lubich. On the stability of Linear Multistep Methods for Volterra Convolution Equations. *IMA Journal of Numerical Analysis*, 3:439–465, 1983.

[134] D. Luo, L. M. Broad, G. S. Bird, and J. Putney, J. W. Signaling pathways underlying muscarinic receptor-induced [Ca^{2+}]i oscillations in HEK293 cells. *J Biol Chem*, 276(8):5613–21, 2001.

[135] H. Maamar, A. Raj, and D. Dubnau. Noise in gene expression determines cell fate in Bacillus subtilis. *Science*, 317(5837):526–9, 2007.

[136] G. Magnus and J. Keizer. Minimal model of beta-cell mitochondrial Ca^{2+} handling. *Am J Physiol*, 273(2 Pt 1):C717–33, 1997.

[137] J. S. Marchant, N. Callamaras, and I. Parker. Initiation of IP3-mediated Ca^{2+} waves in Xenopus oocytes. *EMBO J*, 18(19):5285–5299, 1999.

[138] J. S. Marchant and I. Parker. Role of elementary Ca^{2+} puffs in generating repetitive Ca^{2+} oscillations. *EMBO J*, 20(1-2):65–76, 2001.

[139] M. Marhl, T. Haberichter, M. Brumen, and R. Heinrich. Complex calcium oscillations and the role of mitochondria and cytosolic proteins. *Biosystems*, 57(2):75–86, 2000.

[140] L. Mariani, E. G. Schulz, M. H. Lexberg, C. Helmstetter, A. Radbruch, M. Löhning, and T. Höfer. Short-term memory in gene induction reveals the regulatory principle behind stochastic IL-4 expression. *Mol Syst Biol*, 6:359, 2010.

[141] I. C. Marshall and C. W. Taylor. Biphasic effects of cytosolic Ca^{2+} on Ins(1,4,5)P3-stimulated Ca^{2+} mobilization in hepatocytes. *J Biol Chem*, 268(18):13214–20, 1993.

[142] I. C. Marshall and C. W. Taylor. Two calcium-binding sites mediate the interconversion of liver inositol 1,4,5-trisphosphate receptors between three conformational states. *Biochem J*, 301 (Pt 2):591–8, 1994.

[143] M. J. Mason, C. Garcia-Rodriguez, and S. Grinstein. Coupling between intracellular Ca^{2+} stores and the Ca^{2+} permeability of the plasma membrane. Comparison of the effects of thapsigargin, 2,5-di-(tert-butyl)-1,4-hydroquinone, and cyclopiazonic acid in rat thymic lymphocytes. *J Biol Chem*, 266(31):20856–62, 1991.

[144] H. H. McAdams and A. Arkin. Stochastic mechanisms in gene expression. *Proc Natl Acad Sci U S A*, 94(3):814–9, 1997.

[145] P. Mehta and T. Gregor. Approaching the molecular origins of collective dynamics in oscillating cell populations. *Curr Opin Genet Dev*, 20(6):574–80, 2010.

[146] T. Meyer and L. Stryer. Molecular model for receptor-stimulated calcium spiking. *Proc Natl Acad Sci U S A*, 85(14):5051–5, 1988.

[147] L. Missiaen, C. W. Taylor, and M. J. Berridge. Spontaneous calcium release from inositol trisphosphate-sensitive calcium stores. *Nature*, 352(6332):241–4, 1991.

[148] U. Moran, R. Phillips, and R. Milo. SnapShot: key numbers in biology. *Cell*, 141(7):1262–1262 e1, 2010.

[149] B. Munsky, I. Nemenman, and G. Bel. Specificity and completion time distributions of biochemical processes. *J Chem Phys*, 131:235103, 2009.

[150] J. Murray. *Mathematical Biology*. Springer, 2003.

[151] B. Novak and J. J. Tyson. Design principles of biochemical oscillators. *Nat Rev Mol Cell Biol*, 9(12):981–91, 2008.

[152] E. Oancea and T. Meyer. Protein kinase C as a molecular machine for decoding calcium and diacylglycerol signals. *Cell*, 95(3):307–18, 1998.

[153] E. M. Ozbudak, M. Thattai, I. Kurtser, A. D. Grossman, and A. van Oudenaarden. Regulation of noise in the expression of a single gene. *Nat Genet*, 31(1):69–73, 2002.

[154] A. Paldi. Stochastic gene expression during cell differentiation: order from disorder? *Cell Mol Life Sci*, 60(9):1775–8, 2003.

[155] I. Parker and I. F. Smith. Recording single-channel activity of inositol trisphosphate receptors in intact cells with a microscope, not a patch clamp. *J Gen Physiol*, 136(2):119–27, 2010.

[156] M. Parter, N. Kashtan, and U. Alon. Facilitated variation: how evolution learns from past environments to generalize to new environments. *PLoS Comput Biol*, 4(11):e1000206, 2008.

[157] J. Paulsson, O. G. Berg, and M. Ehrenberg. Stochastic focusing: fluctuation-enhanced sensitivity of intracellular regulation. *Proc Natl Acad Sci U S A*, 97(13):7148–53, 2000.

[158] H. Penzlin. The riddle of 'life,' a biologist's critical view. *Naturwissenschaften*, 96(1):1–23, 2009.

[159] T. J. Perkins and P. S. Swain. Strategies for cellular decision-making. *Mol Syst Biol*, 5:326, 2009.

[160] A. Pikovsky, M. Zaks, M. Rosenblum, G. Osipov, and J. Kurths. Phase synchronization of chaotic oscillations in terms of periodic orbits. *Chaos*, 7(4):680–687, 1997.

[161] F. Plenge-Tellechea, F. Soler, and F. Fernandez-Belda. On the inhibition mechanism of sarcoplasmic or endoplasmic reticulum Ca^{2+}-ATPases by cyclopiazonic acid. *J Biol Chem*, 272(5):2794–800, 1997.

[162] A. Politi. *Systems biology perspectives on calcium signaling and DNA repair*. Dissertation, Humboldt-Universität zu Berlin, 2008.

[163] A. Politi, L. D. Gaspers, A. P. Thomas, and T. Höfer. Models of IP3 and Ca^{2+} oscillations: frequency encoding and identification of underlying feedbacks. *Biophys J*, 90(9):3120–33, 2006.

[164] A. D. Polyanin and A. Manzhirov. *Handbook of Integral Equations*. Chapman and Hall, second edition edition, 2008.

[165] T. Prager. *Synchronization in periodically driven and coupled stochastic systems – A discrete state approach*. Dissertation, Humboldt-Universität zu Berlin, 2006.

[166] T. Prager, M. Falcke, L. Schimansky-Geier, and M. A. Zaks. Non-Markovian approach to globally coupled excitable systems. *Phys Rev E*, 76(1):011118, 2007.

[167] T. Prager, B. Naundorf, and L. Schimansky-Geier. Coupled three-state oscillators. *Physica A*, 325:176–185, 2003.

[168] J. Putney, J. W. A model for receptor-regulated calcium entry. *Cell Calcium*, 7(1):1–12, 1986.

[169] A. Raj and A. van Oudenaarden. Nature, nurture, or chance: stochastic gene expression and its consequences. *Cell*, 135(2):216–26, 2008.

[170] C. V. Rao, D. M. Wolf, and A. P. Arkin. Control, exploitation and tolerance of intracellular noise. *Nature*, 420(6912):231–7, 2002.

[171] J. M. Raser and E. K. O'Shea. Control of stochasticity in eukaryotic gene expression. *Science*, 304(5678):1811–4, 2004.

[172] H. Risken. *The Focker-Planck Equation – Methods of Solution and Applications*. Springer, Berlin, Heidelberg, New York, 1989.

[173] N. Rosenfeld, J. W. Young, U. Alon, P. S. Swain, and M. B. Elowitz. Gene regulation at the single-cell level. *Science*, 307(5717):1962–5, 2005.

[174] E. Rotem, A. Loinger, I. Ronin, I. Levin-Reisman, C. Gabay, N. Shoresh, O. Biham, and N. Q. Balaban. Regulation of phenotypic variability by a threshold-based mechanism underlies bacterial persistence. *Proc Natl Acad Sci U S A*, 107(28):12541–6, 2010.

[175] C. Salazar, A. Z. Politi, and T. Höfer. Decoding of calcium oscillations by phosphorylation cycles: analytic results. *Biophys J*, 94(4):1203–15, 2008.

[176] J. Schaber and E. Klipp. Model-based inference of biochemical parameters and dynamic properties of microbial signal transduction networks. *Curr Opin Biotechnol*, 22:1–8, 2010.

[177] J. Schaber, W. Liebermeister, and E. Klipp. Nested uncertainties in biochemical models. *IET Syst Biol*, 3(1):1–9, 2009.

[178] C. G. Schipke, A. Heidemann, A. Skupin, O. Peters, M. Falcke, and H. Kettenmann. Temperature and nitric oxide control spontaneous calcium transients in astrocytes. *Cell Calcium*, 43(3):285–95, 2008.

[179] R. Schlicht and G. Winkler. A delay stochastic process with applications in molecular biology. *J Math Biol*, 57:613–648, 2008.

[180] B. Schoeberl, C. Eichler-Jonsson, E. D. Gilles, and G. Muller. Computational modeling of the dynamics of the MAP kinase cascade activated by surface and internalized EGF receptors. *Nat Biotechnol*, 20(4):370–5, 2002.

[181] E. Schroedinger. *What is Life?* Cambridge University Press, 1944.

[182] S. Schuster, M. Marhl, and T. Höfer. Modelling of simple and complex calcium oscillations. From single-cell responses to intercellular signalling. *Eur J Biochem*, 269(5):1333–55, 2002.

[183] V. A. Selivanov, F. Ichas, E. L. Holmuhamedov, L. S. Jouaville, Y. V. Evtodienko, and J. P. Mazat. A model of mitochondrial Ca^{2+}-induced Ca^{2+} release simulating the Ca^{2+} oscillations and spikes generated by mitochondria. *Biophys Chem*, 72(1-2):111–21, 1998.

[184] V. Shahrezaei and P. S. Swain. Analytical distributions for stochastic gene expression. *Proc Natl Acad Sci U S A*, 105(45):17256–61, 2008.

[185] V. Shahrezaei and P. S. Swain. The stochastic nature of biochemical networks. *Curr Opin Biotechnol*, 19(4):369–74, 2008.

[186] G. Shinar, R. Milo, M. R. Martinez, and U. Alon. Input output robustness in simple bacterial signaling systems. *Proc Natl Acad Sci U S A*, 104(50):19931–5, 2007.

[187] A. D. Short and C. W. Taylor. Parathyroid hormone controls the size of the intracellular Ca^{2+} stores available to receptors linked to inositol trisphosphate formation. *J Biol Chem*, 275(3):1807–13, 2000.

[188] A. D. Short, G. P. Winston, and C. W. Taylor. Different receptors use inositol trisphosphate to mobilize Ca^{2+} from different intracellular pools. *Biochem J*, 351 Pt 3:683–6, 2000.

[189] J. W. Shuai and P. Jung. Stochastic properties of Ca^{2+} release of inositol 1,4,5-trisphosphate receptor clusters. *Biophys J*, 83(1):87–97, 2002.

[190] A. Sigal, R. Milo, A. Cohen, N. Geva-Zatorsky, Y. Klein, Y. Liron, N. Rosenfeld, T. Danon, N. Perzov, and U. Alon. Variability and memory of protein levels in human cells. *Nature*, 444(7119):643–6, 2006.

[191] A. Skupin. *How does Calcium oscillate? An interdisciplinary approach.* Dissertation, Humboldt-Universität zu Berlin, 2009.

[192] A. Skupin and M. Falcke. Statistical properties and information content of calcium oscillations. *Genome Inform*, 18:44–53, 2007.

[193] A. Skupin and M. Falcke. From puffs to global Ca^{2+} signals: how molecular properties shape global signals. *Chaos*, 19(3):037111, 2009.

[194] A. Skupin, H. Kettenmann, and M. Falcke. Calcium signals driven by single channel noise. *PLoS Comput Biol*, 6(8), 2010.

[195] A. Skupin, H. Kettenmann, U. Winkler, M. Wartenberg, H. Sauer, S. C. Tovey, C. W. Taylor, and M. Falcke. How does intracellular Ca^{2+} oscillate: by chance or by the clock? *Biophys J*, 94(6):2404–11, 2008.

[196] I. F. Smith and I. Parker. Imaging the quantal substructure of single IP3R channel activity during Ca^{2+} puffs in intact mammalian cells. *Proc Natl Acad Sci U S A*, 106(15):6404–9, 2009.

[197] I. F. Smith, S. M. Wiltgen, and I. Parker. Localization of puff sites adjacent to the plasma membrane: functional and spatial characterization of Ca^{2+} signaling in SH-SY5Y cells utilizing membrane-permeant caged IP3. *Cell Calcium*, 45(1):65–76, 2009.

[198] J. Sneyd, A. C. Charles, and M. J. Sanderson. A model for the propagation of intercellular calcium waves. *Am J Physiol*, 266(1 Pt 1):C293–302, 1994.

[199] J. Sneyd and M. Falcke. Models of the inositol trisphosphate receptor. *Prog Biophys Mol Biol*, 89(3):207–45, 2005.

[200] J. Sneyd, K. Tsaneva-Atanasova, V. Reznikov, Y. Bai, M. J. Sanderson, and D. I. Yule. A method for determining the dependence of calcium oscillations on inositol trisphosphate oscillations. *Proc Natl Acad Sci U S A*, 103(6):1675–80, 2006.

[201] J. Stelling, U. Sauer, Z. Szallasi, r. Doyle, F. J., and J. Doyle. Robustness of cellular functions. *Cell*, 118(6):675–85, 2004.

[202] H. Streb, R. F. Irvine, M. J. Berridge, and I. Schulz. Release of Ca^{2+} from a nonmitochondrial intracellular store in pancreatic acinar cells by inositol-1,4,5-trisphosphate. *Nature*, 306(5938):67–9, 1983.

[203] G. M. Suel, J. Garcia-Ojalvo, L. M. Liberman, and M. B. Elowitz. An excitable gene regulatory circuit induces transient cellular differentiation. *Nature*, 440(7083):545–50, 2006.

[204] G. M. Suel, R. P. Kulkarni, J. Dworkin, J. Garcia-Ojalvo, and M. B. Elowitz. Tunability and noise dependence in differentiation dynamics. *Science*, 315(5819):1716–9, 2007.

[205] P. S. Swain, M. B. Elowitz, and E. D. Siggia. Intrinsic and extrinsic contributions to stochasticity in gene expression. *Proc Natl Acad Sci U S A*, 99(20):12795–800, 2002.

[206] D. Swaminathan, G. Ullah, and P. Jung. A simple sequential-binding model for calcium puffs. *Chaos*, 19(3):037109, 2009.

[207] S. Swillens, P. Champeil, L. Combettes, and G. Dupont. Stochastic simulation of a single inositol 1,4,5-trisphosphate-sensitive Ca^{2+} channel reveals repetitive openings during 'blip-like' Ca^{2+} transients. *Cell Calcium*, 23(5):291–302, 1998.

[208] Y. Tang, J. L. Stephenson, and H. G. Othmer. Simplification and analysis of models of calcium dynamics based on IP3-sensitive calcium channel kinetics. *Biophys J*, 70(1):246–63, 1996.

[209] Y. Tateishi, M. Hattori, T. Nakayama, M. Iwai, H. Bannai, T. Nakamura, T. Michikawa, T. Inoue, and K. Mikoshiba. Cluster formation of inositol 1,4,5-trisphosphate receptor requires its transition to open state. *J Biol Chem*, 280(8):6816–22, 2005.

[210] R. Taufiq Ur, A. Skupin, M. Falcke, and C. W. Taylor. Clustering of InsP3 receptors by InsP3 retunes their regulation by InsP3 and Ca^{2+} . *Nature*, 458(7238):655–9, 2009.

[211] C. W. Taylor. Inositol trisphosphate receptors: Ca^{2+}-modulated intracellular Ca^{2+} channels. *Biochim Biophys Acta*, 1436(1-2):19–33, 1998.

[212] C. W. Taylor. Controlling calcium entry. *Cell*, 111(6):767–9, 2002.

[213] C. W. Taylor. Store-operated Ca^{2+} entry: A STIMulating stOrai. *Trends Biochem Sci*, 31(11):597–601, 2006.

[214] C. W. Taylor, P. C. da Fonseca, and E. P. Morris. IP(3) receptors: the search for structure. *Trends Biochem Sci*, 29(4):210–9, 2004.

[215] C. W. Taylor and A. J. Laude. IP3 receptors and their regulation by calmodulin and cytosolic Ca^{2+} . *Cell Calcium*, 32(5-6):321–34, 2002.

[216] C. W. Taylor and P. Thorn. Calcium signalling: IP3 rises again...and again. *Curr Biol*, 11(9):R352–5, 2001.

[217] C. W. Taylor and S. C. Tovey. IP3 Receptors: Toward Understanding Their Activation. *Cold Spring Harb Perspect Biol*, 2(12):a004010, 2010.

[218] M. Thattai and A. van Oudenaarden. Intrinsic noise in gene regulatory networks. *Proc Natl Acad Sci U S A*, 98(15):8614–9, 2001.

[219] M. Thattai and A. Van Oudenaarden. Attenuation of Noise in Ultrasensitive Signaling Cascades. *Biophys J*, 82:2943–2950, 2002.

[220] P. Thorn, A. M. Lawrie, P. M. Smith, D. V. Gallacher, and O. H. Petersen. Local and global cytosolic Ca^{2+} oscillations in exocrine cells evoked by agonists and inositol trisphosphate. *Cell*, 74(4):661–8, 1993.

[221] R. Thul and M. Falcke. Release currents of IP(3) receptor channel clusters and concentration profiles. *Biophys J*, 86(5):2660–73, 2004.

[222] R. Thul and M. Falcke. Stability of membrane bound reactions. *Phys Rev Lett*, 93(18):188103, 2004.

[223] R. Thul and M. Falcke. Waiting time distributions for clusters of complex molecules. *Eur Phys Lett*, 79:38003, 2007.

[224] R. Thul, K. Thurley, and M. Falcke. Toward a predictive model of Ca^{2+} puffs. *Chaos*, 19(3):037108, 2009.

[225] K. Thurley and M. Falcke. Derivation of Ca^{2+} signals from puff properties reveals that pathway function is robust against cell variability but sensitive for control. *Proc Natl Acad Sci U S A*, 108(1):427–432, 2011.

[226] F. Tostevin, P. R. ten Wolde, and M. Howard. Fundamental limits to position determination by concentration gradients. *PLoS Comput Biol*, 3(4):e78, 2007.

[227] S. C. Tovey, P. de Smet, P. Lipp, D. Thomas, K. W. Young, L. Missiaen, H. De Smedt, J. B. Parys, M. J. Berridge, J. Thuring, A. Holmes, and M. D. Bootman. Calcium puffs are generic InsP(3)-activated elementary calcium signals and are downregulated by prolonged hormonal stimulation to inhibit cellular calcium responses. *J Cell Sci*, 114(Pt 22):3979–89, 2001.

[228] S. C. Tovey, S. G. Dedos, E. J. Taylor, J. E. Church, and C. W. Taylor. Selective coupling of type 6 adenylyl cyclase with type 2 IP3 receptors mediates direct sensitization of IP3 receptors by cAMP. *J Cell Biol*, 183(2):297–311, 2008.

[229] J. Tyedmers, M. L. Madariaga, and S. Lindquist. Prion switching in response to environmental stress. *PLoS Biol*, 6(11):e294, 2008.

[230] J. Tyedmers, S. Treusch, J. Dong, J. M. McCaffery, B. Bevis, and S. Lindquist. Prion induction involves an ancient system for the sequestration of aggregated proteins and heritable changes in prion fragmentation. *Proc Natl Acad Sci U S A*, 107(19):8633–8, 2010.

[231] G. Ullah and P. Jung. Modeling the statistics of elementary calcium release events. *Biophys J*, 90(10):3485–95, 2006.

[232] K. Van Acker, N. Nadif Kasri, P. De Smet, J. B. Parys, H. De Smedt, L. Missiaen, and G. Callewaert. IP(3)-mediated Ca(2+) signals in human neuroblastoma SH-SY5Y cells with exogenous overexpression of type 3 IP(3) receptor. *Cell Calcium*, 32(2):71–81, 2002.

[233] N. G. Van Kampen. *Stochastic Processes in Physics and Chemistry*. Elsevier Science B.V., Amsterdam, 2002.

[234] T. Verechtchaguina, I. M. Sokolov, and L. Schimansky-Geier. Interspike interval densities of resonate and fire neurons. *Biosystems*, 89(1-3):63–8, 2007.

[235] A. Wagner. *Robustness and Evolvability in Living Systems*. Princeton University Press, 2005.

[236] A. Wagner. Robustness and evolvability: a paradox resolved. *Proc Biol Sci*, 275(1630):91–100, 2008.

[237] C. Walsh, S. Barrow, S. Voronina, M. Chvanov, O. H. Petersen, and A. Tepikin. Modulation of calcium signalling by mitochondria. *Biochim Biophys Acta*, 1787(11):1374–82, 2009.

[238] K. Wang, W. J. Rappel, and H. Levine. Cooperativity can reduce stochasticity in intracellular calcium dynamics. *Phys Biol*, 1(1-2):27–34, 2004.

[239] H. V. Westerhoff and B. O. Palsson. The evolution of molecular biology into systems biology. *Nat Biotechnol*, 22(10):1249–52, 2004.

[240] P. O. Westermark, D. K. Welsh, H. Okamura, and H. Herzel. Quantification of circadian rhythms in single cells. *PLoS Comput Biol*, 5(11):e1000580, 2009.

[241] D. J. Wilkinson. *Stochastic Modelling for Systems Biology*. Chapman and Hall, 2006.

[242] B. S. Wilson, J. R. Pfeiffer, A. J. Smith, J. M. Oliver, J. A. Oberdorf, and R. J. Wojcikiewicz. Calcium-dependent clustering of inositol 1,4,5-trisphosphate receptors. *Mol Biol Cell*, 9(6):1465–78, 1998.

[243] J. Wolf, J. Passarge, O. J. Somsen, J. L. Snoep, R. Heinrich, and H. V. Westerhoff. Transduction of intracellular and intercellular dynamics in yeast glycolytic oscillations. *Biophys J*, 78(3):1145–53, 2000.

[244] F. Wolfram, E. Morris, and C. W. Taylor. Three-dimensional structure of recombinant type 1 inositol 1,4,5-trisphosphate receptor. *Biochem J*, 428(3):483–9, 2010.

[245] P. H. M. Wolkenfelt. The Construction of Reducible Quadrature Rules for Volterra Integral and Integro-differential Equations. *IMA J Num Anal*, 2:131–152, 1981.

[246] N. M. Woods, K. S. Cuthbertson, and P. H. Cobbold. Repetitive transient rises in cytoplasmic free calcium in hormone-stimulated hepatocytes. *Nature*, 319(6054):600–2, 1986.

[247] X. S. Xie, P. J. Choi, G. W. Li, N. K. Lee, and G. Lia. Single-molecule approach to molecular biology in living bacterial cells. *Annu Rev Biophys*, 37:417–44, 2008.

[248] Y. Yao, J. Choi, and I. Parker. Quantal puffs of intracellular Ca^{2+} evoked by inositol trisphosphate in Xenopus oocytes. *J Physiol*, 482 (Pt 3):533–53, 1995.

[249] J. Yu, J. Xiao, X. Ren, K. Lao, and X. S. Xie. Probing gene expression in live cells, one protein molecule at a time. *Science*, 311(5767):1600–3, 2006.

[250] D. I. Yule and J. A. Williams. U73122 inhibits Ca^{2+} oscillations in response to cholecystokinin and carbachol but not to JMV-180 in rat pancreatic acinar cells. *J Biol Chem*, 267(20):13830–5, 1992.

[251] T. Zhou, L. Chen, and K. Aihara. Molecular communication through stochastic synchronization induced by extracellular fluctuations. *Phys Rev Lett*, 95(17):178103, 2005.

[252] L. Zhu, Y. Luo, T. Chen, F. Chen, T. Wang, and Q. Hu. Ca^{2+} oscillation frequency regulates agonist-stimulated gene expression in vascular endothelial cells. *J Cell Sci*, 121(Pt 15):2511–8, 2008.

[253] P. I. Zhuravlev and G. A. Papoian. Molecular noise of capping protein binding induces macroscopic instability in filopodial dynamics. *Proc Natl Acad Sci U S A*, 106(28):11570–5, 2009.

[254] Z. Zi, W. Liebermeister, and E. Klipp. A quantitative study of the Hog1 MAPK response to fluctuating osmotic stress in Saccharomyces cerevisiae. *PLoS One*, 5(3):e9522, 2010.

Acknowledgment

This work would not have been possible without the support of many people I am indepted to.

My supervisor Dr Martin Falcke went with me through all the ups and downs of this work. He introduced me to the beauty of stochastic Ca^{2+} dynamics, and he shared with me his broad knowledge in this field and his long experience with dynamical systems. I am grateful for all the opportunities I had in his group, most notably the contact to the experimental labs of Prof Colin Taylor's and Prof Ian Parker's. Last not least, I want to thank Dr Falcke for giving me the opportunity to continue the work with Prof Thomas Höfer on spatiotemporal cytokine dynamics in the time of my PhD, which unfortunately did not find a place in this thesis.

I am very much obliged to Prof Colin W Taylor for the great opportunity to verify theoretical predictions by experiments with HEK cells in his lab. I was deeply impressed by his unequalled knowledge about Ca^{2+} signalling and the pharmacology of IP_3Rs, and by the stimulating atmosphere in his group. He always had an open ear, and he was always willing to share his knowledge and his thoughts. I still find it hard to believe that he allowed me, experienced only by a few undergrad lab courses, to utilise all his state-of-the-art microscopic equipment without hesitation.

The help and support I obtained from Dr Alexander Skupin and Dr Stephen C Tovey cannot be overestimated. They introduced me to many technical issues of this work like stochastic modelling and spike-train analysis (AS) and cell culture and fluorescence microscopy (SCT). Even more importantly, they contributed to this work by fruitful discussions in the lab and through countless emails. Especially, I am grateful for the moral support I obtained from them in the final phase of writing this thesis. AS also provided Fig. A.1 and the source-code for spike-train analysis used in Chapters 5 and 6, and he carried the burden of a first corrector of this thesis.

I thank Prof Ian Parker and Dr Ian Smith for the good collaboration and exchange of ideas about statistical properties of Ca^{2+} puffs. Special thanks to Dr Ian Smith for the excellent data from puff sequences in SH-SY5Y cells that contribute to this work.

Moreover, I would like to thank all the members of the Falcke and Taylor labs for the warm and inspiring research atmosphere. Special thanks are given to Heiko Schmidle and to Heather Parker. HS worked out the derivation of cluster opening probability distributions from single-channel models (Appendix A.1) in

his Diploma thesis in the Falcke lab, and he provided excellent source-codes for that issue to me. HP improved Figs. 5.5 and 5.6 by recording some additional spike-sequences as a summer student in the Taylor lab.

I am obliged to Prof Edda Klipp for supporting this work as a faculty supervisor from Humboldt University, and I thank Prof Lutz Schimansky-Geier for the stimulating environment of SFB 555.

I am deeply greatful to my teacher Prof Reinhart Heinrich, from who I received the largest part of my modest knowledge on Theoretical Biophysics. Like so many others, I was deeply impressed by his lectures and just by his presence and his questions in my first seminar talks and in the consultations concerning my student research project. I hope he would have enjoyed this work. I want to thank the supervisors of my student research project and of my Diploma Thesis, Prof Jean-Pierre Mazat and Prof Thomas Höfer, who guided my first scientific experience.

Readability of this thesis has much improved due to the suggestions of Dr Alexander Skupin, Dr Stephen C Tovey, Dr Thomas Handorf and my wife Dr Stefanie Thurley, who read parts of this work prior to final submission.

I would like to express my deep gratitude to my parents Marion and Frank Thurley for their unconditional support in all my years of study.

My wife Stefanie Thurley and my daughter Nora Thurley are the most important people in my life. Stefanie, I thank you for your love and for all you have done for me, and especially for your patience with my many stays abroad in the last two years and with my absence of mind in the time of writing this thesis. Nora, mit Deiner Fröhlichkeit und Deinen wachen Augen zeigst Du mir immer wieder, was wirklich wichtig ist im Leben.

Publications

Kevin Thurley, Alexander Skupin, Stephen C. Tovey, Andrew Thomas, Colin W. Taylor, Martin Falcke.
Structure of dynamic feedback in Ca^{2+} dynamics.
Manuscript in Preparation.

Kevin Thurley and Thomas Höfer.
Cell-communication in the lymph node: Spatiotemporal regulation of paracrine cytokine signalling shapes immune responses.
Manuscript in Preparation.

Kevin Thurley, Ian Smith, Stephen C. Tovey, Colin W. Taylor, Ian Parker, Martin Falcke.
The dynamics of IP_3 receptor channel puff sites.
Manuscript in Preparation.

Kevin Thurley and Martin Falcke (2011).
Derivation of Ca^{2+} signals starting from puffs reveals that pathway function is robust against cell variability and sensitive for control.
PNAS 108:427-432.

Kevin Thurley and Martin Falcke (2010).
Hierarchic stochastic modelling: A new concept based on emergent behaviour of biomolecules.
Proceedings of the 6th Workshop on Computation of Biochemical Pathways and Genetic Networks, p. 81. *Editors: Katrin Hübner, Tim Johann, Ursula Kummer, Jennifer Levering.*

Dorothea Busse, Maurus de la Rosa, Kirsten Hobiger, Kevin Thurley, Michael Flossdorf, Andreas Scheffold, Thomas Höfer (2010).
Competing feedback loops shape IL-2 signaling between helper and regulatory T lymphocytes in cellular microenvironments.
PNAS 107:3058-63.

Rüdiger Thul, Kevin Thurley, Martin Falcke (2009).
Toward a predictive model of Ca^{2+} puffs.
Chaos 19:037108.

Christine Nazaret, Margit Heiske, Kevin Thurley, Jean-Pierre Mazat (2009).
Mitochondrial energetic metabolism: a simplified model of TCA cycle with ATP production.
J Theor Biol 258:455-64.

Berlin, 18. February 2011

Selbstständigkeitserklärung

Ich erkläre, dass ich die vorliegende Arbeit selbstständig und nur unter Verwendung der angegebenen Hilfsmittel angefertigt habe.

Berlin, den 18. Februar 2011

"Wer auf der Welt kann viel? Da sitzt ein Mann jahrelang im Gefängnis und erfindet den Reißverschluss. Ist das – viel? Oder es läuft jemand hundert Meter um eine Zehntelsekunde schneller als alle anderen Sprinter sämtlicher Erdteile, und die Menschheit wirft vor Begeisterung die Hüte ins Stadion. Ein neuer Rekord wurde aufgestellt. Schön und gut. Aber ist es – viel?" "Es ist vielleicht nicht viel", meinte der kleine Mann. "Aber was ist denn dann mehr? Was ist denn überhaupt – viel?" "Einen Krieg verhindern", erwiderte der Jokus. "Eine Hungersnot beseitigen. Eine Krankheit heilen, die für unheilbar gehalten wurde." "Das können wir beide nicht", sagte das Mäxchen.

"Who on earth can do much? A man being jailed for years invents the zip fastener. Is that – much? Or someone runs hundred meters in a tenth second faster than all the other runners on all parts of the world, and all the people throw their hats into the stadium enthusiastically. A new all-time record has been established. Well and good. But is that – much?" "Maybe it is not much", said the little man. "But what is more? What on earth is – much?" "Preventing a war", replied Jokus. "Eliminating a famine. Curating a malady, which was thought to be uncurable." "We both cannot do that", said little Max.

Quoted from Erich Kästner, "Der kleine Mann" (the little man), 1963. Dialogue between the circus conjuror Professor Jokus von Pokus and the little man called Mäxchen Pichelsteiner. Free translation by the author.